Report

Framework for performing NLFEA of deteriorated concrete infrastructures

Outcome of results from main deliverables H3.5

Authors:

Simen Kongshaug, Katarzyna Opstapska, Tore Myrland Jensen, Kathrine Mürer Stemland, Ramon Hingorani and Reignard Tan

Report no.:2026-00025

Partner(s):

SINTEF, Multiconsult, Norconsult.

Report EXCON

Framework for performing NLFEA of deteriorated concrete infrastructures

Outcome of results from main deliverables H3.5

TAGS
Non-linear finite element analysis, Reinforced concrete structures, Material models, Safety format.

VERSION
01

DATE
2025-12-18

AUTHORS
Simen Kongshaug, Katarzyna Opstapska, Tore Myrland Jensen, Kathrine Mürer Stemland, Ramon Hingorani and Reignard Tan

CLIENT(S)
SINTEF, Multiconsult, Norconsult.

CLIENT'S REFERENCE
Tor Arne Hammer

PROJECT NUMBER
102028198/340843

NUMBER OF PAGES AND ATTACHMENTS
100

SUMMARY
A framework for applying nonlinear finite element analysis to assess the current and future condition of reinforced concrete infrastructures has been established. It proposes two approaches for composing material models applicable for that purpose. Both approaches open for either composing available material models or by programming them as user supplied subroutines in commercial general purpose finite element software. Furthermore, methods to account for material degradation due to alkali silica reaction and reinforcement corrosion were formulated along with a safety format applicable for that purpose.

COMPILED BY
Reignard Tan

11.02.2026
Reignard Tan (23. feb.. 2026 10:46:29 GMT+1)
SIGNATUR

CONTROLLED BY
Giovanni Scilipoti

SIGNATUR

ENDORSED BY
Tor Arne Hammer

REPORT NR.	ISBN	GRADATION	GRADING THIS PAGE
2026-00025	978-82-14-07331-7	Open	Åpen

History

SIGNATURE	COMPILED BY	SIGNATURE
01	Reignard Tan	RT

Table of contents

CLICK OR TAP HERE TO ENTER TEXT.

Klikk eller trykk her for å skrive inn tekst.

1 Introduction

1.1 Background and motivation

This report provides guidelines for how nonlinear finite element analyses (NLFEA) can be used to assess the current and future condition of existing concrete infrastructures subjected to deterioration caused by reinforcement corrosion and alkali silica reaction (ASR). These types of deteriorations cause redistribution of forces in reinforced concrete (RC) structures, with the response becoming nonlinear by nature, in addition to other types of non-linearities of both mechanical or geometrical nature. Linear finite element analyses (LFEA) has traditionally been used for such purposes but has its shortcomings in that i) it is not able to realistically account for the nonlinearity caused by reinforcement corrosion and ASR in RC structures as well as for other non-linearities, and ii) the safety format with using partial safety factor method does not allow for utilizing the redundancy and/or the robustness of RC infrastructures. This can lead in many cases to incorrect assessments that trigger unnecessary interventions. In contrast, NLFEA enables a more detailed and realistic representation of damage mechanisms, load redistribution, and structural capacity, corresponding load distributions and their influence on the capacity of the systems under evaluation. The choice to focus on NLFEA is therefore intended to support asset owners and engineers in making well-informed decisions regarding remaining service life, maintenance prioritization, and safety management, based on a more accurate understanding of actual structural behaviour.

1.2 Objectives and scope

The main objectives in the report are to facilitate

- Composition of material models applicable for performing NLFEA to assess the current and future condition of existing concrete infrastructures
- Modelling approach that accounts for deterioration of concrete affected by ASR
- Modelling approach that accounts for deterioration of reinforcing steel affected by corrosion
- Safety format for performing NLFEA of existing concrete infrastructures subjected to deterioration

1.3 Limitations

This report will solely focus on material modelling of reinforced concrete and deterioration caused by specifically reinforcement corrosion and ASR. The framework is formulated so that it is applicable for global assessment of the structural integrity of large concrete infrastructures. This means that only composition of material and degradation models applicable for such purposes will be addressed, naturally computational time being of essence. Furthermore, local assessments, such as anchorage failures due to uniform reinforcement corrosion, are not treated here. Solution strategies related to performing the NLFEA itself will not be addressed and are assumed to be a prerequisite for the reader.

1.4 Framework

The report is structured in such a way that it can serve as a framework for applying NLFEA to assess existing concrete infrastructures subjected to deterioration caused by reinforcement corrosion and ASR. First, two general approaches for composing material models that are applicable for NLFEA of deteriorated concrete structures are addressed. The two general approaches have been chosen carefully with respect to being computationally efficient, while providing realistic and reliable results for large concrete infrastructures. Then, material modelling approaches accounting for ASR and reinforcement corrosion of reinforcing steel have been provided. Thereafter, safety formats applicable to NLFEA of deteriorated concrete structures are addressed. Finally, necessary input required to assess the current and future condition of deteriorated concrete infrastructures applying NLFEA are addressed.

2 Material models applicable for NLFEA of deteriorated concrete structures

2.1 Limitations

There are various ways of modelling the nonlinear behaviour of reinforced concrete structures, and a comprehensive overview is provided in [1]. The modelling approach is among others very dependent on the scale and the failure mode that is expected of the structure. In this report, relevant compositions of material models applicable for analysing large, deteriorated RC infrastructures will be addressed, as computational time becomes an essential parameter. It will thus be emphasized on proposals for material models that are computationally efficient for practical use while providing realistic and reliable results. The material models addressed here are applicable to 3D RC-structures discretized by solid elements. The focus will be on providing practical guidelines for composition of material models that are able to predict the global structural behaviour, while accounting for deterioration caused by reinforcement corrosion and ASR realistically. This means that the report is limited to addressing continuum based smeared cracking approaches only.

2.2 General approaches for composition of material models

Modelling of large, RC structures necessitate a material model for replicating i) the concrete behaviour in compression and tension and ii) the reinforcing steel. The composition of these material models should be consistent with one another. They should also account for the tension stiffening effect to obtain realistic stiffness in the structure [2]. In compression, the concrete should account for being subjected to triaxial stress states, i.e. how confinement and lateral tension affect the behaviour and failure criteria. Furthermore, the behaviour after cracking should also be well defined, e.g. unloading, fixed vs. rotational crack behaviour, closing and opening of cracks, brittle vs. softening branch in tension, effects on the Poisson's ratio and so forth.

Recommended approaches for practical application to the RC structures in this project are plasticity and smeared crack models. The material models for reinforcement should be mechanically consistent with how the concrete has been modelled. Note that the mesh size also should be considered when choosing a composition of material models. This is because tension stiffening is very much dependent on whether it is accounted for by strain localisations in row or column of elements, or if it is inherently accounted for in the material model for the steel e.g. as for tension chord models.

Following general composition of material models are mechanically consistent with one another and are recommended for practical use

1. Fixed crack models accounting for lateral effects such as confinement and lateral tension, without a softening tensile branch can be combined with a tension chord model for the reinforcement. This approach is best suited to relatively coarse mesh sizes, since the tension stiffening effect is inherently accounted for in the tension chord model. This means that there is no additional need to refine the mesh to obtain proper tension stiffening. In fact, one should be aware of not using too small mesh sizes as the tension stiffening effect can be accounted for twice by doing so. This makes the approach suitable for NLFEA of large concrete infrastructures.
2. Fixed crack models and damage plasticity models accounting for lateral effects such as confinement and lateral tension, with a softening tensile branch can be combined with naked steel material behaviour for steel reinforcement. Note that the mesh should be sufficiently small so that tension stiffening is accounted for by strain localization in row or column of elements in the model.

Both approaches can be combined with bond-slip modelling to model anchorage failures in both cases. Bond-slip modelling can also help enhance the tension stiffening effect in the second approach above [3]. However, introduction of bond-slip models will lead to increased computational time, and it is recommended that anchorage failures are investigated separately from the NLFEA as a pragmatic and practical approach. It will thus not be further addressed in detail in this report.

2.3 FE-modelling approaches for practical application of NLFEA

It is recommended that the RC behaviour is modelled using a continuum based smeared cracking approach, with embedded reinforcement elements that are deformation compatible with the solid elements for the concrete. In this manner, the reinforcement elements can be modelled both as smeared and/or discrete. The approach is computational efficient and is compatible with the two approaches for composition of material models addressed in subchapter 2.2.

Both first and second approach in subchapter 2.2 can be applied using general purpose FE software, either directly as available material models or by implementing them in user supplied subroutines. Approaches in accordance with the recommendation in subchapter 2.2 will be addressed in the following. It will also be highlighted which general purpose FE software that offer the various approaches.

2.3.1 Smeared reinforcement with damage model for crack

Most accurate approach at the expense of increasing the computational time considerably. Acceptable in a qualitative study, but not feasible for NLFEA in practical cases. This is mainly due to the need to use softening and small elements to capture reasonable tension stiffening effects.

1. Following modelling techniques are investigated: Solid elements are used for concrete and truss elements for reinforcement with concrete damaged plasticity (CDP) material model and elastic-plastic with bilinear hardening material model respectively, full embedment of the reinforcement within concrete (truss elements within solid) (technique 2)
2. Solid elements for concrete and smeared cracking material model – reference for comparison (technique 1)

Modelling parameters choice in non-linear material models with anisotropic behavior (different failure for different stress state) is time consuming task and practical approach considering sensitivity of the model to different material and numerical settings parameter values for a given class of benchmarks is of interest. Following sensitivity study is planned to provide practical data:
Variation of CDP material parameters with max 5 values for each of the following parameters:

- Dilation angle (30, 35, 40)
- Biaxial to uniaxial stress ratio (1, 1.16, 2)
- Viscous stabilization (0.01, 0.001, 0.0001, 0.0) – a numerical damping parameter that supports convergence and is defined within material definition to simulate energy dissipation, the value needs to be sufficiently small compared to the time increment, default value is 0.0
- Compression softening curve (3 shapes) -
- Tension softening curve (3 shapes)
- Fracture energy (3 values with linear softening, 3 values with exponential softening)
- Mesh size for linear and continuum elements (10mm, 20mm, 30mm, 50mm, 100mm)

2.4 Composition of material models according to the first approach

2.4.1 Relevant material models

The relevant models that will be addressed in the following are total strain models [4] and Kotsovos [5] for the concrete behaviour and tension chord models for the tension stiffening behaviour of reinforced concrete ties. These modelling approaches can be found in the general-purpose FE software DIANA.

2.4.2 Total strain model

Total strain models [4] with fixed crack formulation can be applied together with a tension chord model for the reinforcing steel. A parabolic compressive behaviour can be combined with a brittle tensile behaviour for the concrete. Lateral confinement and cracking effects on the compressive behaviour should be accounted for, as well as effects on the Poisson's ratio in a cracked state. Appropriate modelling approaches for the concrete in compression and tension are provided in [4].

2.4.3 Plasticity models

The Kotsovos model [5] can be applied together with a tension chord model. This is a fully triaxial model meant for modelling the 3D behaviour of large RC structures. As opposed to the total strain modelling approach, it only requires the compressive cylinder strength as input to model the concrete behaviour making it pragmatic and suitable for practical applications.

2.4.4 Tension chord models

Applicable tension chord models compatible with the material models for the concrete addressed above are the original tension chord model (TCM) [6], the simplified modified tension chord model (SMTCM) [7] and the tension chord model deduced from the crack width calculation model in Eurocode 2 (EC2) [8]. It has been proven they all can account for tension stiffening rather efficiently while having rather coarse mesh, making this approach suitable for practical application to large RC structures.

2.5 Composition of material models according to the second approach

2.5.1 Concrete damaged plasticity (CDP)

Concrete damaged plasticity (CDP) is one of the most common concrete material models for advanced and detailed studies among researchers and engineers and can be found in the general-purpose FE software ABAQUS. The material model can be applied together with naked steel behaviour for reinforcing steel in accordance with the second approach in subchapter 2.2. It can predict tension and compression damage initiation and propagation and therefore be applied in complex stress states problems. CDP material model combines the isotropic elasticity, the Drucker-Prager type of compression sensitive plasticity with non-associated flow and the stiffness damage definition based on stress-strain (or traction-separation) definition. While those techniques lie behind the versatile potential of the CDP model, they require multitude material parameters as input. Typically, the data input needed to sufficiently define all CDP material parameters is based on the tests [9]:

1. Uniaxial unconfined compression
2. Uniaxial tension
3. Bi-axial plane stress test (Kupfer curve)
4. Tri-axial compression test (hydrostatic pressure and uniaxial compression combined)

This can also lead to the need for calibration and validation work in the case of new or modified types of concrete, e.g. ultra-high-performance concrete (UHPC), fiber-reinforced concrete, confined concrete, geopolymer concrete. Thus, it is important for practical engineering purposes to define default CDP parameters for a specific type of concrete and structure.

The list over all CDP material parameters with their description and typical values for common concrete are provided in the Table 2-1.

Table 2-1 Overview of CDP material parameters.

Model	Parameter	Description	Value range	Unit
Elasticity				
CDP - elasticity	E – Young modulus	Initial elastic stiffness	15-50	[GPa]
CDP - elasticity	ν – Poisson ratio	Expansion in the direction perpendicular to the applied deformation	0.18-0.25	[-]
Compression: Plasticity + damage				
CDP - plasticity	Dilation angle	Volumetric expansion during plastic deformation, measured in pressure-deviatoric stress space in triaxial test	15-50	[°]
CDP - plasticity	Eccentricity ε	ε=0 aligns with Drucker Prager hypothesis,	0.1-1	
CDP - plasticity	fb0/fc0	Biaxial to uniaxial strength ratio	1.16	[-]
CDP - plasticity	K	Correction of deviatoric failure surface cross section from circle (K=1.0) to differentiate between tension and compression	2/3 = 0.66	[-]
CDP - plasticity	viscosity	Numerical stabilization	0-0.001	[-]
CDP - plasticity	Yield stress-inelastic strain	Stress-strain data based on uniaxial compressive test	curve	[MPa], [-]
CDP - damage	Compression damage	Damage parameter [0-1] defined in function of the inelastic strain	curve	[-]
Tension: damage				
CDP - damage	Tensile strength	Maximum yield stress reached for damage initialization (option 3 and 2)	3-5	[MPa]
CDP - damage	Fracture energy	Damage evolution: linear (option 3)	0.1-0.2	[N/mm]
CDP - damage	Displacement	Damage evolution: linear (option 2)		[mm]
CDP - damage	Tensile damage	Damage parameter [0-1] defined in function of a cracking strain (option 1)	curve	[-]
CDP – damage	Yield stress-cracking strain	Stress-strain curve defining tension stiffening after reaching tensile strength	curve	[MPa], [-]

Besides single numerical value parameters, CDP model requires tabular specification of the stress-strain curves and damage-strain curves for both uniaxial compressive and tensile (option 1) behaviour. Material data for concrete is usually available as Young's modulus and maximum compressive strength, and optionally the corresponding strain. Several models exist to calculate the stress-strain curves in the absence of the uniaxial unconfined compressive test data. Following approaches are commonly applied:

1. Hognestad model:

$$\sigma_c = f_c \left[\frac{2\varepsilon}{\varepsilon_0} - \left(\frac{\varepsilon}{\varepsilon_0} \right)^2 \right] \quad (1)$$

2. Modified Saenz model:

$$\sigma_c = f_c \frac{A\frac{\varepsilon}{\varepsilon_0}}{1 + B\frac{\varepsilon}{\varepsilon_0} + C\left(\frac{\varepsilon}{\varepsilon_0}\right)^2} \quad (2)$$

3. Desayi and Krishana model:

$$\sigma_c = f_c \frac{A\frac{\varepsilon}{\varepsilon_0}}{1 + B\left(\frac{\varepsilon}{\varepsilon_0}\right)^2} \quad (3)$$

4. Eurocode 2 model:

$$\sigma_c = f_c \frac{k\frac{\varepsilon}{\varepsilon_0} - \left(\frac{\varepsilon}{\varepsilon_0}\right)^2}{1 + (k-2)\frac{\varepsilon}{\varepsilon_0}}, \qquad where\ k = 1.05E\frac{\varepsilon_0}{f_c} \quad (4)$$

Where:
σ_c – compressive stress
ε – strain
ε_0 – strain at maximum compressive stress
f_c – maximum compressive stress
E – Young's modulus
A, B, C – constants

All four curves are compared for the same values of material parameters and constants, see Table 2-2.

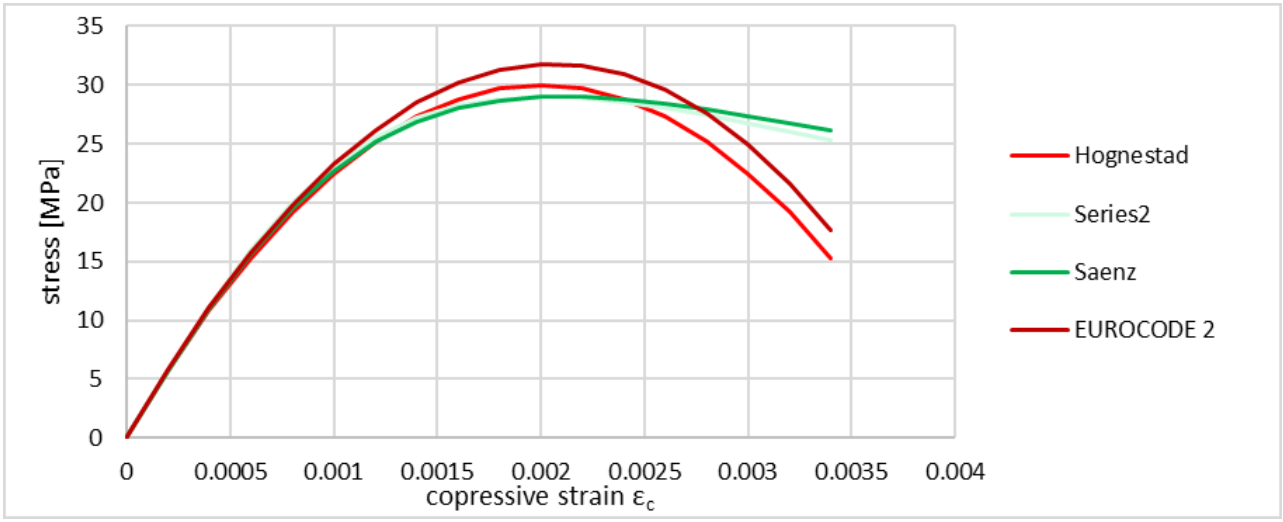

Figure 2-1: Comparison of the stress-strain curves according to input material parameters in Table 2-2.

Table 2-2 Input material parameters for stress-strain curves for uniaxial concrete compression

E	29000 MPa
f_c	30 MPa
ε_0	0.002
k	2.03
A	$E \cdot \varepsilon_0$=58 MPa
B	0.1
C	0.9

It can be noted that models differ after initial elastic response, and the hardening is especially larger for Saenz and Desay-Krishnan model compared to Hognestad and Eurocode. Comparison of modelling with Eurocode 2 and Saenz compression stress-strain curves is shown in different case studies in 2.6.3.

2.5.2 Total strain models

Total strain models can be combined with naked steel behaviour for reinforcing steel. A parabolic compressive behaviour can be combined with a softening tensile behaviour for the concrete. Lateral confinement and cracking effects on the compressive behaviour should be accounted for, as well as effects on the Poisson's ratio in a cracked state. It is recommended by [4] that the element size is smaller than the anticipated average crack spacing to capture the tension stiffening effect properly. Furthermore, bond-slip models might be necessary to enhance the tension stiffening effect. These measures could increase the computational time for large RC structures significantly. This approach can be modelled using both DIANA and ATENA.

2.6 Validation

2.6.1 Case studies

Validation of the material models and modelling techniques was done on several benchmark case studies for which force-displacement curves are available. The following subchapters show comparison of load displacement curves between predicted response either by first or second approach according to that described in subchapter 2.2 and those reported in the experiments. The experiments used in the comparison studies are summarized in Table 2-3 and **Figure 2-2**. The experiments have been chosen carefully to investigate the ability of the NLFEA approaches to predict various failure modes.

Table 2-3: Experiments used for comparison with NLFEA approaches

Authors	Specimen	Failure mode
Vecchio and Shims [10]	C3	Flexural-compression
	OA2	Diagonal tension
	B1	Shear-compression
Kotsovos [11]	CS1	Flexural
Seraj [12]	CS7	Flexural-compression
El-Feky M.H. et al [13]	ELFEKY_1	Flexural

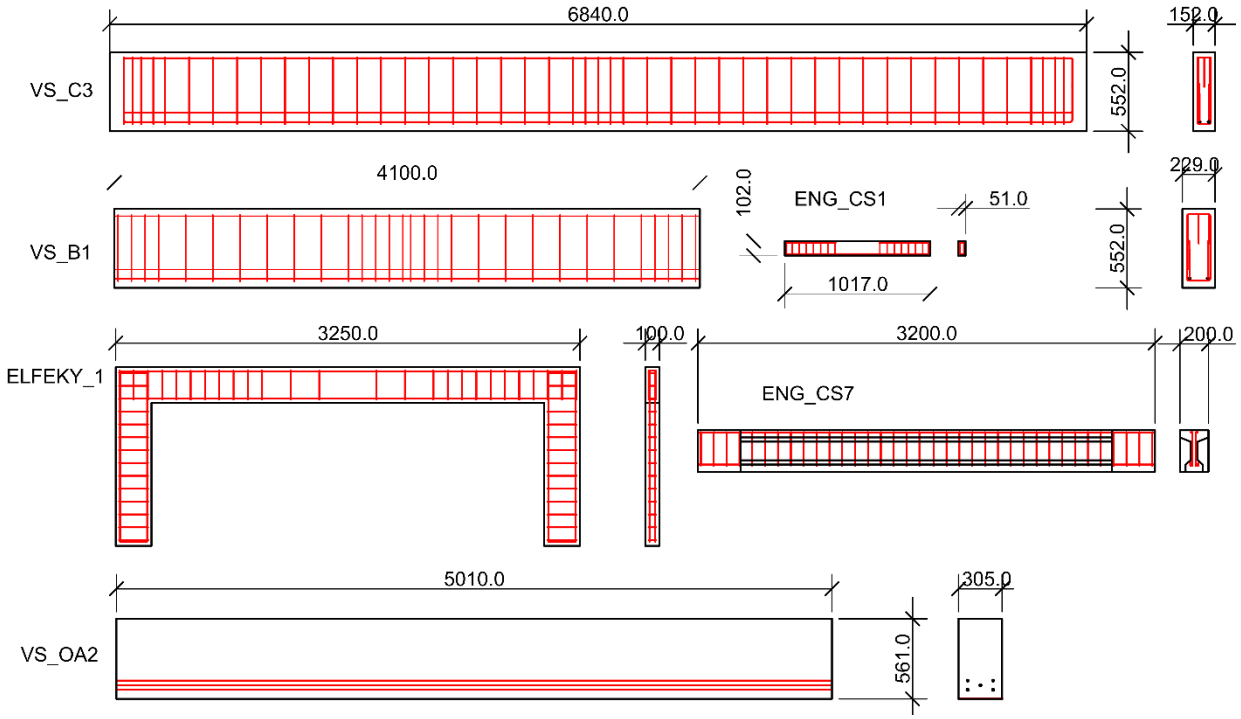

Figure 2-2: Geometry of six benchmark case studies: B1, C3, OA2, CS7 and CS1, and ELFEKY.

2.6.2 Composition of material models according to the first approach

Figure 2-3 to Figure 2-7 show comparison of load-displacement curves with the first approach described in subchapter 2.4. The general-purpose FE software DIANA was used, and the results are extracted from [14]. In these comparisons the tension chord model according to Eurocode 2 [8] was utilized. Note that the responses also include load-displacement curves for which naked steel material behaviour is used for the reinforcement. Furthermore, the specimens were meshed with typically three elements over the thickness. The rather coarse mesh consisting of solid elements was chosen to prove the suitability of the approach for NLFEA of large RC infrastructures. Note that non-converged load steps are provided to visualize the numerical stability of the modelling approach.

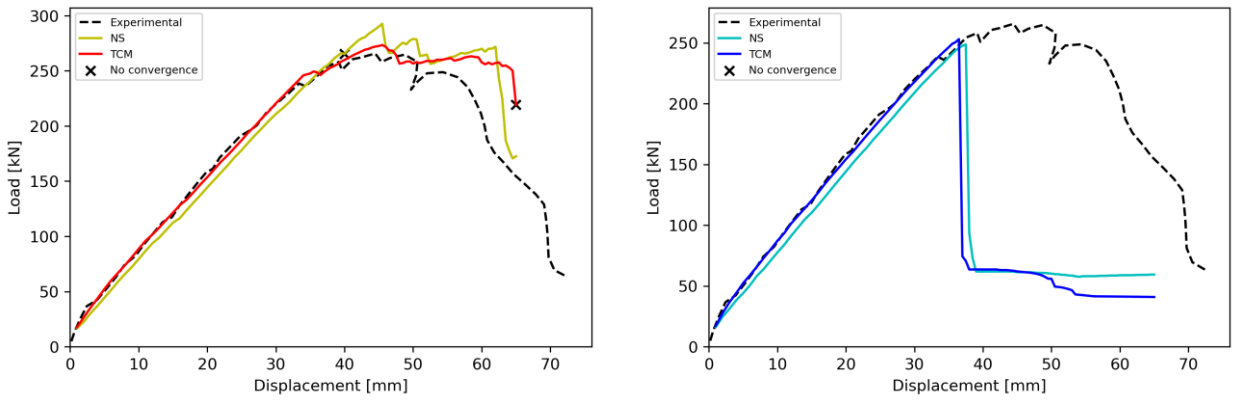

(a) Kotsovos (b) Total strain

Figure 2-3: Load displacement curves for experiment C3.

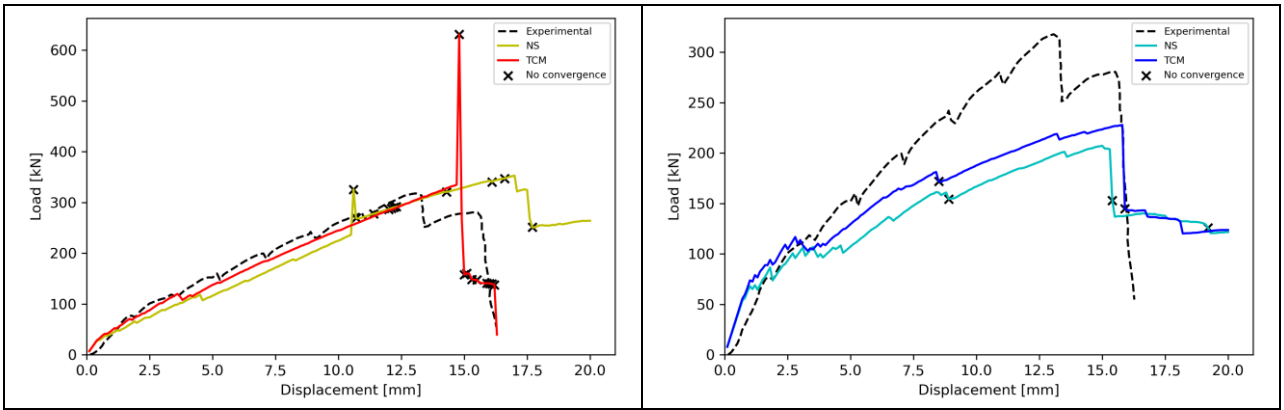

(a) Kotsovos (b) Total strain

Figure 2-4: Load displacement curves for experiment OA2.

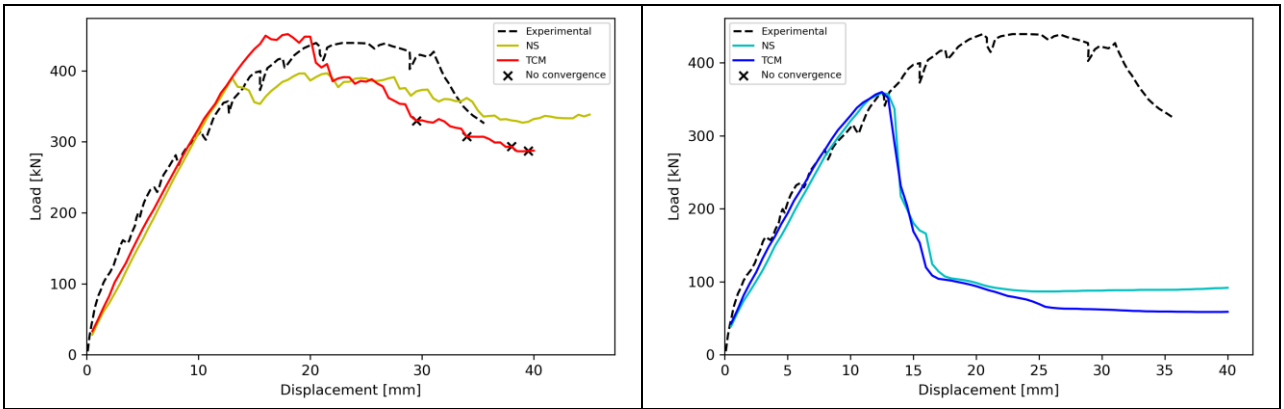

(a) Kotsovos (b) Total strain

Figure 2-5: Load displacement curves for experiment B1.

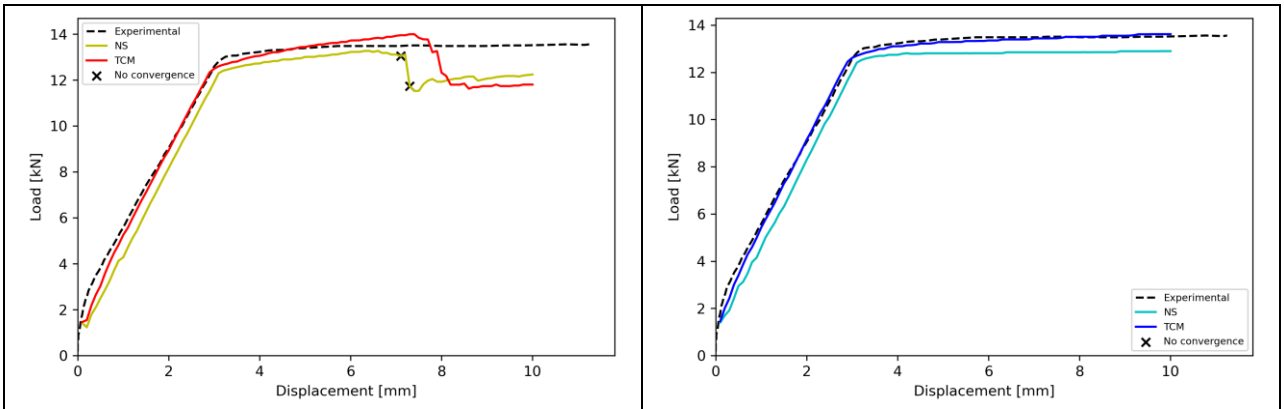

(a) Kotsovos (b) Total strain

Figure 2-6: Load displacement curves for CS1.

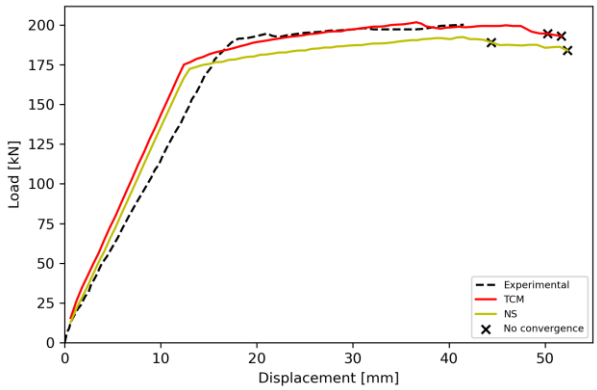

(a) Kotsovos

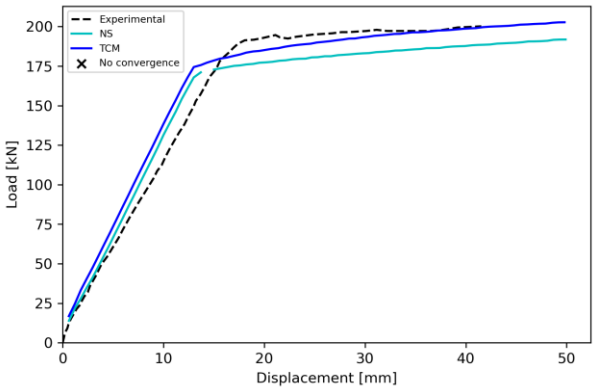

(b) Total strain

Figure 2-7: Load displacement curves for CS7.

2.6.3 Composition of material models according to the second approach

The complete set of material properties was shown for each benchmark model in tables

Figure 2-3 to Figure 2-7 show comparison of load-displacement curves with the first approach described in subchapter 2.5.

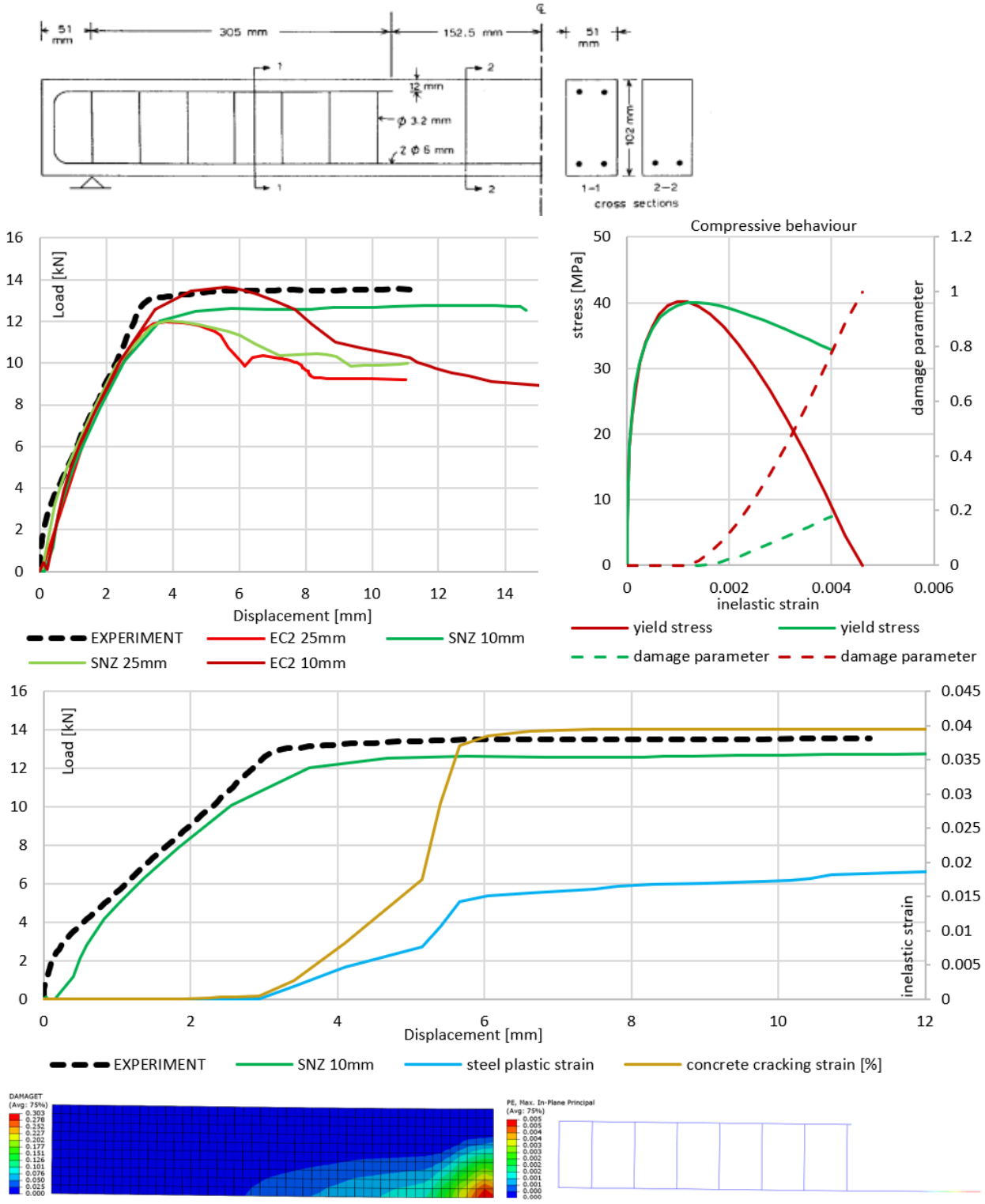

Figure 2-8 Load displacement curves for CS1 with compressive material models and failure mode.

CS1 simulation results are shown in Fig. 2-7. Eurocode 2 compression model of concrete predicts capacity better, but Saenz curve agrees better with overall behaviour – ductile with slight hardening. Mesh size of 25 mm (10% of beam height) was found sufficient. Difference in capacity for Saenz curve simulation is attributed to fracture energy value which was not given for this case and was estimated based on CEB-FIP 2010 equation as $G_F = 73 \cdot \left(\frac{f_c}{10}\right)^{0.18} = 0.9274\ N/mm$. First tensile cracks appear at ca 0.7 mm beam

deflection softening force-displacement curve and concentrated localized cracking occurs under point-load at 2.8 mm beam deflection proceeded by mid-span yielding in tension reinforcement – see bottom right of the Fig. 2-7. Concrete crashing strain was limited here to 4‰. At 11 mm beam deflection the plastic strain in steel is close to 2%.

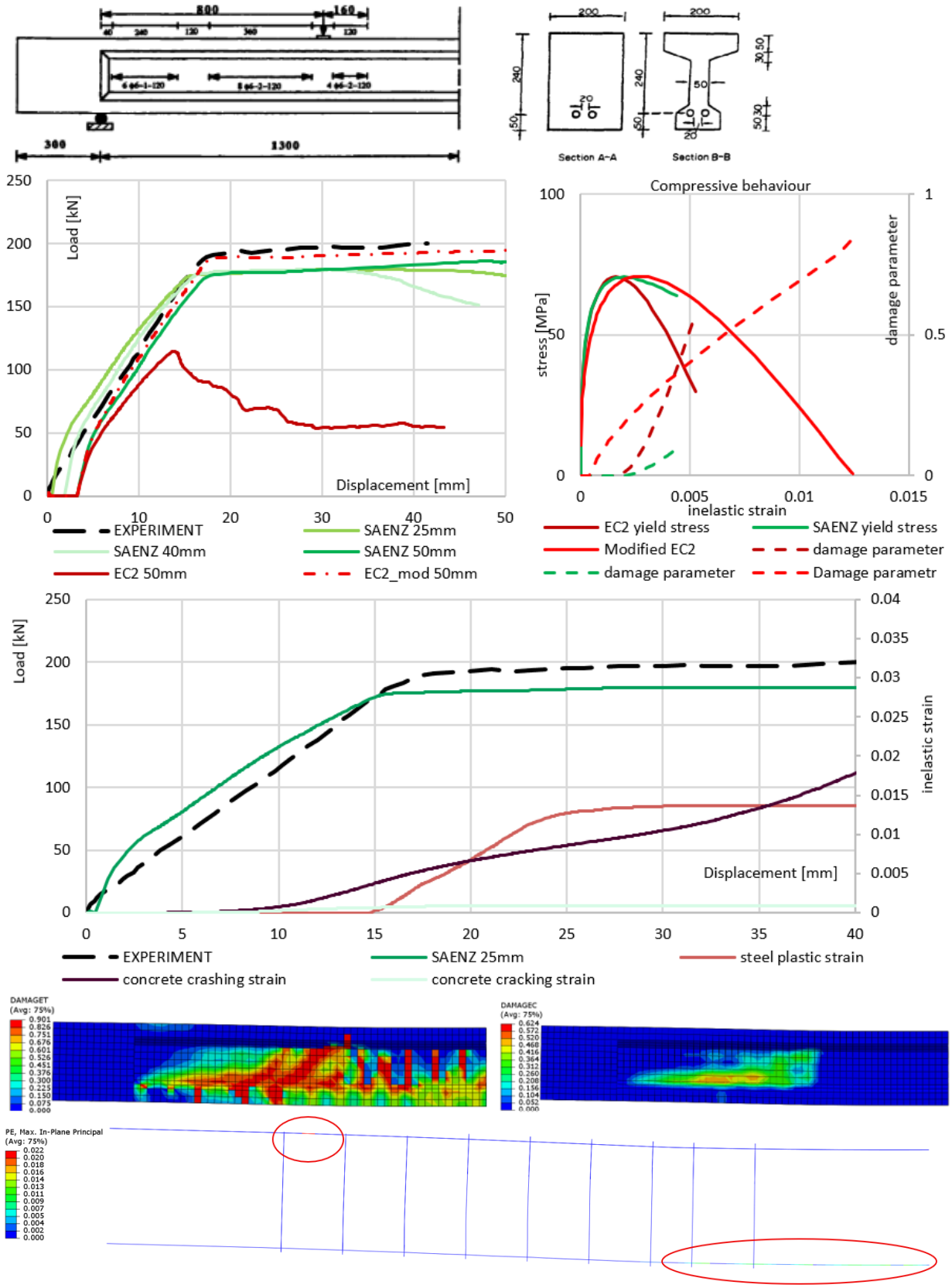

Figure 2-9 Concrete compression curves and load displacement curves for CS7 beam bending test.

CS7 simulation results are shown in Fig. 2-8 together with compression models, i.e. EC2 and Saenz, as well as modified EC2 with higher strain capacity. Mesh of 50mm (17% of beam height) was found sufficient. Modified EC2 compression model shows best agreement with experimental result while EC2 model underestimating capacity. Saenz curve is recommended in case where reinforcement ratio is high, ca 2.4%. Concrete cracking pattern and crashing/shear zone is shown at 15 mm beam deflection, just before steel plastic yield onset. Beam failure is ductile yield in tensile reinforcement with ultimate failure caused by compression rebar localized yield at section profile change.

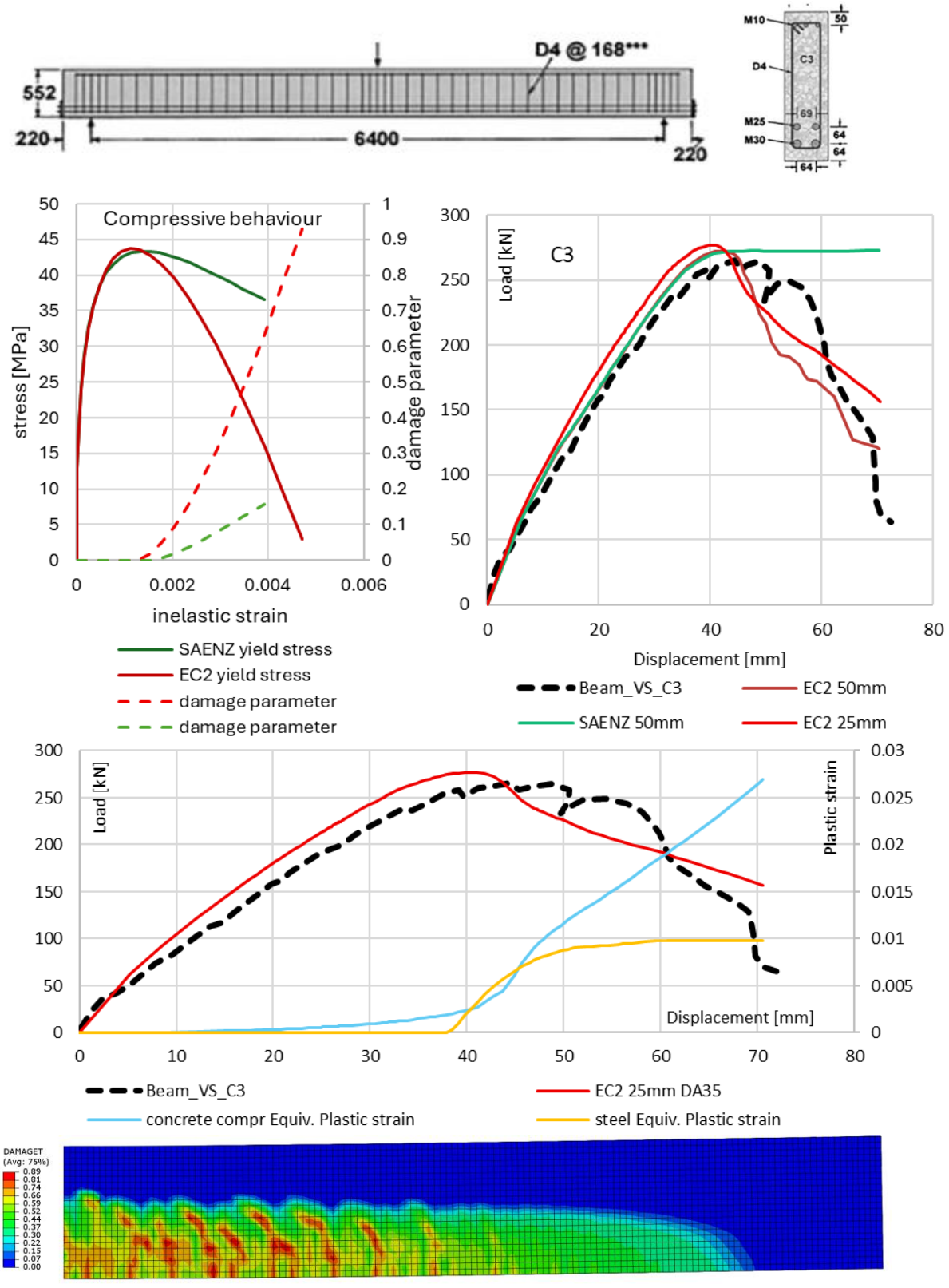

Figure 2-10 Load displacement curves for C3 with concrete compressive models, plastic strains development and crack pattern at maximum capacity.

Beam C3 simulation results and material model for concrete compression are shown in Figure 2-10. Both Saenz and Eurocode 2 curves give good capacity prediction, but Eurocode 2 curve gives better failure mode

prediction. Concrete tensile cracking softens the initial apparent stiffness at around 50kN load before the tensile and shear reinforcement yielding locally under the load point and plastic flow starts just before the maximum load is achieved. The ultimate failure is brittle due to extensive localized crashing and shear of concrete under mid-span load point. Mesh size of 50mm (ca 9% of beam height) is found sufficient.

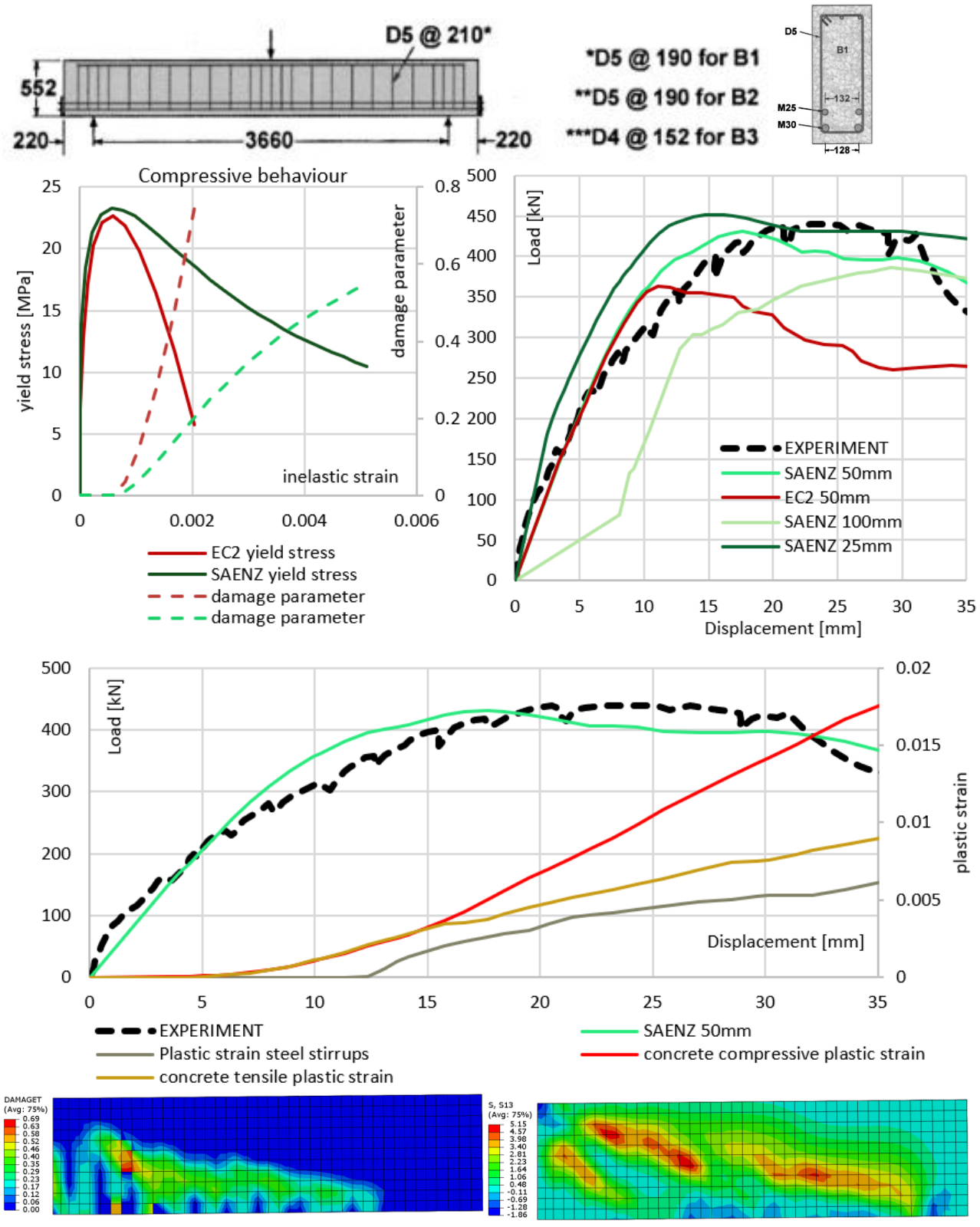

Figure 2-11 Load displacement curves for B1 with concrete compression model, crack pattern and shear stress at maximum load capacity.

B1 simulation results and concrete compression stress-strain curves are shown in Figure 2-11. Concrete tensile cracking leads to force-displacement curve softening from around 200kN load. Concrete shear and

crashing are main failure mode with shear reinforcement yielding onset just before maximum load capacity is reached. Mesh size of 50mm (ca 9% of beam height) is found sufficient. Additional study of the tensile concrete material model was performed for the B1 cases study. See Figure 2-11. Four stress-displacement curves with linear and bi-linear softening are depicted on top with respective force-displacement curves below. Fracture energy is kept constant in the first three tension softening models, one linear and two bi-linear. Tensile damage is linear for all cases. The initial slope of tension softening as well as the fracture energy have large influence on the load capacity. Linear model is found to fit best with the experimental data.

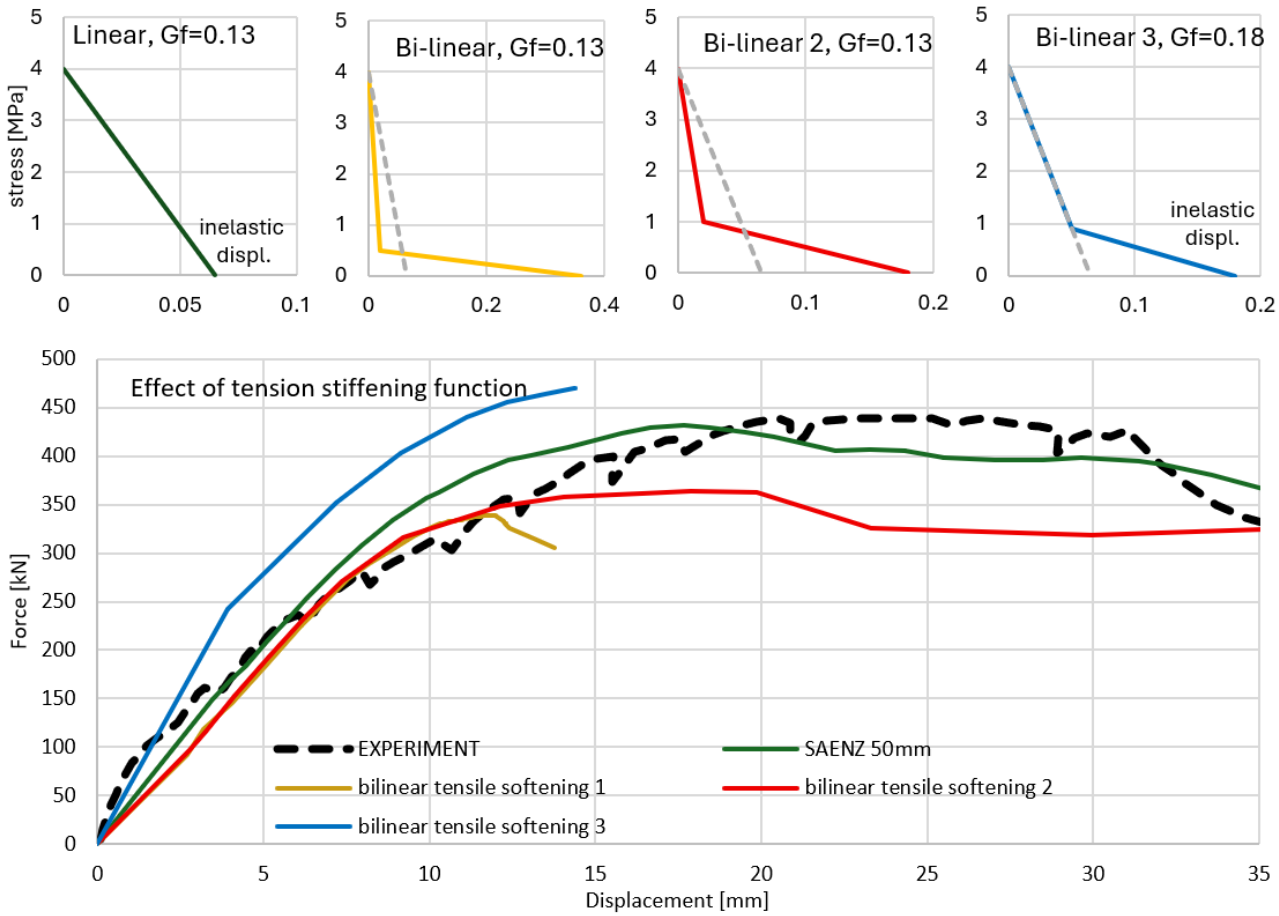

Figure 2-12 Tension stiffening influence on B1 case study simulation results.

Results of OA2 beam simulation are presented in Figure 2-13 together with two concrete compression models, i.e. EC2 and Saenz. EC2 (Eurocode 2) model was found to be best fit with sufficient mesh size of 50 mm (ca 9% of beam height). Saenz model exhibits too ductile behaviour but has accurate capacity prediction. Concrete tensile cracking leads to lowered apparent stiffness at 100 kN load. Concrete crashing and shear is the main failure mode at 300 kN load with brittle collapse. Development of damage of concrete both for tension and compression is shown in the center right of Figure 2-13.

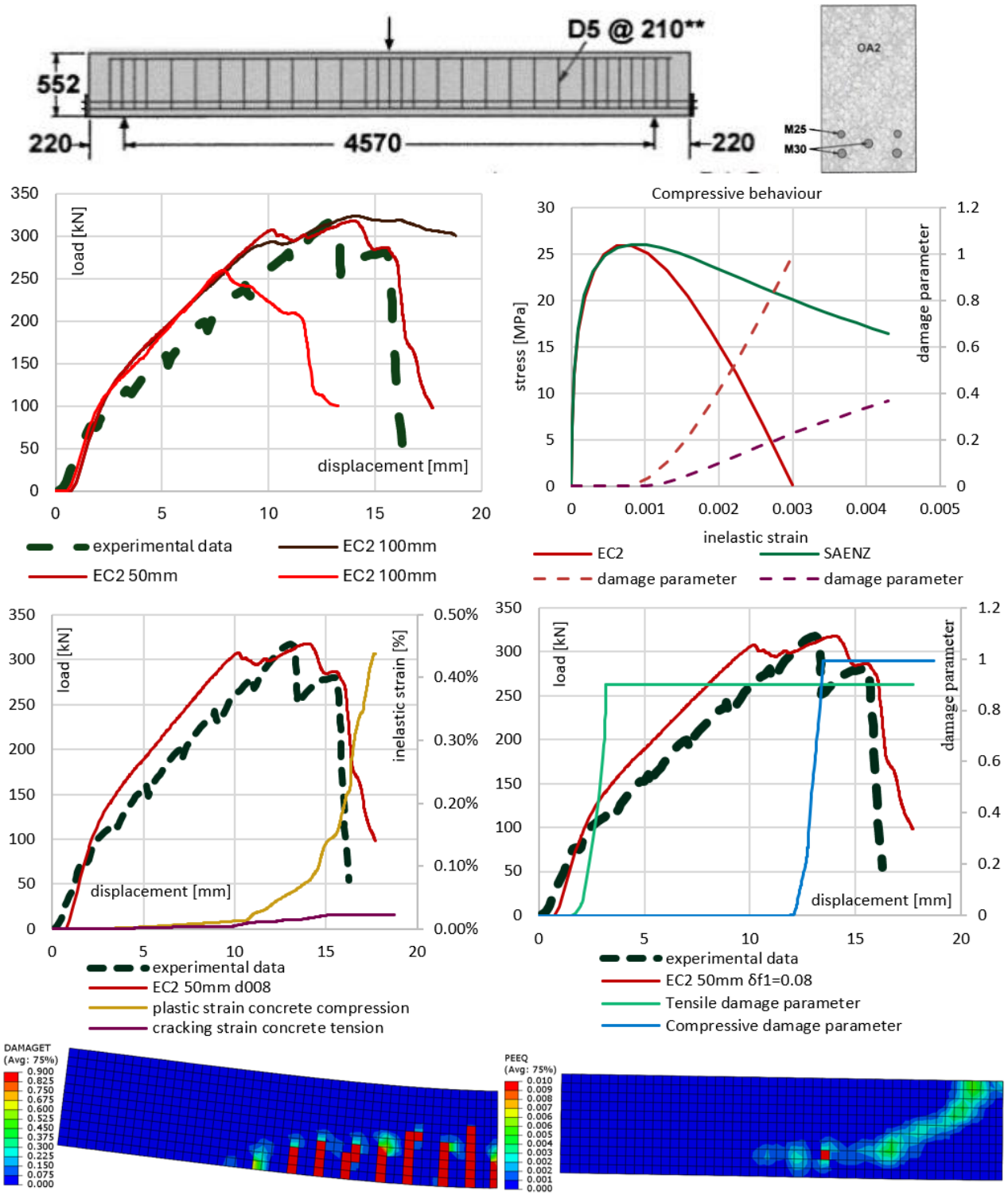

Figure 2-13 Load displacement curves for OA2

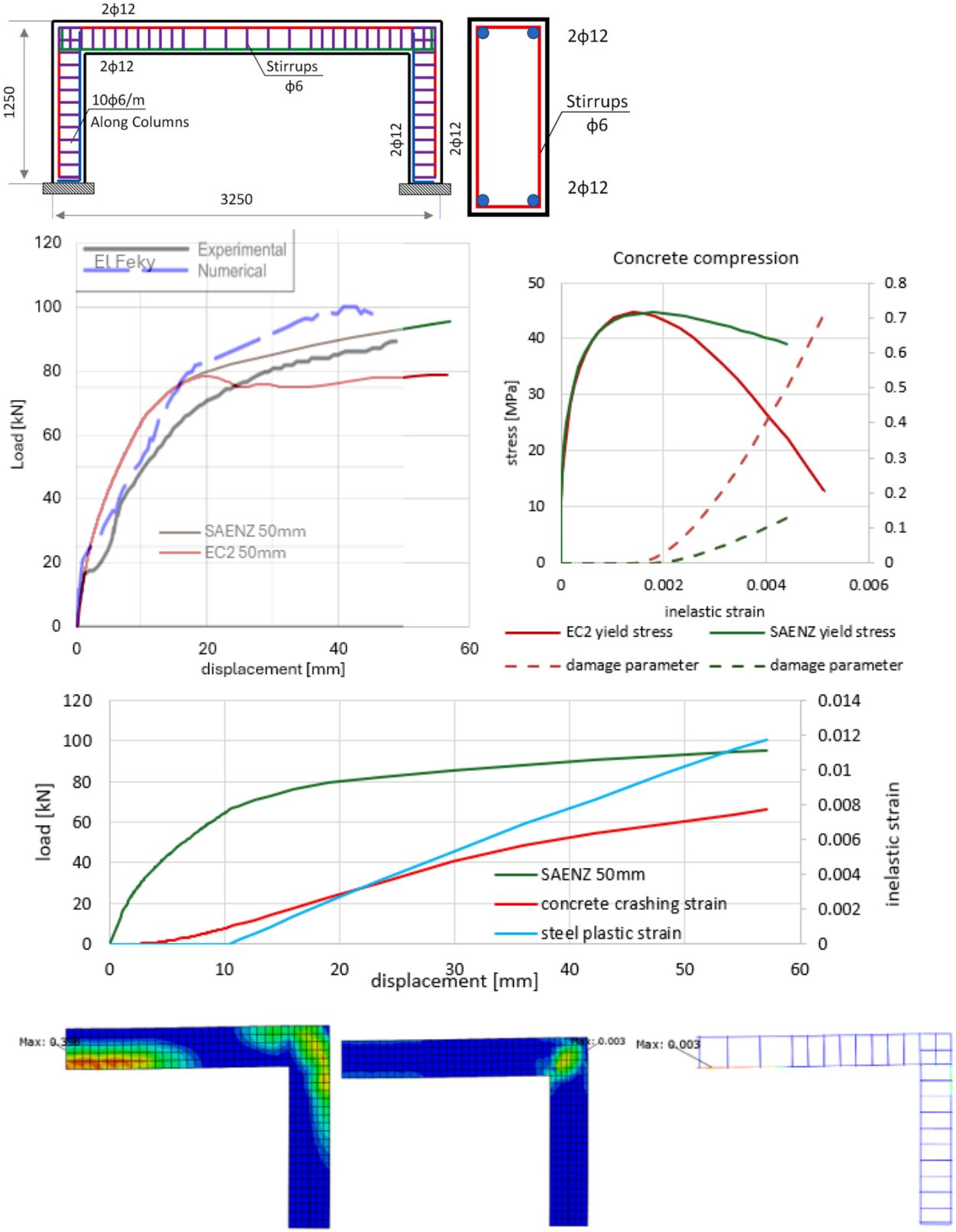

Figure 2-14 Simulation results for portal frame and failure mode.

ELFEKY frame simulation results are presented in Figure 2-14. Saenz curve was found to be the best fit with 50mm mesh size sufficient (20% of section height). EC2 curve gives good prediction within initial loading

before steel plastic yield occurs. Unlike in simply supported beams, boundary conditions applied as fixed under part of column were the most critical factor influencing results. Failure starts with concrete tensile cracking and shearing in the frame corners together with tensile cracking in mid-span and is ductile with tensile rebars plastic deformation in mid-span and confined crashing of concrete in frame corner.

PARAMETRIC STUDY

As there are many model parameters the influence of their variation was studied for a selected set. The parametric study was performed for study case B1, where there are two different experimental results obtained independently (Bresler-Scordelis from 1963 and Vecchio-Shim from 2004). The maximum force of 2004 (Toronto) test is 2% lower than in the original experiment, while the displacement/deflection at the peak force is 61% higher. The original test curves for specimen B1 are depicted in Figure 2-15.

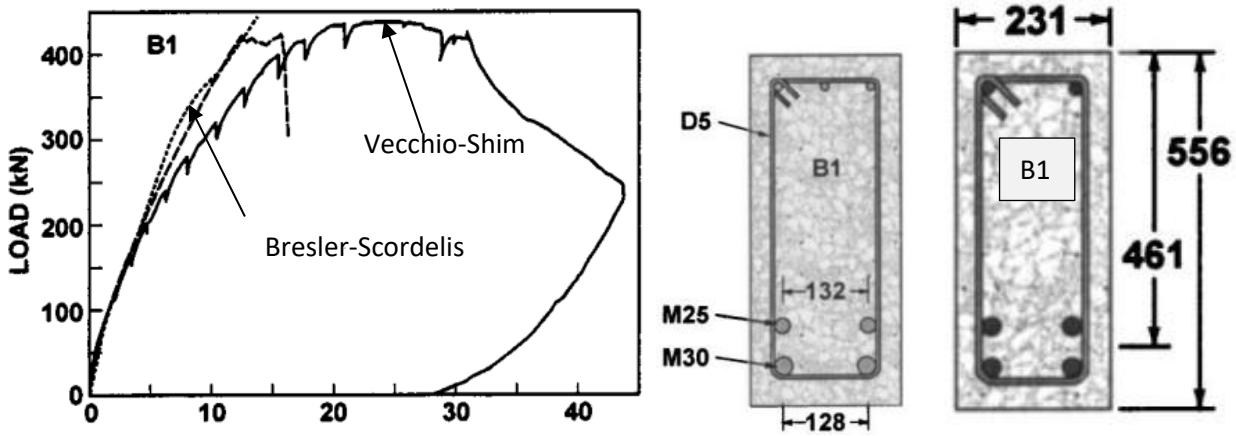

Figure 2-15 Experimental curves from Bresler-Scordelis and Vecchio-Shim beam tests - B1.

The main difference between the beams is the shear reinforcement (D4 for BS and D5 for VS beams) and the curing time (seven days for BS and 4 months for VS). Based on those data, the shear reinforcement (D4, D5), concrete compression stress-strain curve (Saenz, EC2), mesh size (20, 40, 60 mm), and numerical viscous damping (0.001, 0.0001, 0.0001) were varied. Summary of the results with peak force F_{max} and corresponding displacement d, as well as comparison to experimental result (V-S beams) is shown in Table 2-4 below.

Table 2-4 Parametric study for B1 model from Vecchio-Shim

NO	mesh size [mm]	viscous damping [%]	Compression concrete curve	bars	Fmax [kN]	comp. Time [h]	F/Fexp	d/d_exp	CPUs
1	20	0.001	Saez	D4	499	05:05	1.14	2.30	4
2	20	0.001	Saez	D5	501	05:03	1.13	2.18	4
3	20	0.001	EC2	D4	497	08:34	1.13	0.60	8
4	20	0.001	EC2	D5	498	7:57	1.13	0.62	8
5	20	0.0001	Saez	D4	502	16:47	1.14	0.91	8
6	20	0.0001	Saez	D5	492	15:38	1.11	2.21	8
13	40	0.001	Saez	D4	517	00:34	1.18	3.99	8
14	40	0.001	Saez	D5	516	00:29	1.16	4.00	8
15	40	0.001	EC2	D4	481	00:28	1.10	1.05	8
16	40	0.001	EC2	D5	483	00:29	1.10	1.04	8
17	40	0.0001	Saez	D4	504	01:14	1.15	5.11	8
18	40	0.0001	Saez	D5	497	01:29	1.13	2.53	8
19	40	0.0001	EC2	D4	449	01:27	1.02	1.09	4
20	40	0.0001	EC2	D5	464	01:23	1.06	1.24	4
25	60	0.001	Saez	D4	522	00:13	1.19	5.11	8
26	60	0.001	Saez	D5	524	00:08	1.18	3.18	4
27	60	0.001	EC2	D4	494	00:10	1.12	1.11	8
28	60	0.001	EC2	D5	483	00:28	1.10	1.04	8
29	60	0.0001	Saez	D4	484	00:59	1.10	1.73	8
30	60	0.0001	Saez	D5	500	00:20	1.12	3.00	4
31	60	0.0001	EC2	D4	403	00:20	0.92	1.08	8
32	60	0.0001	EC2	D5	414	00:28	0.94	1.08	8
33	60	0.00001	Saez	D4	488	00:53	1.11	4.01	8
34	60	0.00001	Saez	D5	499	00:25	1.14	5.11	8
35	60	0.00001	EC2	D4	418	00:45	0.95	1.34	4
36	60	0.00001	EC2	D5	410	00:41	0.93	1.21	4
37	80	0.00001	Saez	D4	430	00:55	0.98	0.93	8
38	80	0.00001	Saez	D5	446	00:48	1.02	0.98	8
39	80	0.00001	EC2	D4	395	00:37	0.90	0.91	8
40	80	0.00001	EC2	D5	412	00:26	0.94	0.91	8

Peak force and displacement at peak force were divided by the experimental results from Vecchio-Shim curve to present model prediction accuracy ratio. The parametric study shows combined influence of several parameters on the result accuracy and respective computational effort required. The combined effect of mesh size and numerical viscous stabilization on accuracy of prediction is observed. For example, model with 40 mm mesh size and 0.01% damping is only slightly more accurate than model with 60 mm mesh size and 0.001% damping. However, the computational time is doubled for model with 40 mm size mesh. Examples of the load-displacement curves for the selected sets of input parameters are shown in Figure 2-16.

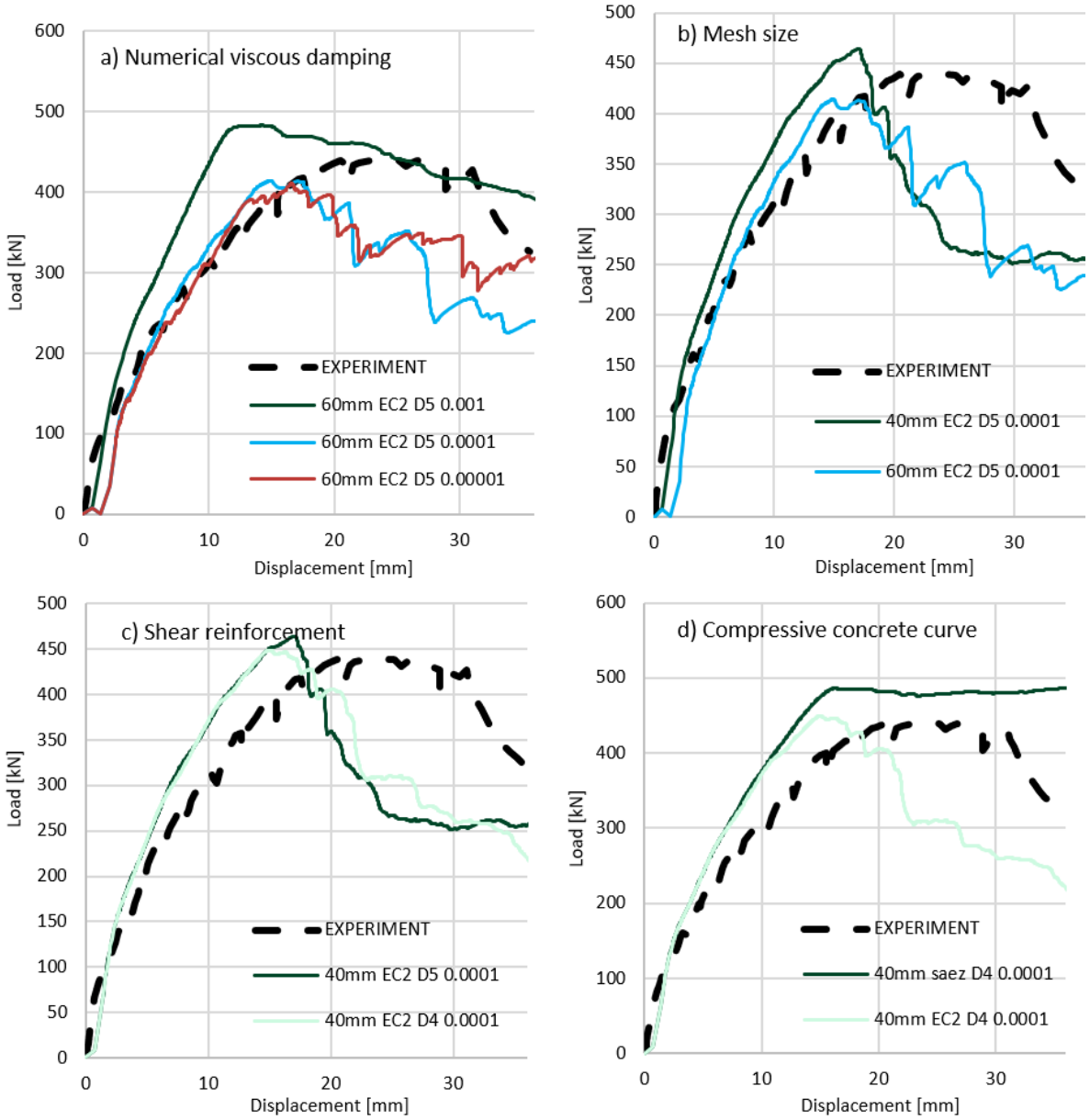

Figure 2-16 Influence of different parameters on CDP model results for benchmark B1.

Crack patterns obtained from numerical analysis can be shown using tensile damage field output that depicts level of damage [0-1] for each element. Examples of crack patterns for studied benchmarks is shown in Figure 2-17.

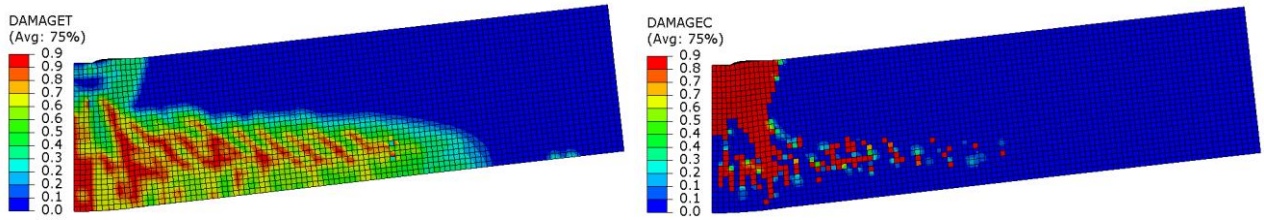

Figure 2-17 Crack pattern (left) and compression damage (right) at 70 mm displacement for B1 case study.

3 Modelling deterioration of concrete affected by ASR

3.1 Introduction

Alkali-silica reaction (ASR) in concrete is a multi-scale phenomenon: it is a chemical reaction that causes material changes, resulting in structural consequences.

On the concrete material scale, the most prominent effects of alkali-silica reaction are expansion and degradation as reduction in tensile strength and modulus of elasticity [15], [16], [17], [18], [19] and [20]. ASR induced expansion depends on the stress, where compressive stress reduces the expansion in the load direction. Consequently, an anisotropic stress state leads to anisotropic expansion. Because the expansion is related to the extent and orientation of micro cracks, an anisotropic expansion corresponds with an anisotropic degradation of the material [19]. Both the stiffness (measured modulus of elasticity) and the tensile strength are reduced with increasing expansion.

To capture the structural consequences of ASR by advanced structural analysis (NLFEA), the effects of ASR must be included in the material model of the concrete.

The multi-scale nature of ASR is reflected in the huge diversity of existing material models, ranging from the chemical to the concrete scale. An overview of existing models is given in the review paper of Esposito and Hendriks [21], where the models were classified based on their starting scale of modelling, and the models were assessed to what extent they can be extended to structural analysis. For structural analysis of large-scale reinforced concrete structures, a material model on the concrete scale must be sought. This means that the constituents at the subscale of concrete are not explicitly modelled, and the subscale physics is included in a smeared or averaged fashion. This modelling approach is presented in the following. Voigt notation is used for stress $\boldsymbol{\sigma}$ and strain $\boldsymbol{\varepsilon}$, where bold-faced letters are vectors.

3.2 Modelling ASR-induced expansion

The most common way to incorporate ASR-induced expansions in structural analysis is to consider the expansion as an imposed deformation/strain [22] [23] [24] [25] [26] [27] [28] [29]. In this way, the total strain of the concrete is decomposed into a mechanical strain $\boldsymbol{\varepsilon}^{\mathrm{m}}$, and an imposed strain $\boldsymbol{\varepsilon}^{\mathrm{i}}$:

$$\boldsymbol{\varepsilon} = \boldsymbol{\varepsilon}^{\mathrm{m}} + \boldsymbol{\varepsilon}^{\mathrm{i}} \tag{5}$$

The mechanical strain $\boldsymbol{\varepsilon}^{\mathrm{m}}$ is caused by stress, and it can be further decomposed to account for cracking or creep. On the other hand, the imposed strain is not caused by stress but by other physical quantities; the most familiar for concrete are thermal dilation/contraction (temperature dependent), and autogenous and drying shrinkage (moisture dependent). Introducing the effect of ASR as an imposed deformation, the total imposed strain is decomposed in three parts: thermal strain $\boldsymbol{\varepsilon}^{\mathrm{th}}$, shrinkage strain $\boldsymbol{\varepsilon}^{\mathrm{sh}}$, and ASR strain $\boldsymbol{\varepsilon}^{\mathrm{asr}}$;

$$\boldsymbol{\varepsilon}^{\boldsymbol{i}} = \boldsymbol{\varepsilon}^{\mathrm{th}} + \boldsymbol{\varepsilon}^{\mathrm{sh}} + \boldsymbol{\varepsilon}^{\mathrm{asr}} \tag{6}$$

All concrete expansion-based models are based on the concept of free ASR expansion $\varepsilon^{\mathrm{asr,free}}$ [23], i.e., the ASR-induced expansion that would have occurred for the same concrete under the same environmental conditions but without stress. It is a scalar measure and corresponds with the uniaxially measured strain in stress-free conditions. In some material models, the free expansion is formulated as a volumetric strain [26] $\varepsilon_{\mathrm{v}}^{\mathrm{asr,free}} = 3\,\varepsilon^{\mathrm{asr,free}}$. The free ASR expansion is considered as a predefined strain field $\varepsilon^{\mathrm{asr,free}}(\boldsymbol{x}, t)$ for the structural analysis, and it is further discussed in Section 3.3. First, the modelling

of the stress-dependency of the ASR expansion is discussed, i.e., the relationship between the free $\varepsilon^{\mathrm{asr,free}}$ and the imposed expansion $\boldsymbol{\varepsilon}^{\mathrm{asr}}$.

The simplest model assumes the imposed ASR expansion equal to the free ASR expansion in all directions, i.e., both stress independent and isotropic. This is considered as a thermal equivalent approach. In three dimensions, with six independent strain components, it reads (Voigt notation)

$$\boldsymbol{\varepsilon}^{\mathrm{asr}} = [1\ 1\ 1\ 0\ 0\ 0]^{\mathrm{T}}\ \varepsilon^{\mathrm{asr,free}} \tag{7}$$

This is a crude simplification. Indeed, ASR expansion is highly stress dependent; the expansion is reduced with compressive stress. In more advanced formulations, the imposed expansion is stated on a rate form and is a function of the current stress state, given by

$$\dot{\boldsymbol{\varepsilon}}^{\mathrm{asr}} = \boldsymbol{W}(\boldsymbol{\sigma})\ \dot{\varepsilon}^{\mathrm{asr,free}} \tag{8}$$

where the over-dot means differentiation with respect to time and $\boldsymbol{W}$ is a vector-valued function of stress ($\boldsymbol{\sigma}$) that accounts for reduction in the imposed ASR expansion in the compressed directions. Four different expansion behaviors have been experimentally observed:

1. total transfer of expansion to the stress-free directions, i.e., volumetric expansion is preserved [30] [31] [32];
2. partial transfer [33] [34] [35];
3. no or negligible transfer to the stress-free directions [36] [37];
4. the expansions in the stress-free directions are reduced [38] [39].

As a result, many formulations of the function $\boldsymbol{W}$ exist in literature.

A one-dimensional version of W (scalar valued function) is shown in Figure 3-1. W expresses the fraction of the imposed to the free ASR expansion rate for uniaxially loaded concrete. The logarithmic function shown in the figure was proposed by Charlwood et al. [40] and is widely used in material modelling. It ranges from 1, no reduction in expansion, for stresses greater than $-\sigma_{\mathrm{L}}$, and to 0, no expansion, for stress less than $-\sigma_{\mathrm{u}}$. A linear or quadratic polynomial, or an exponential function for W in range between σ_{u} and σ_{L} have been proposed by other researchers [24].

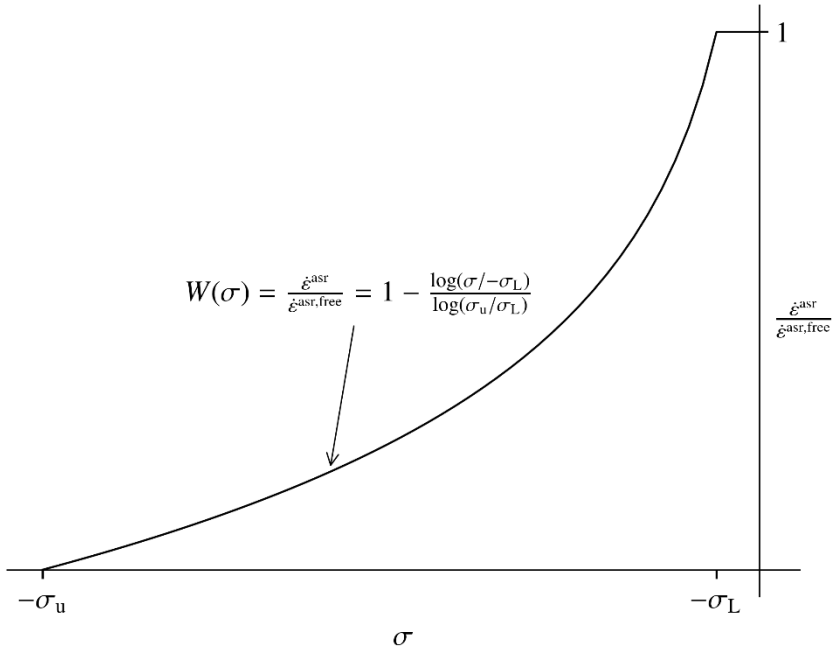

Figure 3-1: Stress-expansion relationship proposed by [40]. $W(\sigma)$ is the imposed expansion relative to the free expansion.

The material constants σ_{L} and σ_{u} depend on the concrete mix and should be determined from uniaxially restrained expansion experiments, see e.g. [36], [33] and [24]. Measured expansions under multiple sustained compressive stress levels are recommended to achieve a model for W. The experimental investigation of [33] found that the expansion under sustained compressive stress of 0.17 MPa was equal to the free expansion irrespective of concrete mix. The compressive stress σ_{u} necessary to stop the expansion ranges from 3 MPa to 10 MPa [41].

An extension of the one-dimensional model to three dimensions can be obtained by considering the expansion in the three principal stress directions independently [40], given by

$$\dot{\varepsilon}_i^{\mathrm{asr}} = W(\sigma_i)\, \dot{\varepsilon}^{\mathrm{asr,free}} \quad ; i = 1,2,3 \tag{9}$$

This model suits the third expansion behavior mentioned above, i.e., when no or negligible expansion transfer occurs. When there is a stronger expansion coupling between the directions, the model by Saouma and Perotti is recommended [26].

3.3 Modelling free ASR expansion versus estimation from field investigations

The free ASR expansion creates the link between the reaction kinetics and the mechanics. Its evolution in time depends on the environmental conditions, where high temperature accelerates the development and high humidity increases its potential. Fortunately, the coupling is unidirectional, i.e., the temperature and moisture affect the free ASR expansion, and hence, the mechanics, but the mechanics does not affect the free ASR expansion. In the most sophisticated material models, the free ASR expansion relies on many

fields such as temperature, moisture, and alkali content [25] [26] [42]. In these advanced formulations, those fields are computed in the time domain for given boundary and initial conditions.

As discussed by [29], a common challenge for the application of material models is the determination of the input fields to the structural analysis. If, for instance, the material model relies on the input of moisture and temperature, these fields—in space and time—must be determined before the structural analysis. This requires solving the corresponding transient problem, and hence, the initial and boundary conditions must be known for the structure's history. These are hardly available for an existing structure. Besides, these models are complex and difficult to implement.

Alternatively, the structural analysis method developed by [29] can be used. In this approach, the free ASR expansion is linear in time, and the spatial variation is a linear combination of assumed shape functions:

$$\varepsilon^{\mathrm{asr,free}}(\boldsymbol{x}, t) = \frac{t}{t_{\mathrm{end}}} \sum_{j=1}^{n} \beta_j \psi_j(\boldsymbol{x}) \tag{10}$$

where t is the time, t_{end} is the age of the structure, β_j are coefficients, and $\psi_j(\boldsymbol{x}) \in [0,1]$ are the shape functions. The shape functions and the corresponding coefficients should be determined based on field investigations as elaborated in Section 6.1. The coefficients β_j can be updated/calibrated by an inverse analysis, where the objective is to determine the set of coefficients that minimize the difference between a calculated and observed quantity, e.g. displacement or crack width. The calibration procedure requires that the number of coefficients (n) is less than or equal to the number of observations.

3.4 Modelling material degradation

ASR leads to a reduction in stiffness and strength. Figure 3-2 shows the reduction in modulus of elasticity and tensile strength with respect to ASR expansion [29]; the results are adapted from the experimental works of [17] and [19]. In the same figure, a model function for the reduction in modulus of elasticity is approximated to the experimental results. This one-dimensional model was first proposed by Wen [24], and later Kongshaug et al. [29] generalized the model to three dimensions. The same one-dimensional model can be used for the reduction in tensile strength, see Figure 3-2.

Compressive strength is much less sensitive to ASR damage compared to modulus of elasticity and tensile strength, and some studies report almost no reduction in compressive strength even at significant expansion levels, see e.g. [43] for an overview. In the experimental investigation by [19], the greatest reduction in compressive strength was approximately 10 % at an expansion of 0.37 %.
ASR also influences the bond strength of concrete, see the review paper by [44]. The recommendation in Model Code 2020 [45] is to use linear reduction in anchorage capacity with increasing volumetric ASR-expansion, ranging from 0% reduction at 0% volumetric expansion to 40% reduction at 1.5% volumetric expansion.

It should be noted that the evolution of mechanical properties with respect to expansion depends on the concrete mix and therefore should be determined from experimental investigation. Nevertheless, a lower bound of the residual mechanical properties with respect to expansion can be based on Table 3-1 [46].

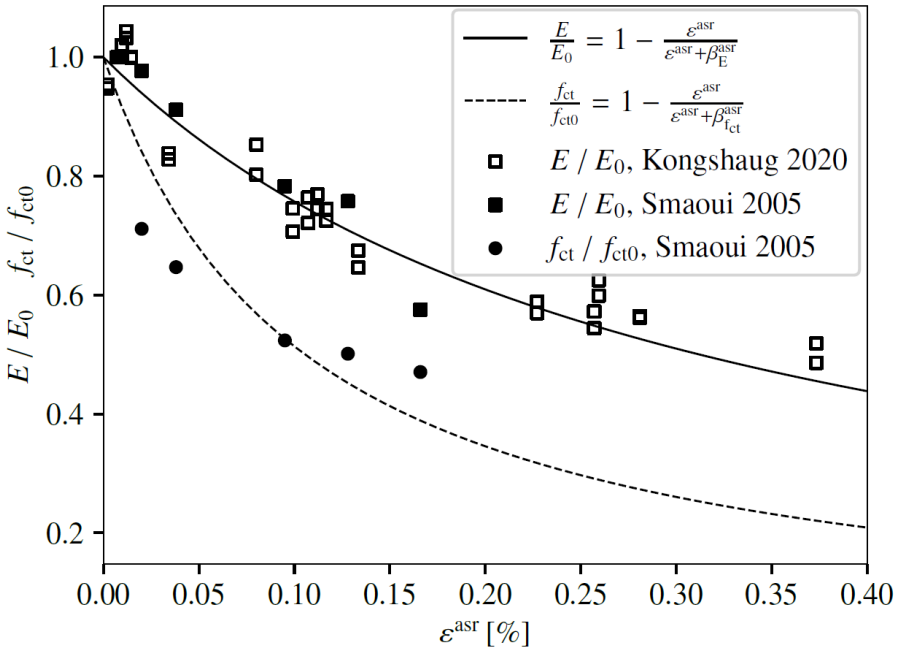

Figure 3-2: Evolution of modulus of elasticity and direct tensile strength relative to undamaged stiffness/strength [29]; $\boldsymbol{\beta_E^{asr} = 0.003}$ and $\boldsymbol{\beta_{f_{ct}}^{asr} = 0.001}$.

Table 3-1: Lower bound residual mechanical properties relative to 28-day unaffected concrete [46].

Expansion [%]	0.05	0.1	0.25	0.5	1
Cylindrical compression strength [%]	95	80	60	60	-
Splitting tensile strength [%]	85	75	55	40	-
Modulus of elasticity [%]	100	70	50	35	30

3.5 Important aspects regarding modelling and assessment of reinforced concrete structures affected by ASR

It is only the concrete that expands due to ASR. Consequently, tensile stresses develop in the reinforcement, and compressive stresses in the concrete, which is often referred to as the pre-stressing effect. To capture this effect, rebars must be part of the structural analysis model. However, an engineering approach that accounts for the reinforcement on the expansion but where the reinforcement is not part of the structural analysis is suggested in ref. [47] and [48]. It should be noted that this method is akin to a drying shrinkage consideration (with opposite sign), where the stress-dependency of the ASR expansion is not part of the analysis but must be considered in advance. Experimental evidence shows that the stress-dependency of the ASR-expansion is strong and non-linear. To capture the stress state due to the ASR expansion, reinforcement should be part of the structural analysis model, and a stress dependent expansion model for the concrete must be used, as described in Section 3.2.

Additional stresses arise when ASR-induced expansion causes displacements that are restricted by boundary conditions, such as in continuous beam bridges [28]. The magnitude of these stresses depends

strongly on the structural stiffness—greater stiffness generally results in larger stresses. To predict the ASR-induced stresses accurately, the structural model must represent the actual stiffness of the system. Cracking and creep will affect structural stiffness, and if these phenomena are present, they should be accounted for in the concrete material model. In addition, the influence of reinforcement on structural stiffness must be accounted for.

The key question is whether ASR reduces the safety of RC structures, expressed by the assessment condition (see Eq. (50) in Section 5.1): $F_d \leq R_d$, where F_d is the action or load, and R_d is the structural capacity. ASR affects the structural resistance (R_d) in two ways:

1. As mentioned in the previous paragraphs, the concrete expansion causes a change of stress state.
2. The material deterioration affects the material strength.

When R_d represents the global structural resistance, determined through NLFEA (Section 5.7), the modelling of ASR-affected concrete should account for the progression of ASR-induced expansion whenever such expansion leads to a reduction in structural capacity. Conversely, when the effect of expansion is beneficial, for example due to the pre-stressing effect, a conservative approach is to consider only the reduction in material strength due to ASR when evaluating the structural resistance.

According to Model Code 2020 [45], NLFEA may be employed to determine load effects for capacity checks of critical sections, particularly where the magnitude of these effects is influenced by concrete cracking or reinforcement yielding—for example, in cases involving deformation actions. In this context, the expansion effect of ASR can be treated as an additional cross-sectional load contribution (F_d), which should then be compared against the corresponding resistance (R_d) while accounting for material deterioration caused by ASR.
It should be noted that even a small ASR-induced expansion can lead to considerable reduction in tensile strength, as discussed in [20]. This reduction may in turn influence the shear capacity. The same investigation reported that reference beams exhibiting only minor ASR expansion—insufficient to benefit from the pre-stressing effect—showed shear capacities below the calculated values from EC2 [49] using $C_{Rd,c} = 0.18$, as well as from the draft of the new EC2 [50] when material safety factors were omitted and the mean concrete compressive strength was used. Consequently, it was proposed that the characteristic reference shear strength for ASR-affected beams should correspond to the basic term in the EC2 [49] expression, but with a reduced coefficient $C_{Rd,c} = 0.18 \cdot 0.75 = 0.135$.

3.6 Traditional (engineering) method for analysing ASR-affected structures

The engineering practice for the prediction of load effects in RC structures is to conduct linear structural analyses, i.e. based on small displacement kinematics and linear elasticity. In addition, the reinforcement is usually excluded from the structural analysis model. Furthermore, ASR expansion is included by a thermal equivalent one. Consequently, the stress dependency of expansion, and the effect of differential expansion between concrete and reinforcement (internal restraint) cannot be captured from the analysis but must be considered in advance. Such a modelling approach is described in ref. [47].

4 Modelling deterioration of steel reinforcement affected by corrosion

4.1 Modelling approach

Reinforcement corrosion causes reduction of the cross-sectional area in rebars and deterioration of bond over time. This will consequently affect the load bearing capacity of structures subjected to corrosion. This can be modelled in an analysis by

1. Explicitly reducing the cross-sectional area of the reinforcement affected by corrosion, in addition to adjusting the stress strain curve to account for material degradation caused by governing corrosion mechanisms.
2. Accounting for both cross-sectional loss and material degradation by modifying the stress strain curve accordingly.

It is recommended to use the second approach in NLFEA to account for the nonlinearity caused by mechanical and material degradation over time due to corrosion. The focus in this report will thus be the second approach. First, the background for the mechanical behaviour of corroded rebars is derived. Then it is argued why the mechanical behaviour needs to be adjusted empirically due to material degradation. Finally, recommended stress strain curves accounting for reinforcement corrosion that can be applied in NLFEA are presented.

Bond-failures caused by reinforcement corrosion will not be considered in this report, in conjunction with not introducing bond-slip models as mentioned in subchapter 2.2. Furthermore, prestressing steel will not be considered in this report.

4.2 Mechanical behaviour and background

4.2.1 Corrosion of naked rebars

The deterioration caused by corrosion is replicated according to [51], and is derived in a mechanical sound manner by considering a naked rebar with a certain length l having an uncorroded part with length l_{uc} and a corroded part with length l_{c}, see Figure 4-1.

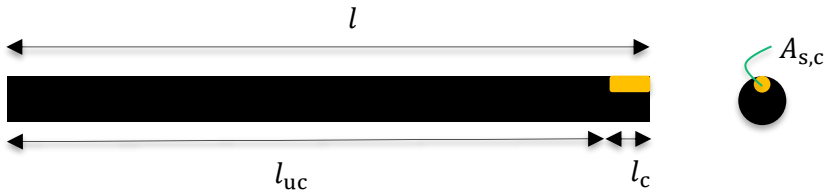

Figure 4-1: Corroded rebar.

The cross-sectional area of the rebar A_{s} is thus reduced over the length l_{c} as

$$A_{\mathrm{s,c}} = (1-\zeta)A_{\mathrm{s}} \tag{11}$$

Where

$$\zeta = \frac{A_{\mathrm{s,lost}}}{A_{\mathrm{s}}} < 1 \tag{12}$$

By equilibrium,

$$F = A_{\mathrm{s}}\sigma_{\mathrm{s,uc}} = A_{\mathrm{s,c}}\sigma_{\mathrm{s,c}} = (1-\zeta)A_{\mathrm{s}}\sigma_{\mathrm{s,c}} \tag{13}$$

By inserting for Eq. (11) in (13) the relation between the stresses for the corroded and uncorroded part becomes

$$\sigma_{\mathrm{s,c}} = \frac{\sigma_{\mathrm{s,uc}}}{(1-\zeta)} \tag{14}$$

The rebar force at yielding is thus limited by

$$F_{\mathrm{y}} = A_{\mathrm{s},c} f_{\mathrm{sy}} = (1-\zeta) A_{\mathrm{s}} f_{\mathrm{sy}} = A_{\mathrm{s}} \sigma_{\mathrm{sy,uc}} \tag{15}$$

And at failure by

$$F_{\mathrm{u}} = A_{\mathrm{s},c} f_{\mathrm{su}} = (1-\zeta) A_{\mathrm{s}} f_{\mathrm{su}} = A_{\mathrm{s}} \sigma_{\mathrm{su,uc}} \tag{16}$$

At which the steel stresses at yielding of the rebar for the uncorroded part are limited to

$$\sigma_{\mathrm{sy,uc}} = (1-\zeta) f_{\mathrm{sy}} \tag{17}$$

And at ultimate to

$$\sigma_{\mathrm{su,uc}} = (1-\zeta) f_{\mathrm{su}} \tag{18}$$

Consequently, the total elongation of the rebar at ultimate is reduced since

$$\varepsilon_{\mathrm{su,uc}} = \varepsilon_{\mathrm{s}}\left(\sigma_{\mathrm{su,uc}}\right) < \varepsilon_{\mathrm{s}}(f_{\mathrm{su}}) \tag{19}$$

The critical cross-section loss ζ_{crit} can be found by exerting the following equilibrium of the uncorroded and corroded part

$$A_{\mathrm{s}} f_{\mathrm{sy}} = (1-\zeta_{\mathrm{crit}}) A_{\mathrm{s}} f_{\mathrm{su}} \tag{20}$$

$$\zeta_{\mathrm{crit}} = 1 - \frac{f_{\mathrm{sy}}}{f_{\mathrm{su}}}$$

Cross-sectional losses larger than ζ_{crit} implies that the uncorroded part remains elastic when the corroded part ruptures. This means that plastic strains localise in the corroded part and that the total elongation at ultimate, or more rigorously speaking the deformation capacity, is drastically reduced. The material models for uncorroded and corroded rebars have been visualized generically in Figure 4-2.

The total elongation of the rebar can be decomposed to

$$u_{\mathrm{tot}} = \frac{F}{A_{\mathrm{s},c} E_{\mathrm{s}}} l_{\mathrm{c}} + \frac{F}{A_{\mathrm{s}} E_{\mathrm{s}}} l_{\mathrm{uc}} = \varepsilon_{\mathrm{s},c} l_{\mathrm{c}} + \varepsilon_{\mathrm{s,uc}} l_{\mathrm{uc}} \tag{21}$$

By defining the following lengths as

$$l_{\mathrm{c}} = \beta l \tag{22}$$

$$l_{\mathrm{uc}} = (1-\beta) l \tag{23}$$

the deformation compatibility of the corroded rebar becomes

$$\varepsilon_{\mathrm{sm}} = \beta \frac{\varepsilon_{\mathrm{s,uc}}}{(1-\zeta)} + (1-\beta)\varepsilon_{\mathrm{s,uc}} \tag{24}$$

This suggests that an uncorroded rebar in general yields a stiffer response than a corroded rebar. The strain at yielding for a corroded rebar can thus be derived from

$$\varepsilon_{\mathrm{sm,y}} = \frac{1}{E_{\mathrm{s,uc}}}\left[\beta f_{\mathrm{sy}} + (1-\beta)(1-\zeta) f_{\mathrm{sy}}\right] \tag{25}$$

Where the corroded Young's modulus becomes

$$E_{\mathrm{s,c}} = \frac{(1-\zeta) f_{\mathrm{sy}}}{\varepsilon_{\mathrm{sm,y}}} \tag{26}$$

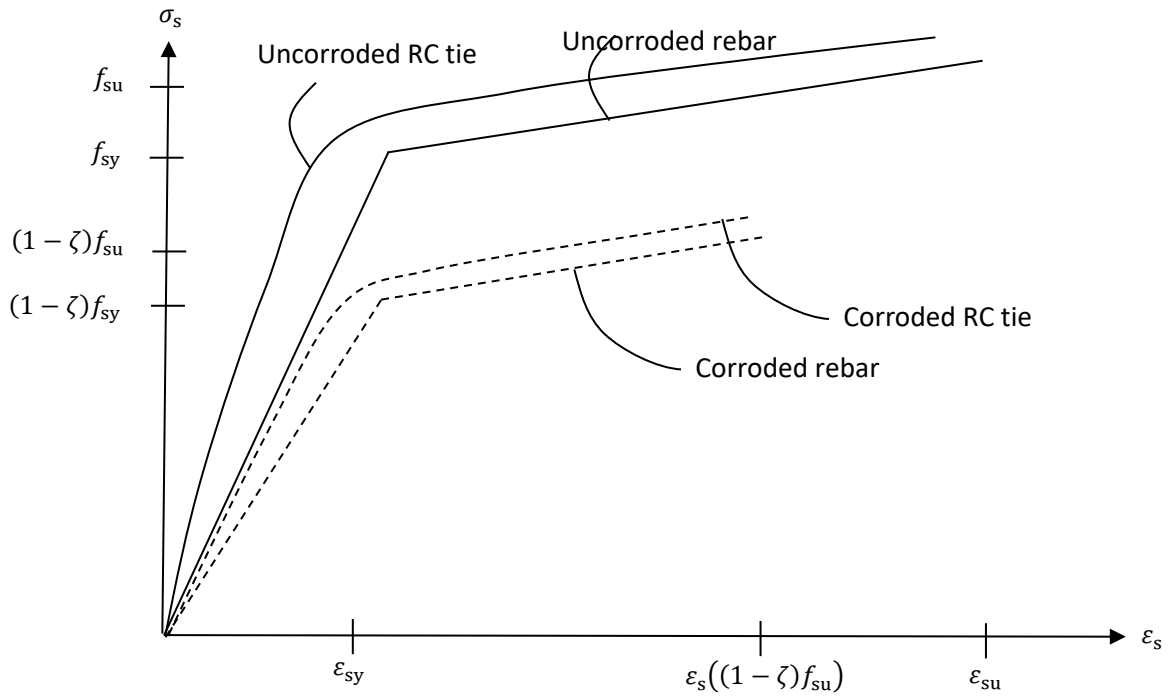

Figure 4-2: Generalized material models for uncorroded and corroded rebars

4.2.2 Experimental behaviour

The mechanical behaviour of corroded rebars has been idealized in the derivations above. However, this idealized behaviour does not necessarily reflect the behaviour observed in experiments of corroded rebars. Haefliger [51] points out that this is caused by the following mechanisms

1. Generally higher stresses in the corroded cross-section compared to the corroded part due to equilibrium of forces
2. Varying strain rate caused by difference in stiffnesses of the corroded and non-corroded parts
3. Distinct microstructure over the cross-section depending on the steel quality
4. Three dimensional stress state
5. Local bending moment in pitting corroded rebars

There have been suggested different approaches to account for these mechanisms. The authors in [52, 53] proposed empirical adjustments for ζ as a function of the yield stress, ultimate stress and strain, degree of corrosion, and whether it is uniform or pitting corrosion governing the deterioration of the rebar. The approach was later adopted by [54] to predict the behaviour of deteriorated RC structures subjected to pitting corrosion applying NLFEA. Another approach that is recommended is the approach suggested in chapter **4.3**.

4.3 Properties of embedded reinforcement affected by corrosion

4.3.1 Flowchart

Figure 4-3 and Figure 4-5 show, respectively, a simplified and a more detailed flowchart illustrating the relationship between corrosion depth (P_X) at the relevant age of the structure (current or future), and the corresponding reinforcement properties used as input in structural analyses.

The figures illustrate a method (flowchart) for determining the properties of embedded reinforcement used as input in structural analysis, including the effects of varying levels of corrosion, such as:

- ✓ Reduction in cross-sectional area (weight loss)
- ✓ Reduction in mechanical properties (stress-strain relationship)
- ✓ Reduction in bond properties
- ✓ Reduction in fatigue properties

When performing non-linear finite element analysis (NLFEA) of reinforced concrete structures subjected to degradation due to reinforcement corrosion, it is essential to consider the effects of such deterioration on structural behaviour. This is complicated by several factors, including the actual corrosion condition (see Section 4.3.2), and the approach used to represent the identified or assumed condition for the reinforcement within the analysis model. For existing structures affected by reinforcement corrosion, certain assumptions and simplifications—preferably on the conservative side—are typically required in order to achieve a practical and reliable representation of the mechanical and bond properties of corroded reinforcement, in accordance with the principles in [49]. A methodological framework for the calculation of corrosion levels (ζ), the application of reduction factors (k_{red}), and the formulation of stress–strain relationships (σ-ε diagrams) for corroded reinforcement is presented in Sections 4.3.3 to 4.3.5.

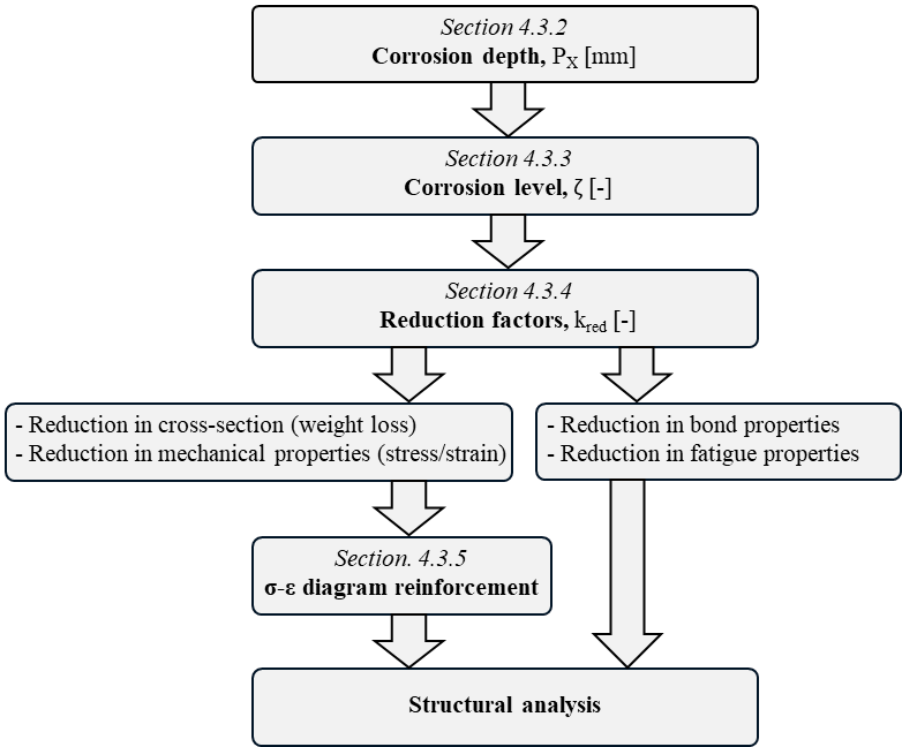

Figure 4-3: Flowchart – Simplified

4.3.2 Corrosion depth, P_X

In each case, the corrosion depth (P_X) — including both the current condition at time t_1 and the future condition at time t_2 – must be assessed based on the corrosion rate up to the present, as well as the estimated or calculated future corrosion rate. Table 4-1 presents typical corrosion rates that may be used in the evaluation of reinforcement corrosion.

For a structure, the corrosion depth (P_X) must be assessed for relevant areas and reinforcement bars with respect to both the current and the expected future condition, i.e.:

- $P_X(t_1)$ = Corrosion depth for the current condition at time t_1
- $P_X(t_2)$ = Corrosion depth for the future condition at time t_2

See example in Figure 4-4. The future condition of a structure at time t_2 exposed to reinforcement corrosion refers to the anticipated state of the structure at a specified time, e.g. for the current condition at t_1, considering ongoing corrosion processes and their projected impact on the reinforcement properties. It is therefore of critical importance that both the corrosion depth (P_X) and its distribution within a reinforced concrete structure are determined with sufficient accuracy, as corrosion depth (P_X) represents a primary input parameter in defining the properties of the embedded reinforcement to be used in structural analyses.

The determination of corrosion depth (P_X) in relevant parts of the structure can be based on, for example:

- NDT (Non-Destructive Testing)
- Instrumentation
- Measurements (e.g., half-cell potential (HCP), chloride profiles, carbonation depth)
- Destructive removal of concrete cover (visual inspection of the current corrosion depths)
- Nominal concrete cover (C_{nom})

Table 4-1: Annual corrosion rate

P_X/year [mm/year]	Level
< 0,001	Insignificant
0,001 – 0,005	Low
0,005 – 0,01	Medium
> 0,01	High

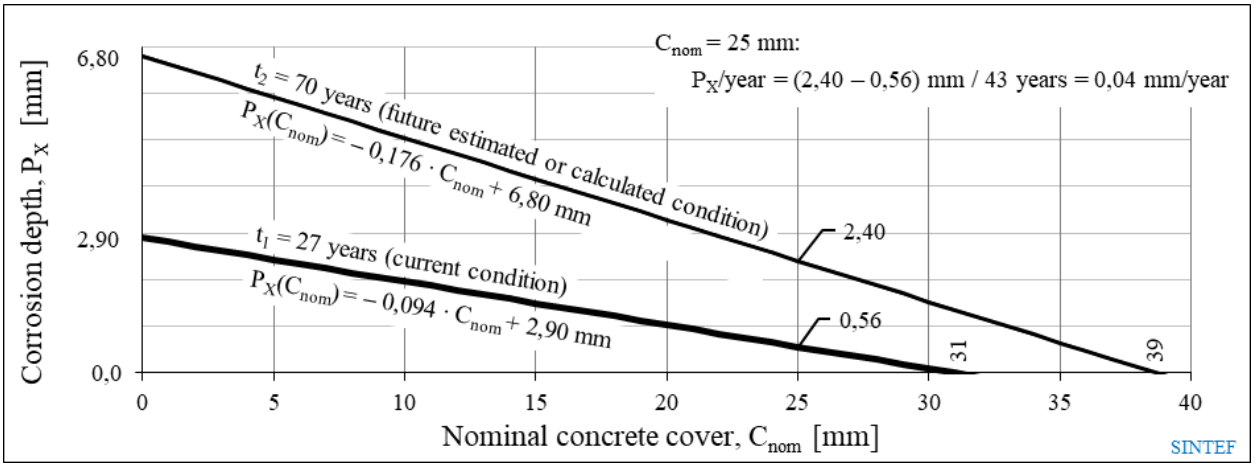

Figure 4-4: Example of corrosion depth (P_X) as a function of nominal concrete cover (C_{nom}) in a reinforced concrete structure exposed to propagating reinforcement corrosion

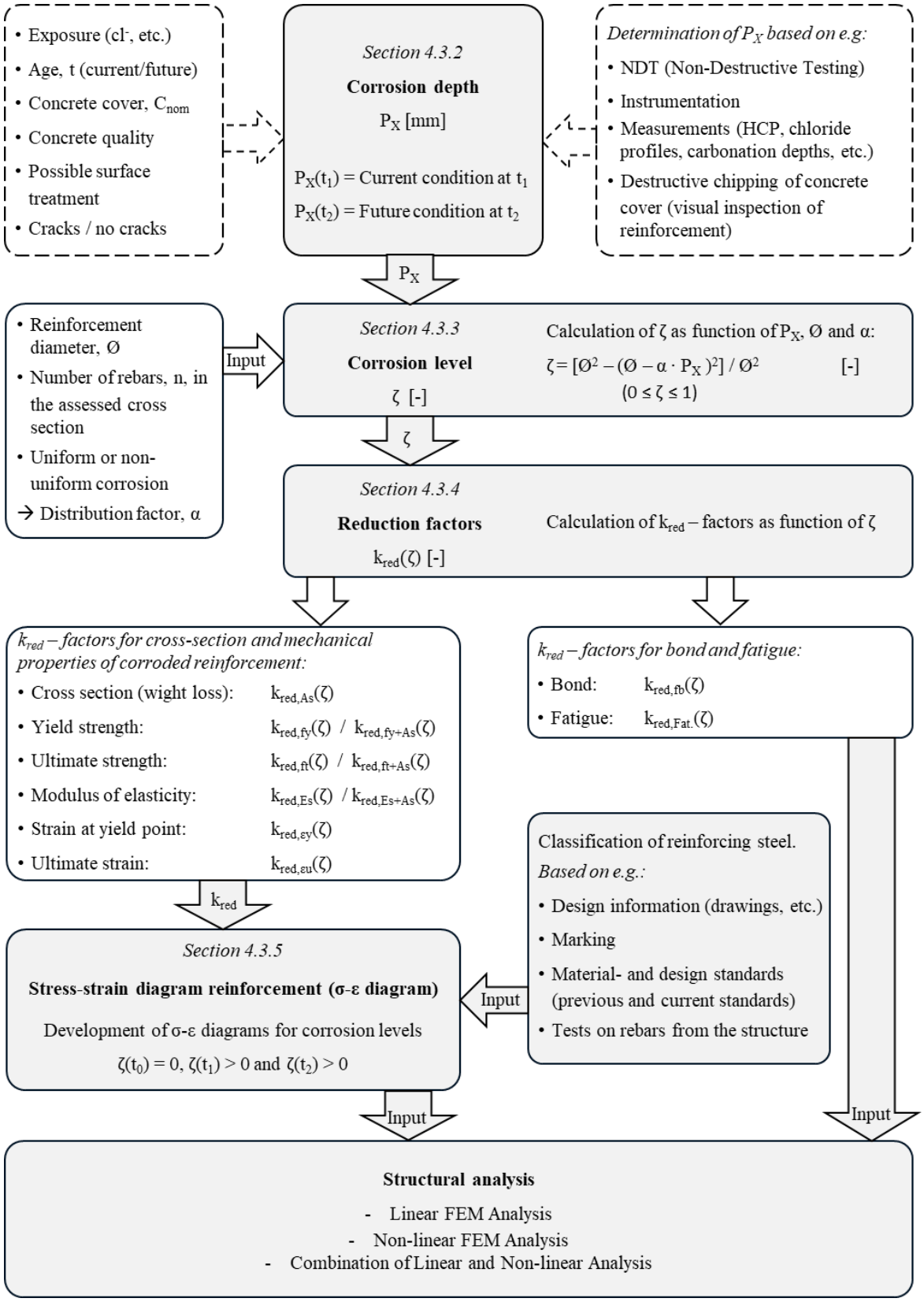

Figure 4-5: Flowchart – Detailed

4.3.3 Corrosion level, ζ

The corrosion level (ζ) represents the cross-sectional loss for the reinforcement within a given structural cross-section. Eq. (27) defines the corrosion level (ζ) as a function of the corrosion depth (P_X) – see Section 4.3.2 – the nominal diameter of the reinforcement ($\emptyset$), and the distribution factor (α).

Corrosion level:

$$\zeta = \frac{A_{S,lost}}{A_S} = \frac{A_S - A_{S,C}}{A_S} = \frac{\emptyset^2 - (\emptyset - \alpha \cdot P_X)^2}{\emptyset^2} \leq 1{,}0 \qquad (27)$$

Where

P_X = Corrosion depth (reduction in the radius of the reinforcing bar), see Section 4.3.2

α = Distribution factor, see Table 4-2

$A_S = \pi/4 \cdot \emptyset^2$ = Nominal cross section of rebar without corrosion

$A_{S,C} = \pi/4 \cdot \emptyset_C^2$ = Effective cross-sectional area of the reinforcement accounting for corrosion

$\emptyset$ = Nominal diameter of reinforcement (uncorroded)

$\emptyset_C = \emptyset - \alpha \cdot P_X$ = Effective diameter of the reinforcement accounting for corrosion

Figure 4-6 shows a model representing different corrosion levels (ζ) according to Eq. (27) in individual reinforcement bars. In the case of uniform corrosion on individual bars (e.g., caused by carbonation), the distribution factor (α) equals 2,0. For asymmetric or pitting corrosion, α for a single bar is generally greater than 2,0.

When multiple reinforcement bars are present within the considered cross-section, it is appropriate to reduce the distribution factor accordingly.

Table 4-2 presents simplified, indicative distribution factors (α) as a function of the number of reinforcement bars (n) in the cross-section and the nominal bar diameter ($\emptyset$), under the assumption of uniform corrosion. When chloride ingress is the primary cause of deterioration, corrosion may initially be localized before gradually developing into a more uniform pattern.

Figure 4-7 shows the corrosion level (ζ) in accordance with Eq. (27), i.e. as a function of the corrosion depth (P_X), reinforcement diameter ($\emptyset$) and the distribution factor (α).

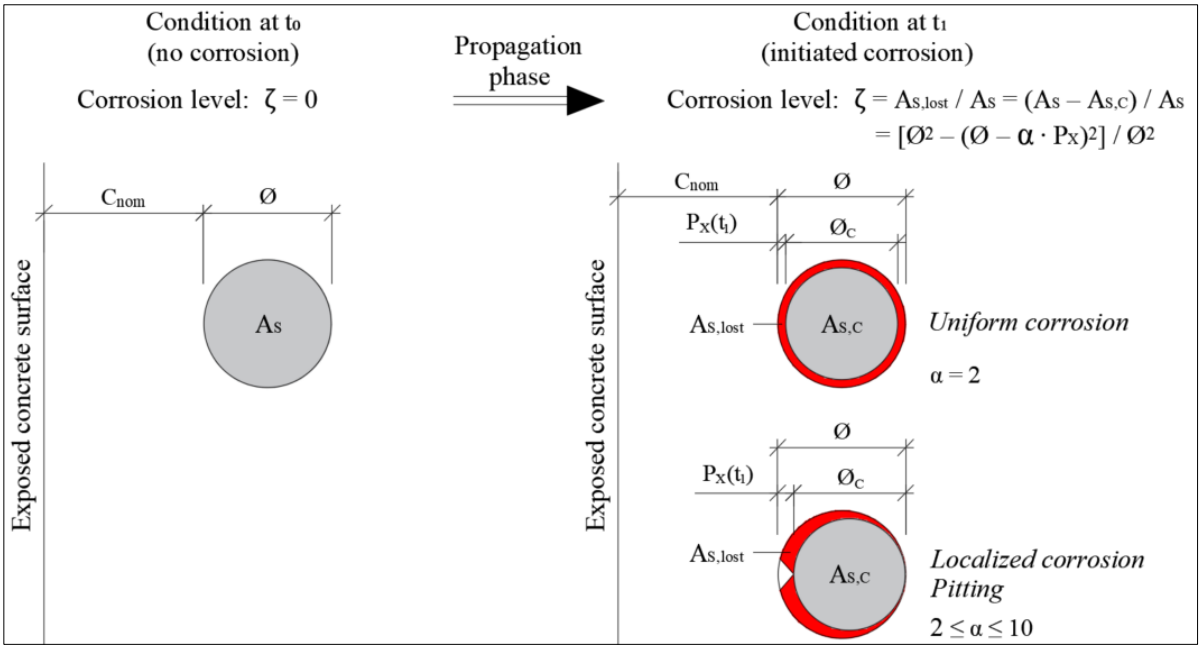

Figure 4-6: Illustration of a model showing varying corrosion levels (ζ) in individual reinforcement bars

Table 4-2: Indicative distribution factors (α) under the assumption of uniform corrosion

Number of reinforcing bars, n [no.]	Nominal rebar diameter, Ø [mm]	Distribution factor, α [-]	Corrosion level, ζ [-]
n ≤ 5	6, 8, 10, 12, 16, 20, 25, 32	2,0	See Figure 4-7 a)
5 < n ≤ 20	6, 8, 10, 12 16, 20, 25, 32	2,0 1,5	See Figure 4-7 b)
20 < n ≤ 50	6, 8, 10, 12 16, 20, 25, 32	1,5 1,0	See Figure 4-7 c)
n > 50	6, 8, 10, 12 16, 20, 25, 32	1,0 0,5	See Figure 4-7 d)

More advanced methods for the assessment and calculation of $A_{s,C}$ under non-uniform reinforcement corrosion can be found in the literature, see for example *Section 5.3.3* in [55].

These methods provide comprehensive approaches to account for spatial variability in corrosion damage, enabling more accurate structural assessments, but are less feasible for application in NLFEA for large real structures.

Note:

The models used to assess reinforcement corrosion are purely deterministic, meaning they only provide the most probable outcome based on the underlying assumptions. Performing probabilistic calculations of the effects of reinforcement corrosion in a structure is considered impractical due to the complexity involved. This complexity arises from uncertainties related to a combination of factors, including:

- the actual corrosion level (ζ)
- the distribution of corrosion among different reinforcement bars
- the actual corrosion rate (P_X/year)
- the actual nominal concrete cover (C_{nom}) and its variation
- the actual impact of corrosion on reinforcement properties for a given level of corrosion (ζ)

As a result, corrosion levels (ζ) are typically expressed as an average within a given area of the structure, based on factors such as nominal (average) concrete cover, exposure conditions, and investigations of the current condition as well as assessments of future corrosion development in the relevant area.

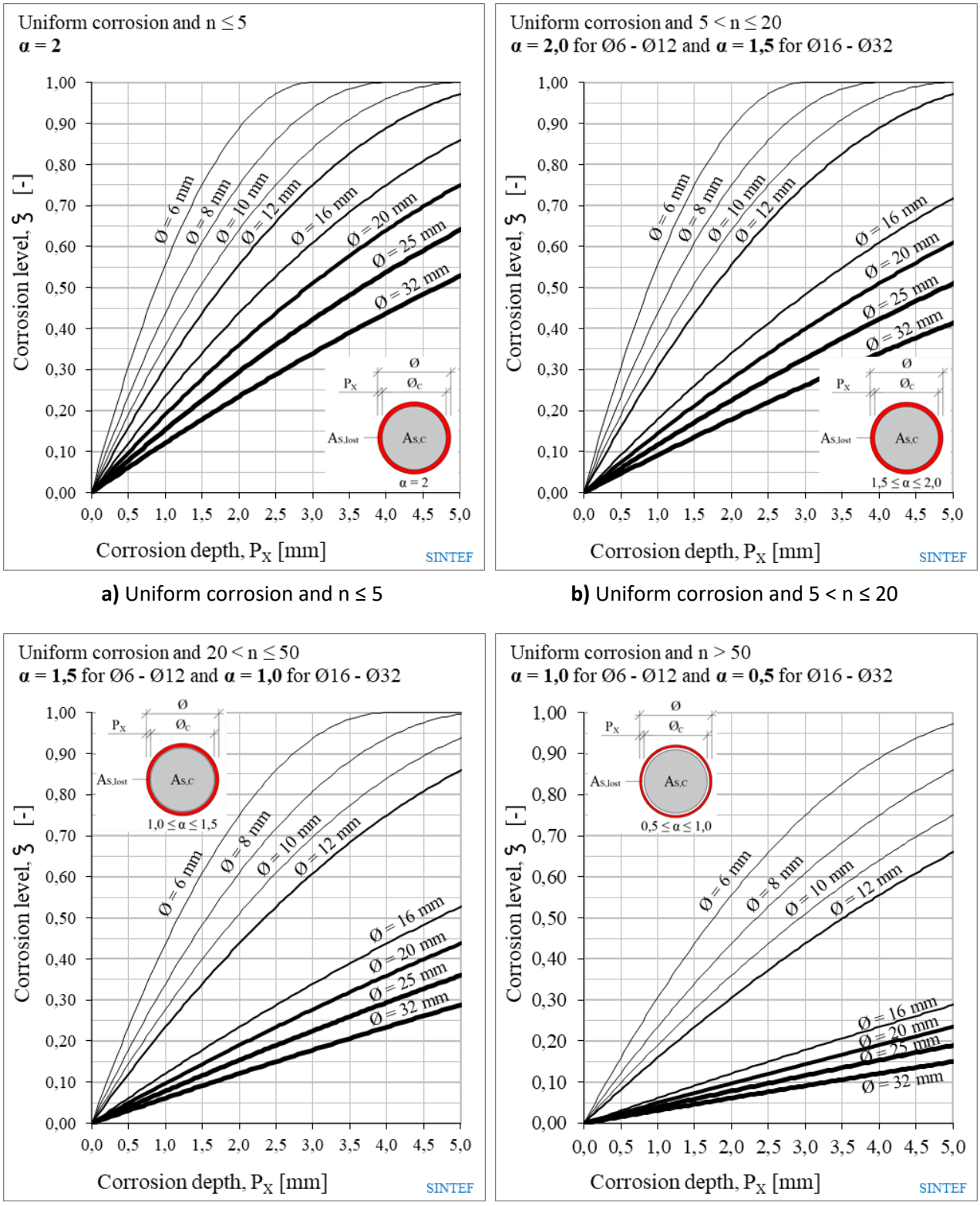

a) Uniform corrosion and n ≤ 5

b) Uniform corrosion and 5 < n ≤ 20

c) Uniform corrosion and 20 < n ≤ 50

d) Uniform corrosion and n > 50

Figure 4-7: Corrosion level (ζ) in accordance with Eq. (27) as function of corrosion penetration depth (P_X), reinforcement diameter (Ø) and the distribution factor (α). Distribution factors according to Table 4-2.

As with corrosion depth (P_x), it is useful to establish an overview of the corrosion levels (ζ) as a function of, for example, the concrete cover (C_{nom}) in relevant areas of a structure. Figure 4-8 shows an example in which the corrosion level is calculated based on the input of the corrosion depth (P_X) from Figure 4-4, using a distribution factor α equal to 2.0. As shown, the threshold for the onset of corrosion (on average) occurs at a nominal concrete cover (C_{nom}) of 31 mm at t_1 = 27 years (current) and 39 mm at t_2 = 70 years (future). This is, of course, consistent with the same threshold values shown in the example for the corrosion depth P_X in Figure 4-4.

For a given structure or structural element where corrosion depths (P_X) have been assessed, it is useful to establish an overview of the corrosion levels (ζ) as a "heat map" on structural drawings, in accordance with Eq. (27) at t_1 (current condition) and t_2 (future condition), based on:

- Nominal concrete cover (C_{nom})
- Exposure conditions
- Reinforcement diameter (Ø)
- Distribution factor (α)

As seen in both the general curves in Figure 4-7 and the example in Figure 4-8, the corrosion level (ζ) increases significantly with decreasing nominal reinforcement diameter (Ø), assuming the same corrosion depth (P_X).

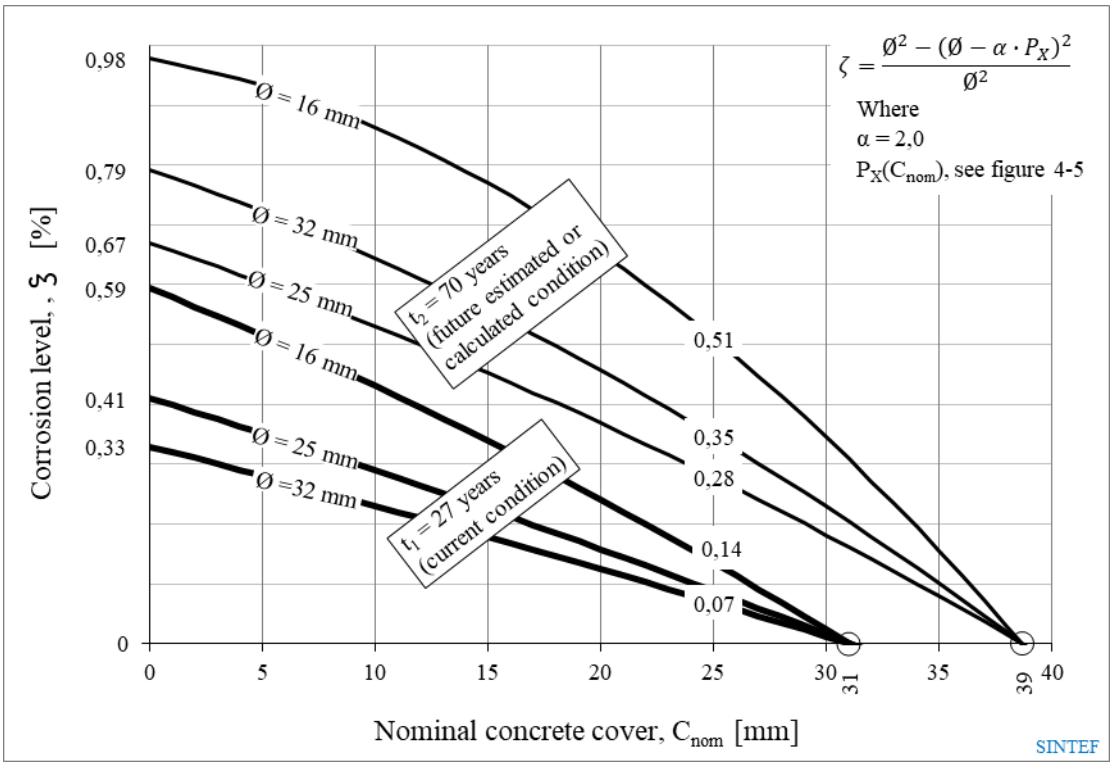

Figure 4-8: Example of corrosion level (ζ) as a function of nominal concrete cover (C_{nom}) in a reinforced concrete structure exposed to propagating reinforcement corrosion in accordance with Eq. (27). The corrosion depth (P_X) as a function of nominal concrete cover (C_{nom}) in accordance with the example in Figure 4-4, reinforcement diameter (Ø = 16 mm, 25 mm and 32 mm) and the distribution factor (α = 2,0) from Table 4-2.

4.3.4 Properties of reinforcing steel subjected to corrosion

4.3.4.1 Reduction factors (k_{red})

The proposed reduction factors (k_{red}) as a function of corrosion level (ζ) are provided in Eqs. (28)–(40) and illustrated in **Figure 4-9**. The literature basis for these reduction factors is summarized in Section **0**. These factors have been derived through curve fitting of various experimental data and should be regarded as indicative values. They are intended as examples of how reinforcement corrosion can be implemented in a general and practical manner within a given project.

Reduction factor accounting for reduced reinforcement area ($A_{S,C}$) due to corrosion:

$$k_{\mathrm{red,As}} = \frac{A_{S,C}}{A_S} = \frac{(Ø - \alpha \cdot P_X)^2}{Ø^2} = 1 - \zeta \tag{28}$$

Reduction factor for yield strength (f_y) accounting for corrosion:

$$k_{\mathrm{red,fy}} = 1 - 1{,}20 \cdot \zeta \tag{29}$$

Reduction factor for tensile strength (f_t) accounting for corrosion:

$$k_{red,ft} = 1 - 1{,}05 \cdot \zeta \tag{30}$$

Reduction factor for elastic modulus (E_S) accounting for corrosion:

$$k_{\mathrm{red,Es}} = 1 - 0{,}70 \cdot \zeta \tag{31}$$

Reduction factor for yield strength (f_y), including reduced reinforcement area ($A_{S,C}$):

$$k_{\mathrm{red,fy+As}} = k_{\mathrm{red,As}} \cdot k_{\mathrm{red,fy}} = 1 - 2{,}20 \cdot \zeta + 1{,}20 \cdot \zeta^2 \tag{32}$$

Reduction factor for tensile strength (f_t), including reduced reinforcement area ($A_{S,C}$):

$$k_{\mathrm{red,ft+As}} = k_{\mathrm{red,As}} \cdot k_{\mathrm{red,ft}} = 1 - 2{,}05 \cdot \zeta + 1{,}05 \cdot \zeta^2 \tag{33}$$

Reduction factor for elastic modulus (E_S), including reduced reinforcement area ($A_{S,C}$):

$$k_{\mathrm{red,Es+As}} = k_{\mathrm{red,As}} \cdot k_{\mathrm{red,Es}} = 1 - 1{,}70 \cdot \zeta + 0{,}70 \cdot \zeta^2 \tag{34}$$

Reduction factor for proportional limit (ε_y) accounting for corrosion:

$$k_{\mathrm{red},\varepsilon\mathrm{y}} = \frac{k_{\mathrm{red,fy}}}{k_{\mathrm{red,Es}}} = \frac{1 - 1{,}20 \cdot \zeta}{1 - 0{,}70 \cdot \zeta} \tag{35}$$

Reduction factor for strain limit (ε_u) accounting for corrosion:

$$k_{red,\varepsilon u} = 1 - (50/35) \cdot \zeta \tag{36}$$

Reduction factor for fatigue accounting for corrosion:

Δσ = 150 MPa: $k_{red,Fat,150} = e^{-7 \cdot \zeta}$ (37)

Δσ = 200 MPa: $k_{red,Fat,200} = e^{-12 \cdot \zeta}$ (38)

Δσ = 300 MPa: $k_{red,Fat,300} = e^{-16 \cdot \zeta}$ (39)

Reduction factor for bond accounting for corrosion [1)]:

$0 < \zeta \leq 0{,}05$: $k_{red,fb} = f_{b,C}/f_b = 0{,}75$ (40)

$\zeta > 0{,}05$: $k_{red,fb} = f_{b,C}/f_b = 0{,}85 - 1{,}875 \cdot \zeta$

[1)] *Methods for modeling the bond of corroded reinforcement under different conditions can be found in e.g. Section 6.1.2 of* [55].

Where

ζ = Corrosion level, see Section 4.3.3

The reduction factors (k_{red}) are applied to the original (uncorroded) reinforcement properties in order to account for the effects of corrosion, see Section 4.3.5.2.

Note:

It is considered appropriate to simultaneously incorporate the effects of reduced reinforcement cross-sectional ($A_{S,C}$) area and degraded mechanical properties (yield strength, ultimate strength, and elastic modulus), see Eqs. (32), (33) and (34), thereby enabling the use of the original nominal reinforcement diameter (Ø) in the structural modelling within NLFEA. This is shown as part of the development of the stress–strain relationships (σ-ε diagrams) for corroded reinforcement in Section 4.3.5.2.

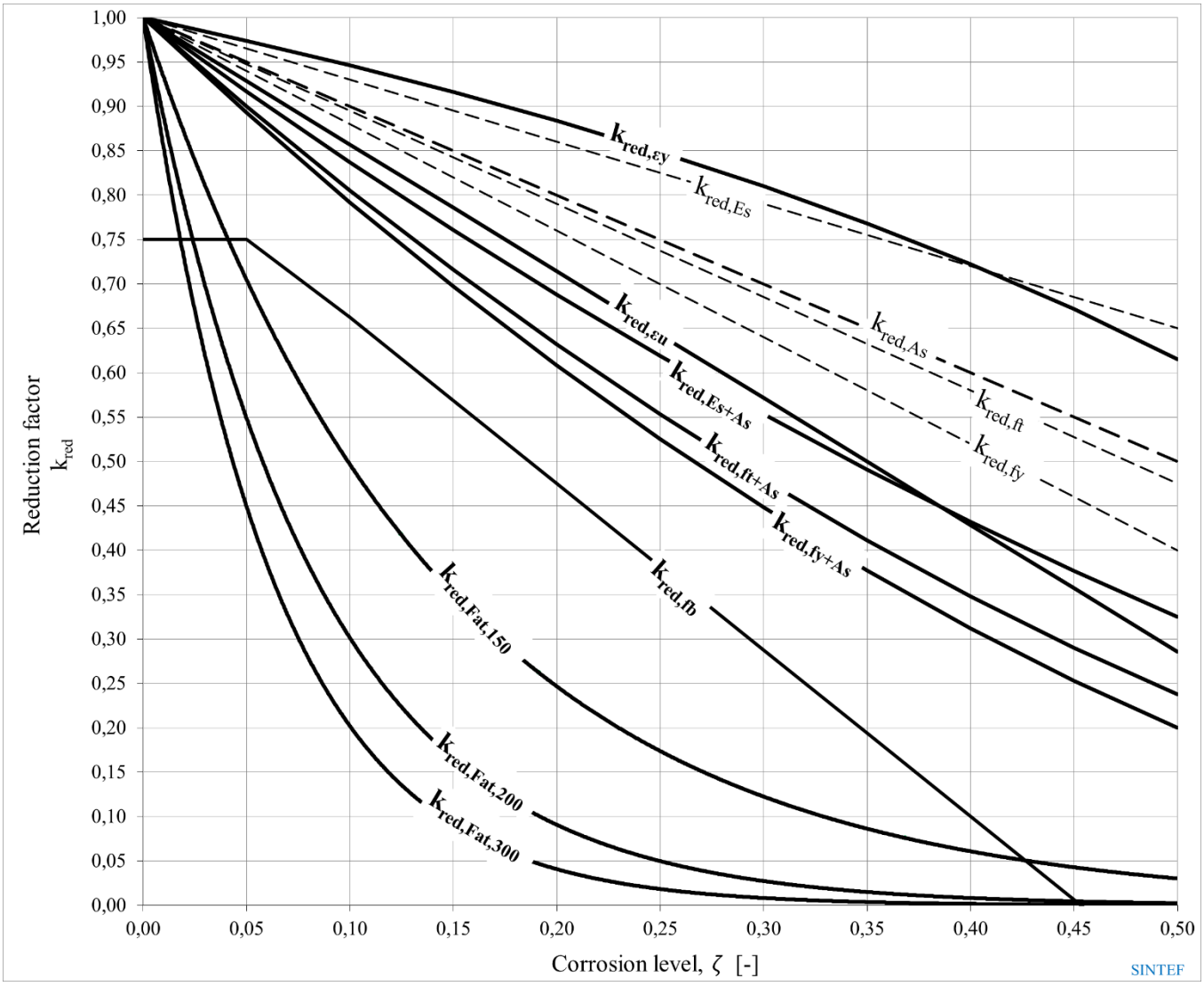

Figure 4-9: Indicative reduction factors (k_{red}) according to Eqs. (28) to (40)

4.3.4.2 Background literature for the proposed reduction factors (k_{red})

Reduction in <u>mechanical properties</u> of reinforcement due to corrosion:

The following literature has been reviewed and evaluated in connection with the development of the proposed and simplified k_{red}-factors in Eqs. (29) to (36):

- Modelling structural performance of existing concrete structures [55], *Section 5.3.3 – Properties of reinforcing steel subjected to deterioration*
- Stress-Strain curves and mechanical properties of corrosion damaged super ductile reinforcing steel [56]
- Corrosion effects on the mechanical properties of reinforcing steel bars. Fatigue and σ–ε behavior [57]
- Service life of concrete structures [58]
- Influences of corrosion degree and corrosion morphology on the ductility of steel reinforcement [59]

The mechanical properties of non-corroded reinforcement are presented in Section 4.3.5.1, based on the following standards and referenced clauses:

- *Clause 11.3.6* in [60]
- *Clause 3.2.7* / *NA.3.2.7* and *Annex C* in [49]

When verifying the capacity of reinforcement, corrosion effects may be accounted for by introducing reduction factors, k_{red}, applied to the properties of non-corroded reinforcement. Proposed reduction factors (k_{red}) for the mechanical properties of reinforcement as a function of corrosion level (ζ) are presented in Section 4.3.4.1, see Eqs. (29) to (36) and Figure 4-9.

These k_{red}-factors may be used as a basis for structural calculations to demonstrate the structural integrity at a given level of corrosion (ζ).

Reduction in <u>bond properties</u> of reinforcement due to corrosion:

The following literature has been reviewed and evaluated in connection with the development of the proposed and simplified $k_{red,fb}$-factor in Eq. (40):

- Modelling structural performance of existing concrete structures [55], *Section 6 - Bond*
- Fatigue of Concrete Structures [61]
- Post-Corrosion Bond-Slip Models for super Ductile Steel with Concrete [62]
- Service life of concrete structures [58], *Section 5.2 – Bond*
- Model Code 2010 – *Volume 1* [63], *Section 6.1.7.1 – Corrosion*
- Model Code 2020 [45], Section 30.1.10.3 – Structures with corroded reinforcement

The bond capacity of reinforcement depends on several factors related to the specific structure. For non-corroded reinforcement, the bond capacity is typically calculated in accordance with one of the following standards and referenced sections:

- *Section 12.8.5* in [60]
- *Section 6.11.1.16* in [64]
- *Section 8.4.2* in [49]

Where applicable, the bond capacity is also verified with respect to fatigue, in accordance with e.g. the following standards and referenced sections:

- *Section 13.5* in [60]
- *Section 6.13.5* in [64]
- *Section 6.8.2* in [49]

See below for considerations related to reduction in fatigue properties of the reinforcement steel itself.

When assessing the bond capacity of reinforcement in accordance with the sections listed above, reinforcement corrosion can be accounted for by introducing the reduction factor, $k_{red,fb}$, applied to the calculated bond capacity of non-corroded reinforcement. Suggested reduction factor as a function of corrosion level (ζ) are provided in Section 4.3.4.1, see Eq. (40) and Figure 4-9.

This $k_{red,fb}$ factor can then be used as input in structural calculations to demonstrate the structural integrity at a given corrosion level (ζ).

Note:

Eq. (40) is considered conservative, as it likely provides a reduction factor ($k_{red,fb}$) that does not account for the significant residual capacity resulting from mechanical force transfer via the remaining reinforcement ribs. When considering multiple reinforcement bars and increased anchorage lengths, it is unlikely that reduced bond characteristics will present a critical issue for the structural integrity for structures and structural components with typical corrosion levels. This applies in cases of both uniform corrosion and, in particular, when pitting corrosion is present.

Reduction in <u>fatigue properties</u> of reinforcement due to corrosion:

The following literature has been reviewed and evaluated in connection with the development of the proposed and simplified k_{red}-factors in Eqs. (37), (38) and (39):

- Corrosion effects on the mechanical properties of reinforcing steel bars. Fatigue and σ–ε behavior [57]
- Fatigue of Concrete Structures [61], *Clauses 4.1.3.3*, *4.1.3.4*, and *4.1.4*

The fatigue properties and fatigue loading of reinforcement depend on several factors specific to the structure in question. The fatigue capacity of non-corroded reinforcement steel is typically verified in accordance with one of the following standards and referenced clauses:

- *Clauses 13.1*, *13.2.1*, *13.2.2*, and *13.5* in [60]
- *Clause 6.13* in [64]
- *Clauses 6.8.1*, *6.8.2*, *6.8.3*, *6.8.4*/*NA.6.8.4*, *6.8.5*, and *6.8.6*/*NA.6.8.6* in [49]

Fatigue verification related to bond capacity is addressed on the previous page.

When verifying the fatigue capacity of reinforcement steel in accordance with the standards listed above, reinforcement corrosion may be accounted for by introducing the reduction factor, $k_{red,Fat}$, applied to the calculated fatigue capacity of non-corroded reinforcement.

Suggested reduction factors for selected stress ranges ($\Delta\sigma$), as a function of corrosion level (ζ), are presented in Section 4.3.4.1, see Eqs. (37), (38) and (39), and Figure 4-9.

These $k_{red,Fat}$ factors may then be used as input in structural analyses to demonstrate the structural integrity at a given level of corrosion (ζ).

Note:

Fatigue performance curves for reinforcement steel generally lie below those of plain steel, as the rib pattern introduces stress concentrations. Consequently, the reduction factors for reinforcement steel should normally be lower than those used for smooth steel.

The reduction factors ($k_{red,Fat}$) given in Eqs. (37), (38) and (39) are likely to be significantly conservative.
Fatigue, in combination with possible pitting corrosion, should be assessed separately, depending on the extent to which parts of the structure are exposed to fatigue loading.

4.3.5 Stress-strain diagram reinforcement (σ-ε diagram)

4.3.5.1 Uncorroded reinforcing steel (σ-ε diagram)

To determine the mechanical properties of reinforcement steel, including the effects of corrosion (see Section 4.3.5.2), it is essential that the uncorroded reinforcement is properly classified. Accordingly, the relevant reinforcement bar dimensions from the structure under assessment must be classified to enable reliable determination of the properties of the uncorroded material.

The classification may be based on one or a combination of the following methods, such as:

- Design information from drawings, calculations, etc.
- Former material and/or design standards applicable at the time of design and construction
- Current material and/or design standards
- Marking present on the steel surface
- Tests on rebars from the structure

Tests performed on samples taken from the structure according to [65] and [66].

Regarding the classification of reinforcement steel (sound) in existing structures, also refer to the general information provided in the following literature and referenced sections:

- Modelling structural performance of existing concrete structures [55],
  Section 5.3.1 – Classification by strength
  Section 5.3.2 – Classification by nominal values of strength
- Model Code 2010 – *Volume 2* [67]
  Section 7.11.8 – Statistical analyses of test results

Table 4-3 and

Table 4-4 summarize the mechanical properties (characteristic and design values) of standard reinforcement steel in accordance with [60] and [49], respectively.

The corresponding stress–strain diagrams according to methods given in *clause 3.2.7(2)* in [49] for uncorroded reinforcement steel type B500N (Class A, B and C), with characteristic yield strength (f_{yk}) equal to 500 MPa, are presented in Figure 4-10 and Figure 4-11.

Table 4-3: Mechanical properties of uncorroded reinforcing steel. Design assumptions according to withdrawn [60]

Mechanical properties			Type of reinforcement		Ref. clause in [60]
			K400TS	K500TS	
Material factor (Ultimate Limit State – ULS)	γ_s	[-]	1,25	1,25	*10.4.3*
Material factor (Accidental and Fatigue Limit States)	γ_s	[-]	1,10	1,10	
Material factor (Serviceability Limit State – SLS	γ_s	[-]	1,00	1,00	
Characteristic yield strength	f_{yk}	[MPa]	400	500	-
Design yield strength (ULS)	$f_{yd} = f_{yk} / \gamma_s$	[MPa]	320	400	*10.4.2*
Characteristic modulus of elasticity	E_{sk}	[MPa]	200 000	200 000	*9.2.5*
«Design» modulus of elasticity (ULS)	$E_{sd} = E_{sk} / \gamma_s$	[MPa]	160 000	160 000	*11.3.6*
Proportional strain limit ($\varepsilon_{sy} = \varepsilon_{sd}$) (Characteristic / Design)	$\varepsilon_{sy} = f_{yk} / E_{sk}$ $\varepsilon_{sd} = f_{yd} / E_{sd}$	[‰]	2,00	2,50	
Ultimate strain (ULS)	ε_{su}	[‰]	10	10	

Table 4-4: Mechanical properties of uncorroded reinforcing steel. Design assumptions according to [49]

Mechanical properties			Method a)						Method b)		Ref. Clause and Annex in [49]
			Technical Class A		Technical Class B		Technical Class C		For reinforcement with high ductility		
			B400NA	B500NA	B400NB	B500NB	B400NC	B500NC	B400	B500	
Material factor – Ultimate and Fatigue Limit States	γ_s	[-]	1,15	1,15	1,15	1,15	1,15	1,15	1,15	1,15	*2.4.2.4/ NA.2.4.2.4*
Material factor – Accidental and Serviceability Limit States	γ_s	[-]	1,00	1,00	1,00	1,00	1,00	1,00	1,00	1,00	
Characteristic yield strength	f_{yk}	[MPa]	400	500	400	500	400	500	400	500	*3.2.7/NA.3.2.7*
Design yield strength (ULS)	$f_{yd} = f_{yk} / \gamma_s$	[MPa]	347,8	434,8	347,8	434,8	347,8	434,8	347,8	434,8	
Characteristic tensile strength at ε_{uk}:	$f_{tk} = k \cdot f_{yk}$	[MPa]	k = 1,01		k = 1,02		k = 1,04		k = 1,0		
			404,0	505,0	408,0	510,0	416,0	520,0	400,0	500,0	
Design tensile strength at ε_{ud}:	$f_{td} = k \cdot f_{yk}/\gamma_s$	[MPa]	k = 1,01		k = 1,02		k = 1,04		k = 1,0		
			351,3	439,1	354,8	443,5	361,7	452,2	347,8	434,8	
Required minimum value of k in testing	$k = f_{tk} / f_{yk}$		k ≥ 1,05		k ≥ 1,08		1,15 ≤ k < 1,35		-		*C.1*
Modulus of elasticity (design value)	E_S	[GPa]	200	200	200	200	200	200	200	200	*3.2.7/NA.3.2.7*
Characteristic yield strain	$\varepsilon_{yk} = f_{yk} / E_S$	[‰]	2,00	2,50	2,00	2,50	2,00	2,50	2,00	2,50	
Design yield strain	$\varepsilon_{yd} = f_{yd} / E_S$	[‰]	1,74	2,17	1,74	2,17	1,74	2,17	1,74	2,17	
Characteristic strain at maximum stress	ε_{uk} (= A_{gt})	[‰]	25	25	50	50	75	75	100	100	*3.2.7/NA.3.2.7 and C.1*
Design strain at maximum stress	$\varepsilon_{ud} = 0{,}4 \cdot \varepsilon_{uk}$	[‰]	10	10	20	20	30	30	-	-	

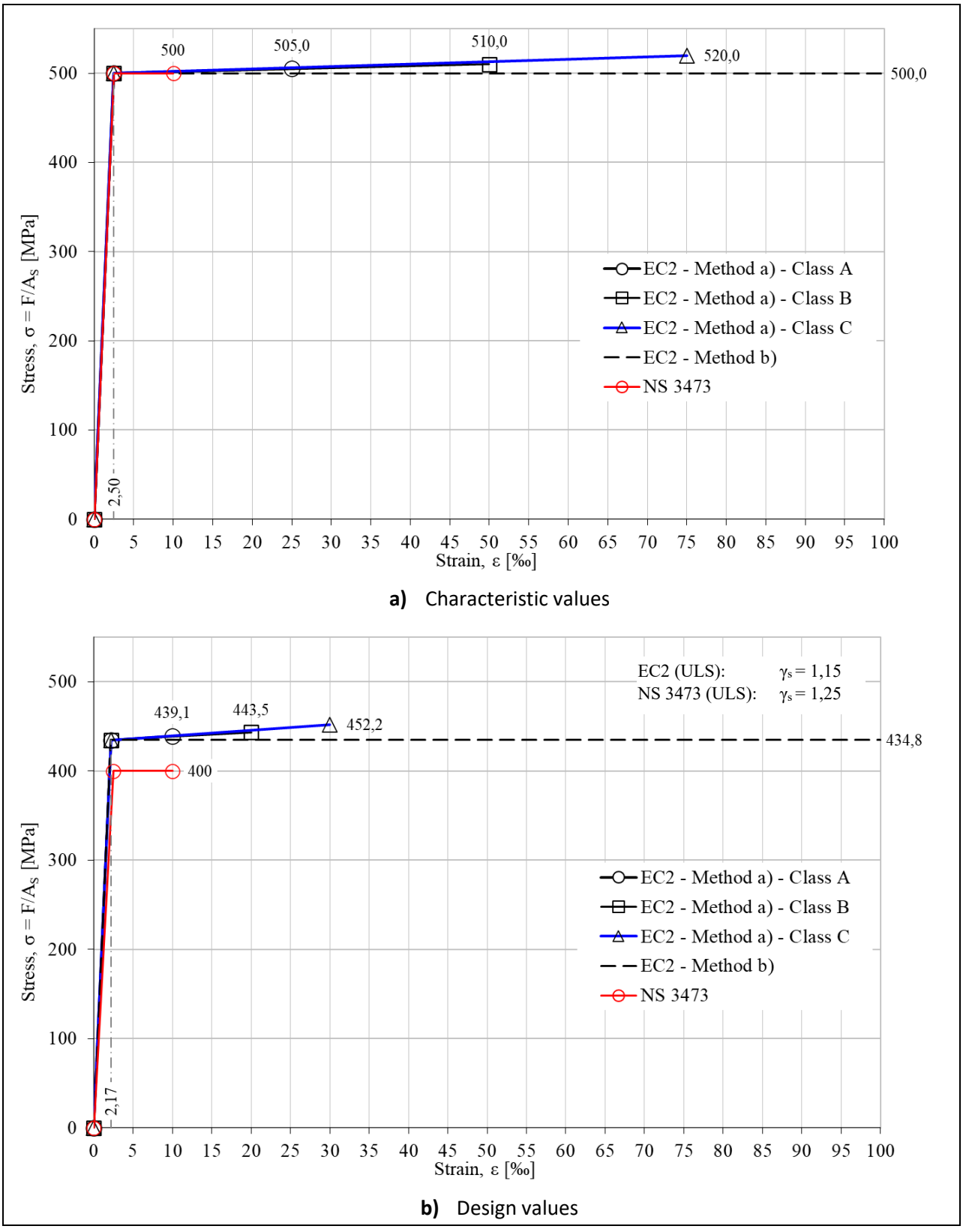

Figure 4-10: Idealized and design stress–strain relationship for conventional uncorroded reinforcing steel with f_{yk} = 500 MPa, in accordance with [60] and [49].

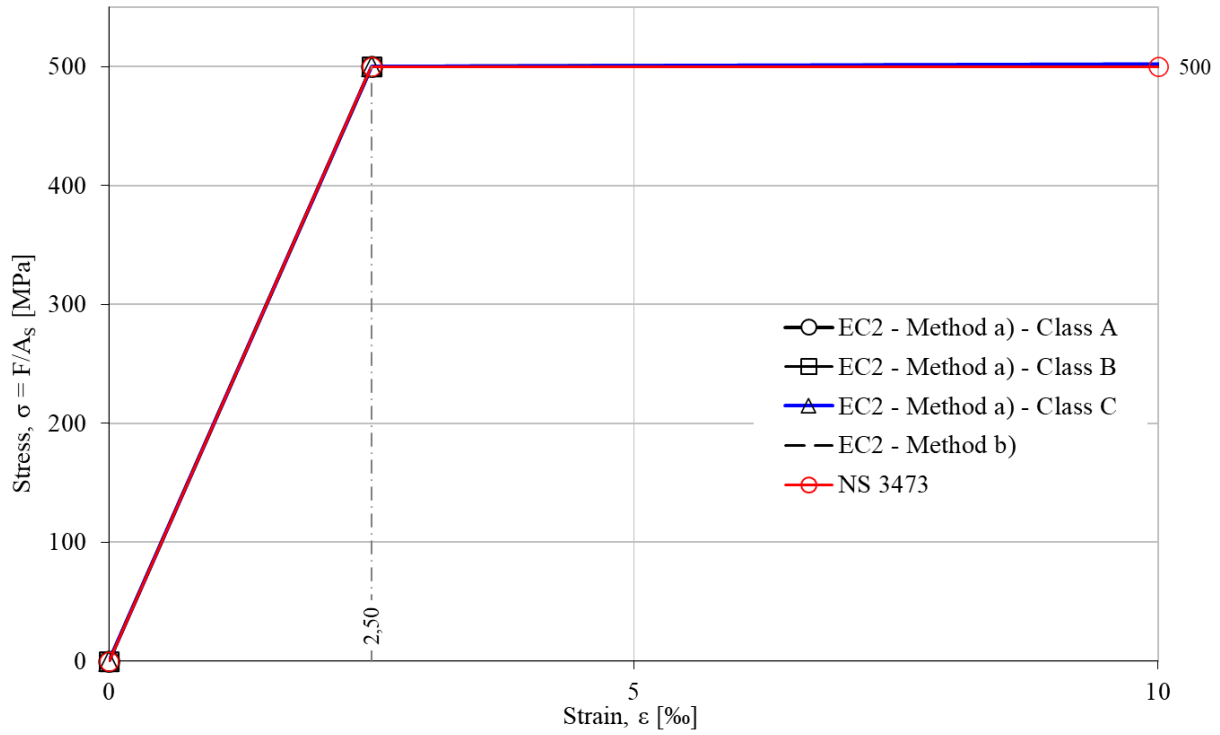

a) Characteristic values (section from Figure 4-10a)

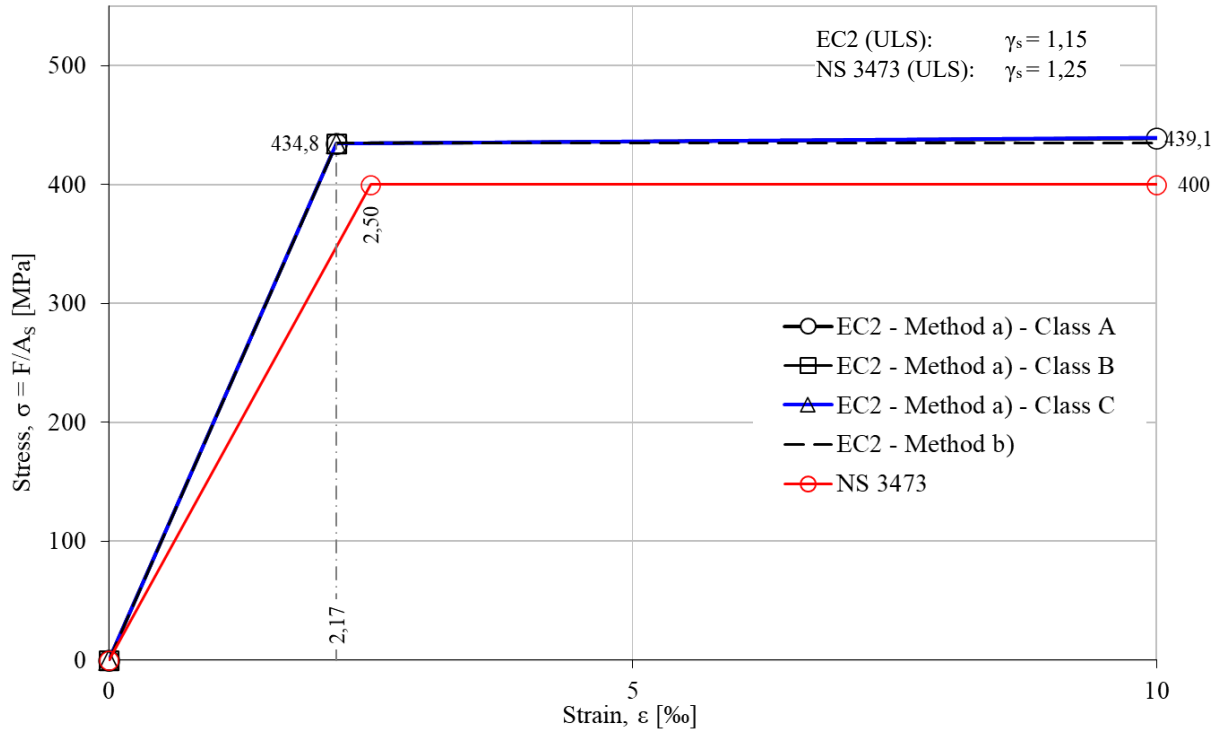

b) Design values (section from Figure 4-10a)

Figure 4-11: Section from Figure 4-10 (σ-ε relationship up to 10 ‰ strain).

4.3.5.2 Corroded reinforcing steel (σ-ε diagram)

Figure 4-12 illustrates the procedure for developing stress-strain diagram (σ-ε diagram) for corroded reinforcing steel.

The procedure shown in Figure 4-12 is practically implemented by multiplying the reduction factors (k_{red}) for the mechanical properties of corroded reinforcing steel (Section 4.3.4.1) with the corresponding characteristic and/or design values of the mechanical properties for uncorroded reinforcing steel (Section 4.3.5.1), see Eqs. (41)–(48). These equations are then used to develop the stress–strain relationship for corroded reinforcement.

Figure 4-13 to Figure 4-16 demonstrate the development of general stress–strain relationships for various corrosion levels (ζ). These figures are based on reinforcement grade B500NA, i.e. reinforcement (Class A) with characteristic yield strength (f_{yk}) equal to 500 MPa, and the use of method a) in *clause 3.2.7(2)* in [49].

Equivalent relationships can be established for all combinations of ductility classes (Class A–C) using method a), as well as method b), in *clause 3.2.7(2)* in [49].

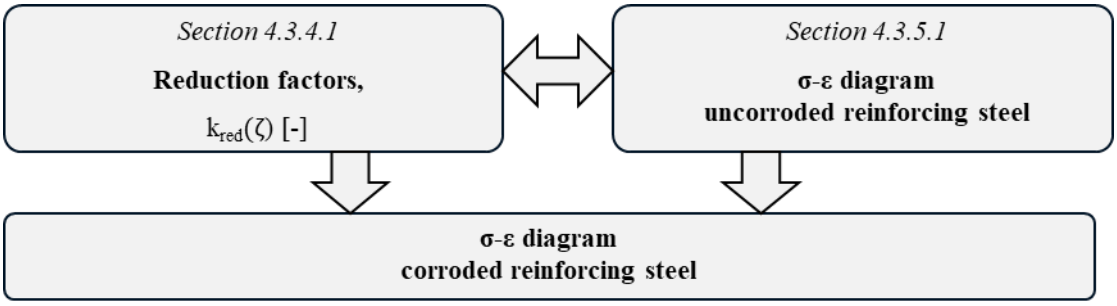

Figure 4-12: Flowchart illustrating the procedure for developing stress–strain diagram (σ-ε diagram) for corroded reinforcing steel.

Yield strength (f_y) accounting for corrosion:

$$f_{yk,C} = k_{red,fy} \cdot f_{yk}$$
$$f_{yd,C} = k_{red,fy} \cdot f_{yd} \quad (41)$$

Tensile strength (f_t) accounting for corrosion:

$$f_{tk,C} = k_{red,ft} \cdot f_{tk}$$
$$f_{td,C} = k_{red,ft} \cdot f_{td} \quad (42)$$

Elastic modulus (E_S) accounting for corrosion:

$$E_{S,C} = k_{red,Es} \cdot E_S \quad (43)$$

Yield strength (f_y), including reduced reinforcement area ($A_{S,C}$), accounting for corrosion:

$$f_{yk,C,As} = k_{red,fy+As} \cdot f_{yk} = (k_{red,As} \cdot k_{red,fy}) \cdot f_{yk}$$
$$f_{yd,C,As} = k_{red,fy+As} \cdot f_{yd} = (k_{red,As} \cdot k_{red,fy}) \cdot f_{yd} \quad (44)$$

Tensile strength (f_t), including reduced reinforcement area ($A_{S,C}$), accounting for corrosion:

$$f_{tk,C,As} = k_{red,ft+As} \cdot f_{tk} = (k_{red,As} \cdot k_{red,ft}) \cdot f_{tk}$$
$$f_{td,C,As} = k_{red,ft+As} \cdot f_{td} = (k_{red,As} \cdot k_{red,fd}) \cdot f_{td} \quad (45)$$

Elastic modulus (E_S), including reduced reinforcement area ($A_{S,C}$), accounting for corrosion:

$$E_{S,C,As} = k_{red,Es+As} \cdot E_S = (k_{red,As} \cdot k_{red,Es}) \cdot E_S \quad (46)$$

Proportional limit (ε_y) accounting for corrosion:

$$\varepsilon_{yk,C} = k_{red,\varepsilon y} \cdot \varepsilon_{yk} = \frac{k_{red,fy}}{k_{red,Es}} \cdot \varepsilon_{yk}$$
$$\varepsilon_{yd,C} = k_{red,\varepsilon y} \cdot \varepsilon_{yd} = \frac{k_{red,fy}}{k_{red,Es}} \cdot \varepsilon_{yd} \quad (47)$$

Strain limit (ε_u) accounting for corrosion:

$$\varepsilon_{uk,C} = k_{red,\varepsilon u} \cdot \varepsilon_{uk}$$
$$\varepsilon_{ud,C} = k_{red,\varepsilon u} \cdot \varepsilon_{ud} \quad (48)$$

Where

ζ = Corrosion level, see Section 4.3.3
k_{red} = Reduction factor, see Eqs. (29) to (36) in Section 4.3.4.1
f_{yk} = Characteristic yield strength of uncorroded reinforcement, see Section 4.3.5.1
f_{yd} = Design yield strength of uncorroded reinforcement, see Section 4.3.5.1
f_{tk} = Characteristic tensile strength of uncorroded reinforcement, see Section 4.3.5.1
f_{td} = Design tensile strength of uncorroded reinforcement, see Section 4.3.5.1
E_S = Design value of modulus of elasticity of uncorroded reinforcement, see Section 4.3.5.1
ε_{yk} = Characteristic yield strain of uncorroded reinforcement, see Section 4.3.5.1
ε_{yd} = Design yield strain of uncorroded reinforcement, see Section 4.3.5.1
ε_{uk} = Characteristic strain at maximum load of uncorroded reinforcement, see Section 4.3.5.1
ε_{ud} = Design strain at maximum load of uncorroded reinforcement, see Section 4.3.5.1

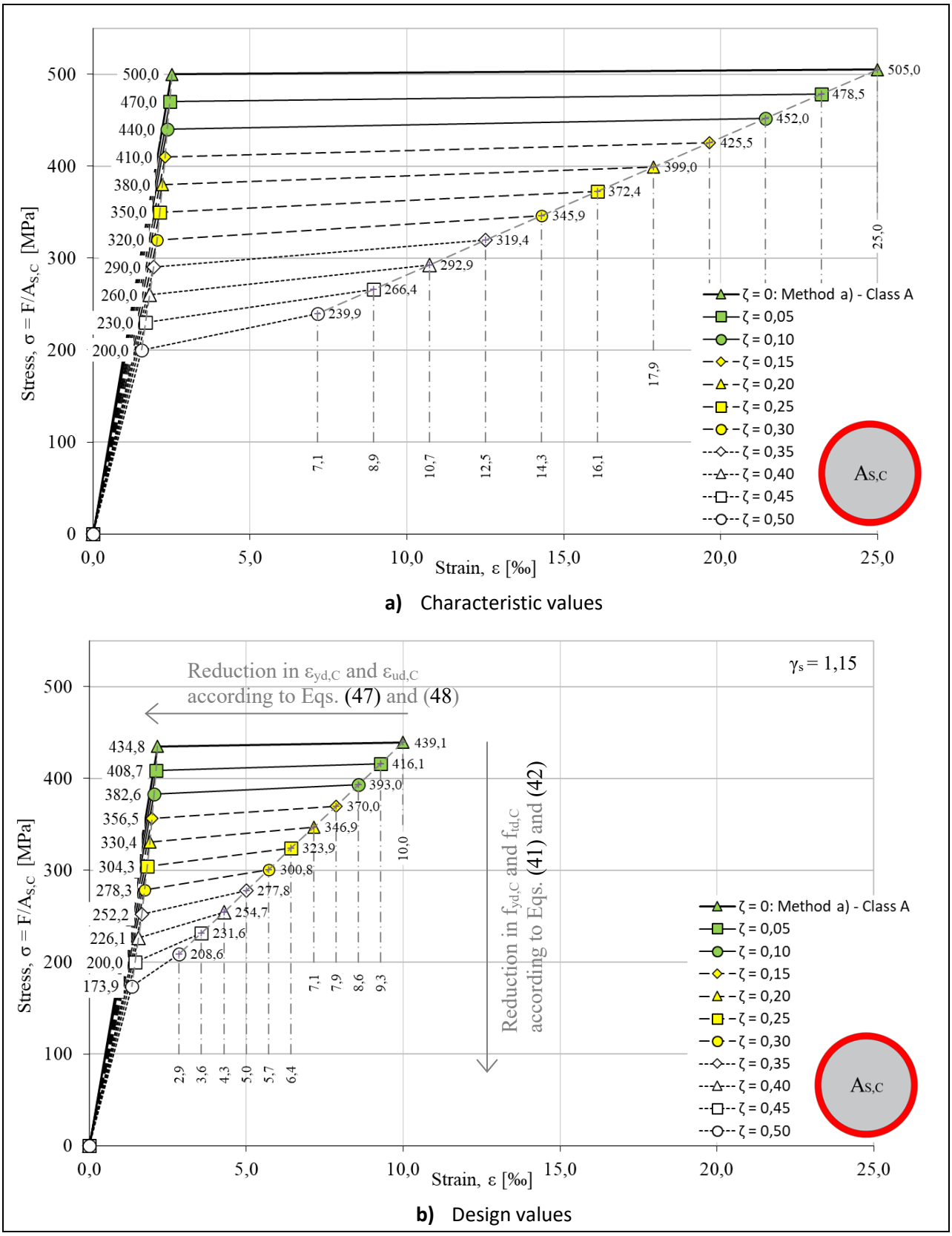

Figure 4-13: Idealized and design stress–strain relationships for various corrosion levels (ζ) from 0 to 0,5.
Note: The stress values (σ) are applied to the reduced corroded reinforcement cross-sectional area ($A_{s,C}$).

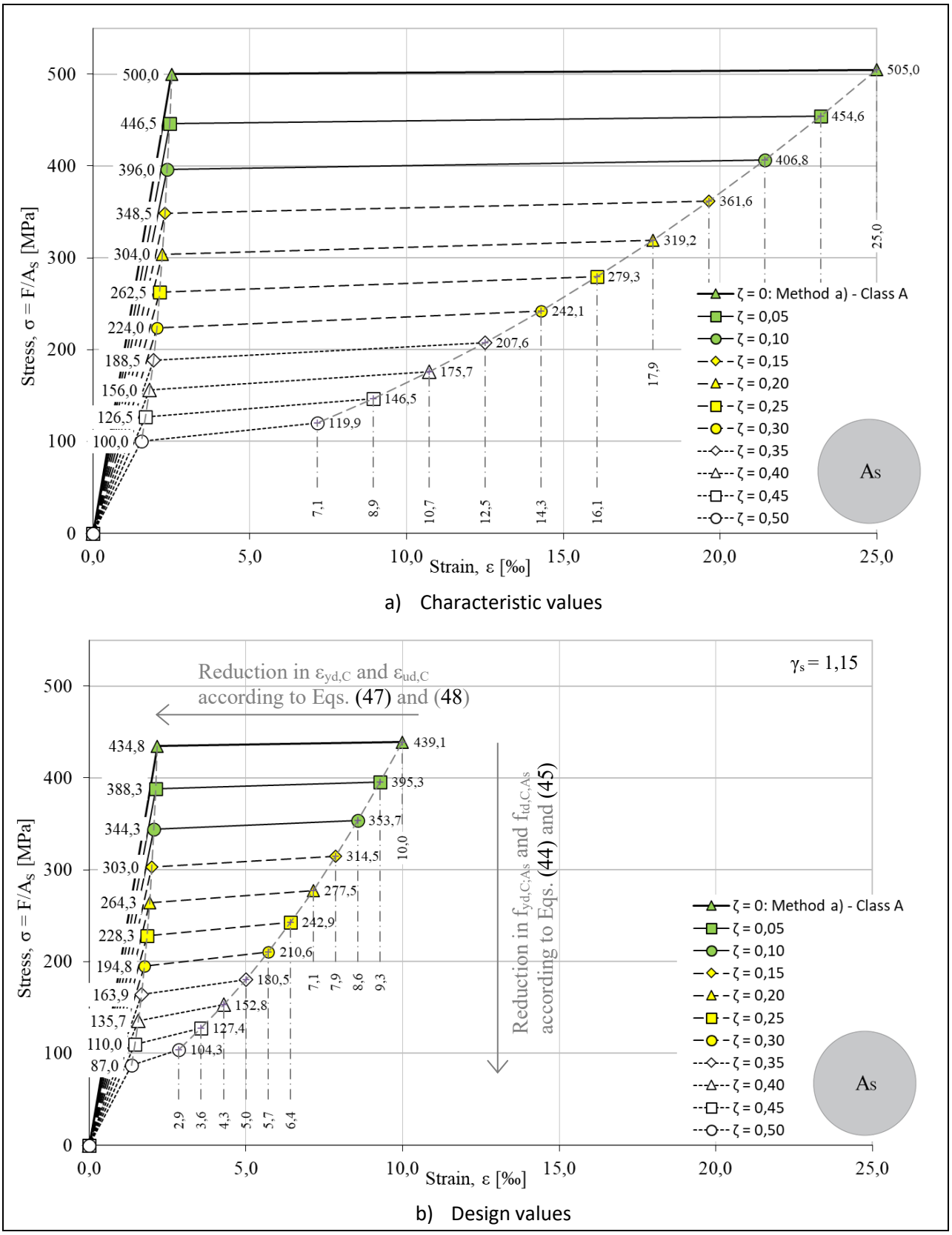

Figure 4-14: Idealized and design stress–strain relationships for various corrosion levels (ζ) from 0 to 0,5, including the effect of reduced reinforcement area, $A_{s,c}$. *Note:* The stress values (σ) are applied to the original nominal reinforcement cross-sectional area (A_s).

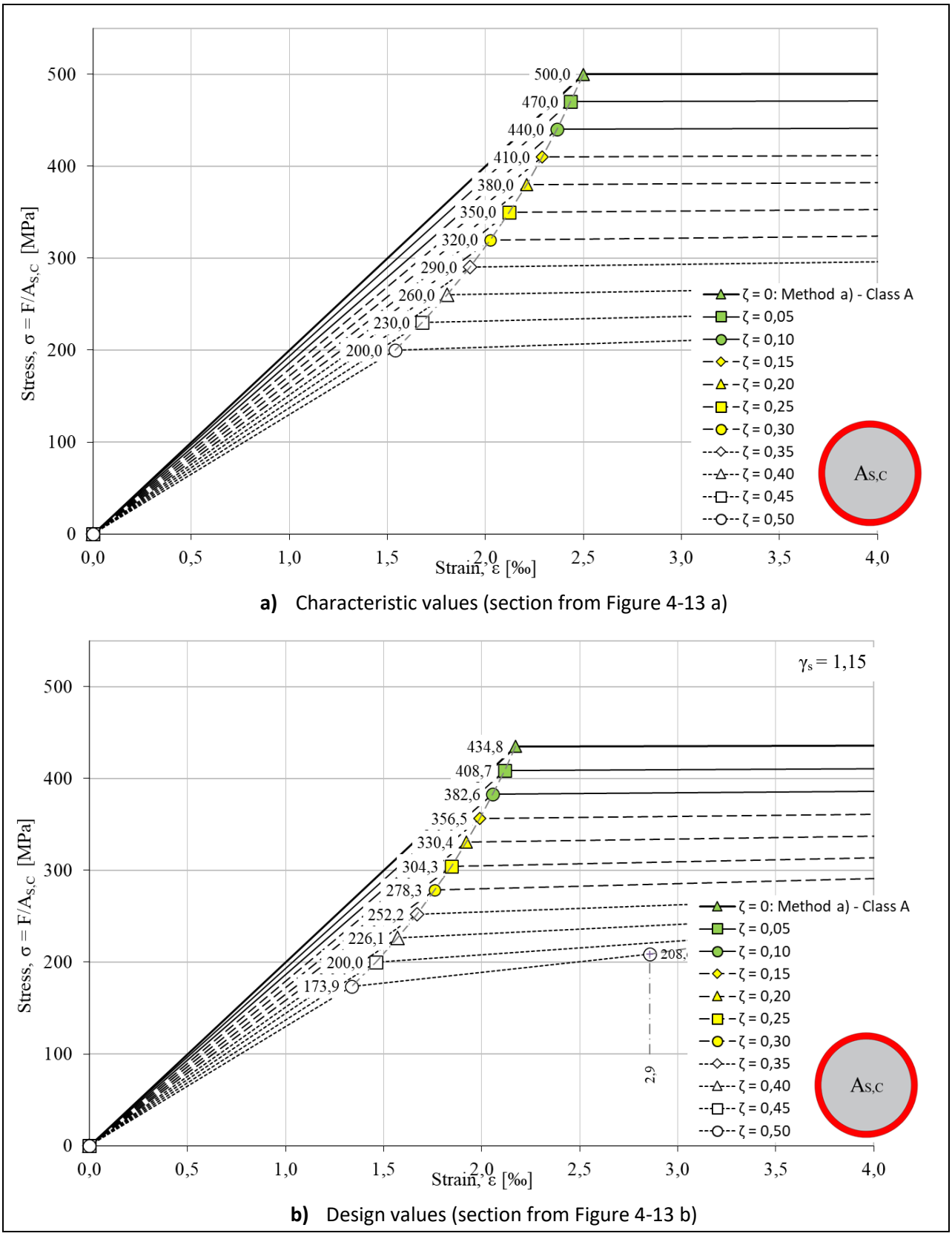

Figure 4-15: Section from Figure 4-13 (σ-ε relationship up to 4 ‰ strain).
Note: The stress values (σ) are applied to the reduced corroded reinforcement cross-sectional area ($A_{s,c}$).

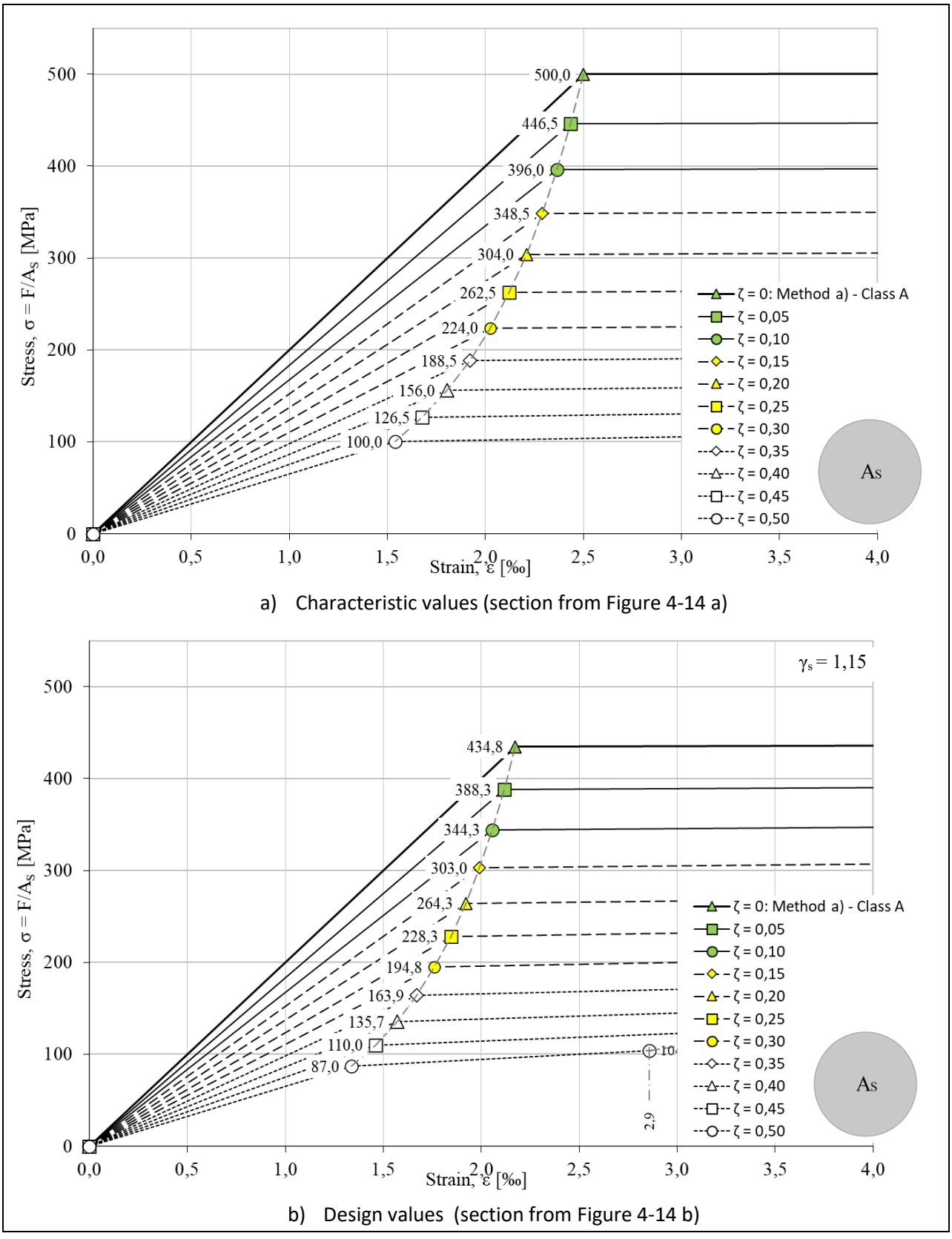

a) Characteristic values (section from Figure 4-14 a)

b) Design values (section from Figure 4-14 b)

Figure 4-16: Section from Figure 4-14 (σ-ε relationship up to 4 ‰ strain).

Note: The stress values (σ) are applied to the original nominal reinforcement cross-sectional area (A_S).

4.4 Corrosion of RC ties

The stress-strain curve for RC ties subjected to corrosion can be obtained by using a tension chord model with material parameters as suggested in the previous subsections. Note that the mean steel strain ε_{m} of the corroded RC tie should be adjusted as suggested by [51]

$$\varepsilon_{\mathrm{m,c}} = \frac{(1-\beta)s_{\mathrm{r}}\varepsilon_{\mathrm{m}} + \beta s_{\mathrm{r}}\varepsilon_{\mathrm{s}}(\sigma_{\mathrm{s,c}})}{s_{\mathrm{r}}} = (1-\beta)\varepsilon_{\mathrm{m}} + \beta\varepsilon_{\mathrm{s}}\left(\frac{\sigma_{\mathrm{s,uc}}}{1-\zeta}\right) \tag{49}$$

It is thus necessary to obtain input on the deterioration parameters related to the relative loss of cross-sectional area ζ and the length of the damaged section βs_{r}, where s_{r} is the transfer length. The stress strain curves for uncorroded and corroded RC ties are exemplified in Figure 4-2. Note that β is a parameter describing how the bond, or more rigorously speaking, how the tension stiffening effect is affected by corrosion. It could be an additional input to ζ, but can also be determined according to the recommendations in [51].

4.5 Accounting for development of corrosion over time

The development of corrosion can be effectively accounted for in a time analysis by providing stress-strain curves at distinct times. This is exemplified in Figure 4-2, where the uncorroded stress-strain curves represents the behaviour for an undamaged structure, e.g. right after opening of the structure, whereas the corroded rebar represents the behaviour according to the inspected one. If those two curves are provided at distinct times a priori, most general-purpose FE software's will be able to interpolate the response in between. The fact that the stress-strain curve alters over time for the corroded rebars in a NLFEA will eventually reveal if the structure is able to redistribute the internal forces, while maintaining equilibrium with the external applied forces.

5 Safety format

5.1 Introduction

The safety assessment of existing structures requires verifying that the design value of the structural demand does not exceed the design value of the structural capacity or resistance, typically expressed by the general verification format:

$$F_d \leq R_d \tag{50}$$

where F_d is the design value of the action effects in the relevant combination, and R_d is the design value of the corresponding structural resistance.

When NLFEA is used in the assessment of existing structures, this verification must account for the nonlinear and path-dependent response of the structure. In addition, verifying structural safety requirements implies dealing with manifold uncertainties. Among them are uncertainties associated with material and geometrical structural properties, loads and environmental influences. Such uncertainty can be principally reduced through information acquisition by means of measurements and tests on the existing structure, a process that itself is associated with uncertainties, e.g. due to imperfect observations (test uncertainties) and limited sample sizes (statistical uncertainties) [68, 69]. Another important source of uncertainties is the variability in the prediction capacity of the finite element models employed for the assessment (model uncertainties).

Different approaches can be distinguished to verify the basic requirements given by Eq. (50) in the context of NLFEA:

- Full probabilistic methods, in which uncertainties in basic variables are explicitly modelled using probability density functions, and both action effects and structural resistance are characterized e.g. via simulation techniques such as Monte Carlo or Latin Hypercube sampling, or approximate methods like first- or second-order reliability methods (FORM/SORM), see e.g. [70];

- Semi-probabilistic methods, which simplify the treatment of uncertainties by using safety factors applied to representative values of actions and resistances.

While full probabilistic methods in connection with NLFEA generally allow for a more accurate representation of structural performance under specific loads and influences, and hence, can activate hidden structural reserve capacities, they are comparatively cumbersome and time intensive. This chapter focuses therefore on the semi-probabilistic methods commonly used in engineering practice:

- Partial Factor Method (PFM): The design capacity is obtained by applying partial safety factors to the representative values of basic variables that influence the structural performance.

- Global Factor Method (GFM): The design capacity is determined by applying a global safety factor to structural resistance, which accounts in a global manner for uncertainty across basic variables.

The selection of an appropriate method depends on engineering judgment and should consider the type of capacity model used and the nature of the non-linearities and uncertainties involved. For some problems the complex, non-linear interaction of basic variables resulting in uncertain structural behaviour and possible interaction between different local failure mechanisms, could make the PFM difficult to implement transparently and the GFM might preferably be used. In other cases, the PFM might be more convenient due to its comparatively more user-friendly format.

The remainder of this chapter is structured as follows. Section 5.2 discusses the selection of target reliability levels crucial for the adjustment of partial and global safety factors. Another instrumental process in the safety assessment of existing structures is the updating of the knowledge state on the structure, based on new information gained, what is briefly addressed in section 5.3. Subsequently, section 5.4 focuses on the treatment and updating of model uncertainties, which are of particular importance in NLFEA-based safety assessments. Following considerations on loads and load effects in section 5.5, the main verification formats and methods, i.e. the PFM (section 5.6) and the GFM (section 5.7) are introduced and discussed. Finally, section 5.8 illustrates the application of the different safety formats and methods by means of a case study.

5.2 Target reliabilities

5.2.1 General

The design of new or the assessment/upgrading of existing structures, or parts thereof, can ultimately be viewed as a form of decision analysis. The aim is to determine the layout, materials, and dimensions required to meet specified performance criteria with a certain level of (structural) reliability, while considering relevant constraints [68].

Most modern structural codes and standards include probabilistic reliability requirements for structural design or assessment. Formulated in terms of target reliability indices (β_t), in turn related to admissible failure probabilities $p_{f,adm}$ via the cumulative probability distribution function of the standardised normal

operator $\Phi(.)$ – see Eq. (51)– such (nominal) requirements may be used for decision making based on explicit probabilistic analysis, e.g. in unusual design situations regarding the involved uncertainties or potential failure consequences. Moreover, they serve as a basis for calibration of user-friendly semi-probabilistic safety rules for addressing design and assessment situations in routine engineering practice.

$$\beta_t = -\Phi^{-1}(p_{f,adm}) \tag{51}$$

A target reliability index is always associated with a specific reference period T_{ref}, which is used for the statistical assessment of extreme values of variable actions, their combined effects, as well as accidental actions or degradation where relevant [71]. It is further important to recognize that codified failure probabilities should generally not be interpreted as absolute values, but rather as nominal targets, which are derived based on particular probabilistic modelling assumptions. These assumptions include for example the type of statistical distributions and their parameters (probabilistic representations of the basic variables), correlations between basic variables, or the form of the limit state functions. As a result, $p_{f,adm}$ and β_t are dependent on these modelling choices and simplifications.

5.2.2 Reference period

For new structures, *codified target reliability levels* are typically associated with a T_{ref} that is aligned with the design working life. For example, both the current and next generation of the Eurocodes demand structural members to be designed for a target reliability index $\beta_{t,50}$=3.8 for a 50-year reference period [72]. In a similar vein, for existing structures the anticipated remaining service life can be adopted as T_{ref}. However, recent standards and recommendations, including [73, 74, 45], propose the adoption of annual reliability indices (T_{ref} = 1 year) what has several motivations [71]:

- It aligns reliability indices with the time scale of variable loads, which are typically defined using annual maxima.
- It reduces confusion related to differences between the intended remaining service life (often shorter than the design working life of new structures) and reference periods.
- It better supports condition-based assessments, which are particularly relevant for deteriorating structures where failure probability usually increases with time. In such cases, the final year of the remaining service life is decisive for structural reliability verifications.
- It enables integration into economic and risk-based decision-making frameworks, where cost-benefit calculations are typically annualized.

A naïve transformation from lifetime to annual reliability might assume that annual failure events are independent, leading to the approximation:

$$p_{f,50} \approx 50 \cdot p_{f,1} \tag{52}$$

This results in an annual target value of approximately $\beta_{t,1}$ = 4.7 to match the 50-year $\beta_{t,50}$ = 3.8 used in [72] for new structures and consequence class CC2 (moderate consequences). Likewise transformations between $\beta_{t,50}$ and $\beta_{t,1}$ are given in [72] for CC1 and CC3 – see Table 5-1. However, it has been recognized that this assumption is overly conservative —especially for concrete structures— where significant contributions of permanent loads introduce correlation of failure events over subsequent years, leading to comparatively higher (acceptable) failure probabilities, hence lower target reliability indices. Depending on the modelling assumptions, annual *average* values of the order of $\beta_{t,1}$ = 4.2-4.5 have been observed to provide a better correspondence to the 50-year target $\beta_{t,50}$ = 3.8 [75, 76, 77, 68].

Table 5-1: Target reliabilities defined in EN1990 associated with annual and 50-year reference periods [72].

Relative cost of safety measure	Consequence Class (CC)		
	CC1	CC2	CC3
T_{ref} = 1y	4.2	4.7	5.2
T_{ref} = 50y	3.3	3.8	4.3

5.2.3 Influences and indicative values in codes and standards

Most structural codes, e.g. the Eurocodes [72], use mainly the expected failure consequences (encompassing human safety, economic loss, and also environmental impact) to explicitly differentiate target reliability levels, see Table 5-1. The JCSS Probabilistic Model Code [73] recognizes the relevant role of other parameters for fixing such levels, among them the relative cost of safety measures to increase reliability or the variability in actions, influences and structural resistance parameters. In compliance with the JCSS recommendations, the international standard ISO 2394 [74] and the fib Model Code 2020 [45] support the use of annual target reliabilities as given per Eq. (53), which expresses that any economically optimal solution, associated with a target value $\beta_{t,eco}$, should be subject to a constraint $\beta_{t,hs}$ that ensures human safety risks are within the bounds of acceptability.

$$\beta_t = \max\left(\beta_{t,eco}; \beta_{t,hs}\right) \tag{53}$$

Following the recommendations in [73, 74, 45], the target reliability constraint $\beta_{t,hs}$ should be adopted in compliance with the marginal lifesaving cost principle (MLSC). On the basis of this approach, implemented in practice by the Life Quality Index (LQI), the conformity of structural decisions can be assessed with respect to the societal preferences for investments into life safety - see [78, 79, 80, 81] for further guidance. The LQI approach aligns with the ALARP principle, with a range of tolerable risks when reduced to "*As Low As Reasonably Practicable*" [74]. The lower limit of the ALARP range corresponds to negligible risks and the upper limit to the intolerable level at which risks must be kept below regardless of the cost. For the upper limit, [82] suggested a unifying metric that can be used to compare human safety risks among different fields, the expected value of the number of deaths per person-year. Reference [83] proposed target reliability levels $\beta_{t,hs}$ for the design and assessment of building structures based on implicitly acceptable life safety risks, addressing also time-dependent risk exposure. Specific developments for human safety reliability targets for bridges can be found, e.g. in [84].

ISO 2394 and fib MC both propose indicative annual $\beta_{t,eco}$ values, as summarized in Table 5-2 below, based on the fundamental work by Rackwitz [79] and further developed by others, e.g. [80]. As a default case for design of new structures, consequence class CC2 and normal relative cost of safety measures (class B) are identified and associated with medium variabilities of the yearly extreme values of the loads and resistances. For the assessment of existing structures, there is consensus in the literature and guidelines that lower target reliabilities than for design are justified on the grounds of comparatively higher costs for achieving specific safety levels [85, 86, 87, 71] provided that human safety requirements are met according to Eq. (53). For the minimum target level, below which an existing structure should be upgraded, large relative cost of safety measures (class C) may be assumed according to [45].

Table 5-2: Tentative values for annual target reliabilities $\beta_{t,eco}$ for Ultimate Limit States based on economic optimization, adopted from [73, 74, 45].

Relative cost of safety measure	Consequence Class (CC)*		
	CC1	CC2	CC3
Large (A)	3.1	3.3	3.7
Normal (B)	3.7	4.2	4.4
Small (C)	4.2	4.4	4.7

* Note that the definition of consequence classes (CC) in, respectively, [73], [74], and [45] obeys different criteria.

The assessment of the current condition of a structure and its upgrading should be treated separately. Following [87] and the [45], it is recommended to first evaluate the structure against a baseline target reliability index $\beta_{t,0}$ (based on Eq. (53), with $\beta_{t,eco}$ typically from Table 5-2 above). If this criterion is not met, a decision must be made whether to upgrade the structure toward a higher index $\beta_{t,up}$. Cost-optimisation studies suggest that slightly lower reliability levels than for new structures may be acceptable for upgrading [86]. A reduction of $\Delta\beta \approx 0.5$ relative to design targets (for new structures) has been suggested as a rule of thumb, see [87] and [45]. However, it is common and reasonable to require upgrading levels that comply with those of design [71].

5.3 Updating

5.3.1 General

A key difference between assessing new and existing structures is that, in existing structures, many characteristics can be measured directly rather than assumed. The actual condition of the structure—including effects of construction, aging, deterioration, and past use—can be observed and considered in the assessment. This allows for more accurate evaluations, enabling verifications of compliance with reliability targets, and hence life-time extensions of structures that are deemed unsafe when assessed on the grounds of the design rules for new structures [69].

Improving the accuracy of structural assessments typically involves gathering additional information about both the structure and the loads acting on it, followed by a probabilistic evaluation of the obtained data and its incorporation into structural verifications. This process is known as probabilistic updating and should be a core part of a reliability assessment of an existing structure. Note that in cases where multiple similar structures have been built and used under comparable conditions, performance data from one can potentially inform the assessment of another structure. Two complementary updating approaches can be distinguished [71, 88]:

1. Updating of structural performance based on global information such as load testing or observed performance over time.
2. Updating of individual basic variables—such as e.g. geometry, material properties, or degradation variables—through inspections, measurements or tests.

The first approach, such as updating resistance values of bridge girders via proof load tests, e.g. [89], can significantly reduce uncertainty but tends to be comparatively complex and cost intensive. The second approach, focusing on updating variables like material strength, geometrical properties, specific loads or degradation parameters [90], is often more practical—though its benefits must be evaluated case by case. In the following, approach 2 is briefly outlined below.

5.3.2 Updating of basic variables

Bayesian methods offer a consistent framework for updating probabilistic models of basic variables. In this context, prior information (e.g., from databases, literature, or background reports to standards) is combined with new data (e.g., test results, monitoring data) to improve estimates of variable distribution properties. The new data are incorporated using a *likelihood function*. Often, the prior and updated (posterior) distributions are assumed to belong to the same family (e.g., lognormal for material strength) [71].

The quality and representativity of both the prior information and the test data should always be critically assessed. Depending on this, different updating scenarios may arise [71, 91]:

- Strong prior, weak likelihood: For example, well-established databases on steel properties are updated with a small number of tests. These tests mainly serve to confirm existing assumptions.
- Weak prior, strong likelihood: For example, the compressive strength of in-situ concrete may be uncertain due to construction variability, but sufficient core testing can significantly reduce this uncertainty.
- Balanced prior and likelihood: Both sources provide useful information, and the combination improves reliability estimates.

From a computational perspective, Bayesian updating may be carried out using numerical methods such as FORM/SORM/simulation techniques (e.g., Markov Chain Monte Carlo) when analytical solutions are not feasible. Guidance on available closed form solutions can be found in [73] or [45]. Annex A4 of prEN 1990-2 [92] includes Eqs. (54) to (57) for combining prior information and new data constituted by *n* observations (with ν degrees of freedom) in order to determine the parameters of the posterior distribution of a normally (or log-normally) distributed basic variable. In the mentioned equations, m^{II} and s^{II} represent, respectively, the posterior mean and standard deviation, with v^{II} and n^{II} representing the posterior degrees of freedom and sample size n^{II}. In Eqs. (54) to (57), m, s, v and n are the sample parameters and m^I, s^I, v^I and n^I are the prior parameters of the distribution. If no prior information is available, then n^I = v^I = 0 and m^{II}, n^{II}, s^{II}, v^{II} are equal to the sample characteristics m, s, v and n. See e.g. [71, 93, 68] for further guidance.

$$m^{II} = \frac{1}{n^{II}}(nm + n^I m^I) \tag{54}$$

$$s^{II\,2} = \frac{1}{\nu^{II}}(\nu s^2 + \nu^I s^{I\,2} + nm^2 + n^I m^{I\,2} - n^{II} m^{II\,2}) \tag{55}$$

$$\nu^{II} = \nu^I + \nu + \delta(n^I) \tag{56}$$

$$n^{II} = n^I + n \tag{57}$$

Where:
$\delta(n') = 0$ for $n' = 0$;
$\delta(n') = 1$ for $n' > 0$;
$\nu = n - 1$.

Besides the inherent variability of a measured variable, the updating should take into account measurement or test errors, model uncertainty when a parameter is measured indirectly and a model is needed for

converting the measured parameter into the corresponding variable under investigation, and statistical uncertainty due to limited number of measurement of test results [71].

When updating a characteristic value, e.g. for a material property *M*, statistical uncertainties associated with a limited sample size *n* can be accounted for by using the posterior predictive distribution. Under the conjugate normal (or lognormal, after transformation to the log-space Y=lnX) model with unknown population standard deviation, the updated characteristic value is obtained by inserting the posterior hyperparameters (m^{II}, n^{II}, s^{II}, υ^{II}) into Eq. (58) based on the predictive Student t distribution. Here $t_{\upsilon'',\alpha}$ is the α-fractile (e.g. 5%) of the Student t-distribution with posterior degrees of freedom υ^{II}. The t-factor accounts for the additional uncertainty introduced by estimating the unknown population standard deviation from a finite sample. The term $\sqrt{1+1/n''}$reflects uncertainty in the population mean.

$$M_{k,upd} = m'' - t_{\nu'',\alpha}\mathrm{s}''\sqrt{1+\frac{1}{n''}} \tag{58}$$

It should be noted that Eq. (58) is valid for normal basic variables, or for lognormal variables after transforming the data, performing the Bayesian update in Y-space, and then back-transforming the resulting quantile to the original X space. Alternatively, the updated characteristic value may be obtained through a Monte Carlo posterior predictive simulation. This involves drawing (μ,σ) from the posterior distribution (using the inverse-chi-square distribution for the variance in case of normal/lognormal distributed variables), simulating future observations conditional on these parameters, and computing the empirical p-quantile of the simulated predictive values. The MC approach is more generally applicable and coincides with the analytical Student-t result when the conjugate assumptions hold.

5.4 Model uncertainty

5.4.1 Background and representation

In NLFEA of reinforced concrete structures, the reliability of the results depends not only on the accuracy of the input data but also on the adequacy of the selected modelling approach (i.e. the solution strategy). It is essential that engineers recognize this and do not treat the use of NLFEA software as a black-box exercise. Instead, the analyst bears full responsibility for verifying and validating the selected solution strategy. Proper *verification* ensures that simulation results are not sensitive to mesh or load step size, and that the numerical, iterative solution scheme can adequately reproduce the intended nonlinear behavior. Proper *validation* of the solution strategy examines whether the verified numerical model represents the physical behavior sufficiently well and forms the basis for quantifying the modelling uncertainty (MU).

While models are generally not “right or wrong”, they can be more useful for a given problem if the associated uncertainties are quantified and accounted for [94]. MU arise from the idealizations and simplifications inherent to the formulation and solution of physical models and express how well they capture the structural behavior relevant to the problem at hand. MU capture all residual influences not explicitly represented in the numerical model, such as uncertainties regarding the idealization of structural geometry, loading or boundary conditions, uncertain spatial distribution of material parameters, or uncertain relations between such parameters within the test specimen [45]. Moreover, the MU accounts for the physical uncertainty of the experimental outcomes, which are hardly possible to eliminate [95].

Formally, the MU can be expressed by the ratio Θ of the structural capacity observed in experiments R_{exp} and the predicted capacity R_{NLFEA}. Ratio Θ is treated as a lognormal random variable with mean μ_Θ and coefficient of variation V_Θ.

$$\Theta = \frac{R_{\text{exp}}}{R_{\text{NLFEA}}} \tag{59}$$

To support the practical application of NLFEA in structural assessment, the following subsections describe the key elements of handling MU. Section 5.4.2 discusses requirements for test coverage and parameter consistency of benchmark analyses performed. Subsequently, section 5.4.3 outlines how to update prior modelling uncertainty distributions based on the results of benchmark analyses. Following a description of the formulation of partial factors to consider MU in a semi-probabilistic assessment format (section 5.4.4), section 5.4.5 addresses the model sensitivity to aleatory uncertainties in material properties. Finally, section 5.4.6 provides a practical illustration of how prior modelling uncertainty parameters can be updated using available benchmark data.

5.4.2 Benchmarking

Based on Eq. (59), the modelling uncertainty Θ should be characterized by benchmarking analyses, comparing experimental (R_{exp}) and numerical (R_{NLFEA}) results. The latter are obtained by consistently applying a specific solution strategy during all the benchmark analyses performed, as well as during solution of the actual structural assessment problem it is intended for [95]. This includes consistent modelling assumptions, material models, discretization strategies, and solution algorithms. Any variation in these elements between the benchmarking process and the actual assessment can invalidate the derived uncertainty representation.

The selection of benchmark experiments is critical. The experiments should be chosen to reflect the structurally significant subsets of the actual problem—i.e. they should exhibit similar structural behavior and failure modes to those expected in the structure being assessed. Where the target structure includes multiple behavioral mechanisms, the benchmarking suite should aim to cover these representative conditions.

While there is no strict minimum requirement on the number of experiments, at least 3 relevant and well-documented benchmark tests are recommended to derive a meaningful result for the updated modelling uncertainty following the procedure in section 5.4.3. The analyst is encouraged to perform a larger number of benchmarks since this helps to reduce statistical uncertainty and improve confidence in the resulting parameters of the MU, and hence on the corresponding safety factor.

To limit the influence of material-related uncertainty on the benchmarking outcome, it is recommended to perform specific material testing alongside the structural experiments. The numerical predictions R_{NLFEA} should then be based on the measured material parameters, rather than nominal or assumed values. For geometric properties, nominal values are typically sufficient, unless specific tolerances or imperfections are known to have a critical influence on the response.

Finally, it is important to document all aspects of the benchmark analyses — including experimental setup, boundary conditions, material tests, and the modelling approach — to ensure traceability and facilitate future updates of the modelling uncertainty representation as additional data become available.

5.4.3 Updating based on benchmark studies

If a solution strategy is validated by performing a series of benchmark analyses, the mean μ_Θ and coefficient of variation V_Θ representing the parameters of the lognormally distributed variable Θ can be calculated by Bayesian updating of prior parameters based on the sample mean and variance from the series of

benchmark analyses [95, 45]. From a sample of *n* observations $y_i = \ln(\Theta)_i$, the sample mean $\bar{y}$ and variance s_y^2 can be calculated from Eqs. (60) and (61):

$$\bar{y} = \frac{1}{n}\sum_{i=1}^{n} y_i \tag{60}$$

$$s_y^2 = \frac{1}{n-1}\sum_{i=1}^{n}(y_i - \bar{y})^2 \tag{61}$$

The population mean value and variance of Θ can then be derived from Eqs. (62) and (63), which represent posterior (updated) distribution parameters based on the assumption of a non-informative prior with unknown mean and variance and account for statistical uncertainty due a limited sample size (where $\nu_y = n-1$ degrees of freedom). A non-informative prior means that all values of the mean are assumed equally likely, and all scales of variance are treated without preference. This avoids injecting subjective assumptions about the accuracy of the NLFEA model and ensures that the estimated modelling uncertainty is primarily informed by the benchmark data y_i.

$$\mu_\theta = \exp(\bar{y}^{II}) \tag{62}$$

$$V_\theta = {s_y}^{II}\sqrt{\frac{{\nu_y}''({\nu_y}''+2)}{({\nu_y}''-2)({\nu_y}''+1)}} \tag{63}$$

The posterior parameters $\bar{y}^{II}$, ${s_y}^{II}$ v^{II} and n^{II} are established by Eqs. (54) to (57), where *m* (= $\bar{y}$), *s* (= s_y), v and n are the sample parameters and m^I (= $\bar{y}^I$), s^I (= ${s_y}^I$), v^I and n^I are the prior parameters according to Table 5-3 derived by Engen et al. [95] from a maximum likelihood estimation of a representative range of series of benchmark analyses gathered from the literature. These prior parameters reflect the initial belief on the model uncertainty when applying a specific solution strategy.

Table 5-3: Prior parameters for the distribution of y = ln (Θ) [95, 45]

$\bar{y}^I$	s_y^I	ν^I	n^I	$\delta(n^I)$
0.02	0.1	6.2	1.4	1

Using the updated distribution parameters μ_θ and V_θ determined based on Eqs. (62) and (63), the partial factor accounting for the model uncertainty, γ_{Rd}, can be determined as described in section 5.4.4 below, for use in the direct PFM (section 5.6.2) or the GFM as formulated in the Eurocodes (section 5.7.2). Alternatively, parameters μ_θ and V_θ can be used for calculating the global safety factor γ_R under the approach in the fib MC [45] (see section 5.7.3) or serve as input for a full probabilistic structural assessment.

5.4.4 Partial factors

The partial factor γ_{Rd} accounting for model uncertainties can be obtained based on Eq. (64):

$$\gamma_{Rd} = \frac{\exp(\alpha_{R,ND}\beta_t V_\Theta)}{\mu_\Theta} \tag{64}$$

Where:
$\alpha_{R,ND}$ = Sensitivity factor for non-dominant resistance variables
μ_θ = Mean value of the model uncertainty θ
V_θ = Coefficient of variation of the model uncertainty θ

The parameters characterizing the model uncertainty, $\boldsymbol{\mu_\theta}$ and $\boldsymbol{V_\theta}$, should be deduced from benchmark analyses comparing numerical predictions of the structural capacity with test results (section 5.4). In the exceptional case where no benchmark studies are available for derivation of solution-strategy-specific model uncertainty parameters, the $\boldsymbol{\gamma_{Rd}}$ provided in Table 5-4 can be used for assessment. The Eurocode indicates a default value $\boldsymbol{\gamma_{Rd} = 1.3}$, while the fib MC 2020 **[45]**, based on the work by Engen et al. **[95]**, suggests a slightly higher value ($\boldsymbol{\gamma_{Rd} = 1.35}$). The mentioned study, in which model uncertainty parameters ($\boldsymbol{\mu_\theta}$ and $\boldsymbol{V_\theta}$) were derived from a significant set of benchmark tests, including both the "within" (within a specific solution strategy) and the "between" (between different solution strategies) model uncertainties (section 5.4.3), informed also the determination of the values based on indicative values for $\beta_{t,eco}$ in Table 5-4 for respectively, normal and large safety costs. For the latter case, a slightly lower $\boldsymbol{\gamma_{Rd}}$ is obtained, due to the correspondingly lower target value (see section 5.2).

Table 5-4: Default partial factors for the representation of the uncertainties of NLFEA models for the assessment of existing concrete structures when no benchmark studies are available

PF	Eurocode prEN 1991-1-1, Annex F [50]	Fib MC 2020, section 30.10 [45] *	Based on indicative values for $\beta_{t,eco}$ (CC2) in JCSS PMC, ISO 2394, fib MC (see Table 5-2) *	
			Normal safety costs	Large safety costs
T_{ref} (years)	50	50	1	1
γ_{Rd}	1.30	1.35	1.35	1.26

* Based on benchmark series evaluated in [95].

Note that the adoption of lower γ_{Rd} might be reasonable for simple 2D or 1D models, provided that the failure mode under investigation can be well represented by such a model. For the former, a value $\gamma_{Rd} = 1.15$ was suggested in [96] assuming moderate failure consequences and a 50 year reference period in a comprehensive study including 225 NLFEAs of walls, deep beams and panels. For 1-dimensional beam elements (rods) and bending failure mode, Annex F of [50] suggests $\gamma_{Rd} = 1.06$.

5.4.5 Model sensitivity to probability distribution of materials

When the design structural resistance is evaluated using a non-linear numerical model, consideration should be given to the sensitivity of the model response to the variability of material properties. This was investigated in [97], where it was observed that, when the design ultimate resistance is estimated using a specific NLFEA safety format that does not account for how changes in the structural response and failure mode affect the distribution of structural resistance, the resulting safety level may be inadequate. They proposed to include a partial factor γ_{FM} accounting for the failure-mode sensitivity of the structure.

The suggestion in Annex F of prEN 1992-1-1 [50] to account for this sensitivity is to increase the partial factor γ_{Rd} for the model uncertainties based on Eq. (65). The sensitivity may be assessed by carrying out three preliminary NLFEA simulations with different combinations of material properties with the aim of representing a wide range of possible values for these properties:

(a) Mean concrete properties combined with design reinforcement properties

(b) Design concrete properties combined with mean reinforcement properties

(c) Design concrete properties combined with design reinforcement properties

According to prEN 1992-1-1 [50], if the load-carrying capacities obtained from simulations (a) or (b) are lower than that of case (c), the response is considered sensitive to material variability. In such cases, and unless a more detailed probabilistic analysis is performed, prEN 1992-1-1 Annex F [50] recommends increasing γ_{Rd} by 15%.

The described procedure for assessing the model sensitivity has been conceived for the design of new structures. For the assessment of existing structures, the uncertainties associated with the material parameters can be reduced by means of in-situ tests. Updated probability density functions should be considered for the sensitivity analysis when test results are available (section 5.3).

5.4.6 Example

Problem statement and assumptions

A case study is conducted to demonstrate how Bayesian updating can be applied to quantify and reduce the model uncertainty associated with NLFEA when assessing the resistance of existing RC structures. The context is a scenario in which an engineer intends to evaluate the safety of a simply supported RC bridge girder by means of NLFEA.

Before applying the NLFEA model to the real bridge, the analyst verifies the predictive capability of the chosen solution strategy by performing a set of benchmark analyses. These consist of numerically reproducing previously tested structural members that are considered similar in geometry and reinforcement layout (longitudinal and shear reinforcement), loading and boundary conditions (one- or two-point loaded, simply supported beams), as well as expected failure mechanisms (generally characterized by flexural behavior, in two of the four cases with concomitant shear stresses). Further details of the four benchmark tests considered are provided in section 2.6.1 of this report. For each test, the experimental ultimate load R_{exp} is compared with the NLFEA-predicted ultimate load R_{NLFEA}, resulting in one model uncertainty realization Θ according to Eq. (59).

Two different constitutive models for concrete compression are investigated in the benchmark studies (see section 2.5.1):

- Model *i*: Modified Saenz model [98]
- Model *ii*: Eurocode-2 concrete model [8]

All other modelling choices characterizing the solution strategy, e.g. software (Abaqus 2019), analysis type (displacement-control with step size maximum of 0.01), element types (a truss 2-node linear T2D2 element for rebars and a continuum 8-node linear brick C3D8 element for concrete), mesh size (25-100 mm rectangular mesh), and reinforcing steel constitutive models (ideal elastic-plastic) and boundary conditions (rebars embedded in concrete without bond-slip)—are held constant across all benchmark simulations (see section 2.6.1 for details).

Using these consistent modelling assumptions, the analyst conducts four benchmark analyses for each model variant ($n = 4$ per strategy *i* and *ii*, respectively). The corresponding sample parameters are evaluated based on Eqs. (60) and (61). These sample parameters are then combined with the prior parameter values given in Table 5.3, according to Eqs. (54) to (57), leading to the posterior parameters of the MU distribution.

These are then plugged into (62) and (63) to obtain the population parameters of the model uncertainty distribution, μ_Θ and V_Θ.

Given μ_Θ and V_Θ, the computation of the partial factor γ_{Rd} follows Eq. (64). For the target reliability index, two values are considered, both assuming moderate failure consequences (CC2): i) $\beta_t = 3.3$ ($T_{ref} = 1y$), assuming economic criteria to govern target reliability over human safety, and assuming large relative costs for increasing the safety level of the existing structure, according to the recommendation in [73, 74, 45], see Table 5-2; ii) $\beta_t = 4.7$ ($T_{ref} = 1y$) based on the approach in the Eurocodes [92], see Table 5-1. The sensitivity coefficient for non-dominant resistance variables is taken as $\alpha_{R,ND} = 0.7 \cdot 0.4 = 0.28$ ($T_{ref} = 1y$), following recommendations in [45, 68].

Results and interpretation

Table 5-5 below summarises the benchmark results, the computed sample statistics, the Bayesian-updated posterior parameters, the resulting model-uncertainty statistics μ_Θ and V_Θ, and the corresponding partial factors γ_{Rd} for strategies *i* and *ii*.

Table 5-5: Assumptions and results for the conducted benchmarking case studies for updating of the model uncertainty and the corresponding partial factor gRd based on two different modelling strategies for concrete in compression (i: Saenz model; ii: EC2 model).

Study	Case	Failure mode	R_{EXP} (kN)	$R_{NLFEA,A}$ (kN)	$R_{NLFEA,B}$ (kN)	$R_{exp}/R_{NLFEA,\,i}$	$R_{exp}/R_{NLFEA,\,ii}$
	CS1	flexure (ductile)	13.56	12.80	12.64	1.06	1.07
	CS7	flexure (ductile)	200.18	186.10	179.57	1.08	1.11
	C3	flexure-compression	265.00	273.13	276.95	0.97	0.96
	B1	flexural-shear	497.00	449.00	434.00	1.11	1.15
Sample parameters					**n**	4	4
					ν	3	3
					m	0.050	0.068
					s	0.057	0.079
Posterior parameters					**n''**	5.4	5.4
					ν''	10.20	10.2
					m''	0.043	0.055
					s''	0.084	0.090
Model uncertainty					**μ_θ**	1.043	1.057
					V_θ	0.098	0.105
Partial factor					**$\gamma_{Rd,\beta t=3.3}$**	1.05	1.04
					$\gamma_{Rd,\beta t=4.7}$	1.09	1.09

Figure 5-1 shows the probability density functions (PDF) of Θ before and after combining the sample data with prior information.

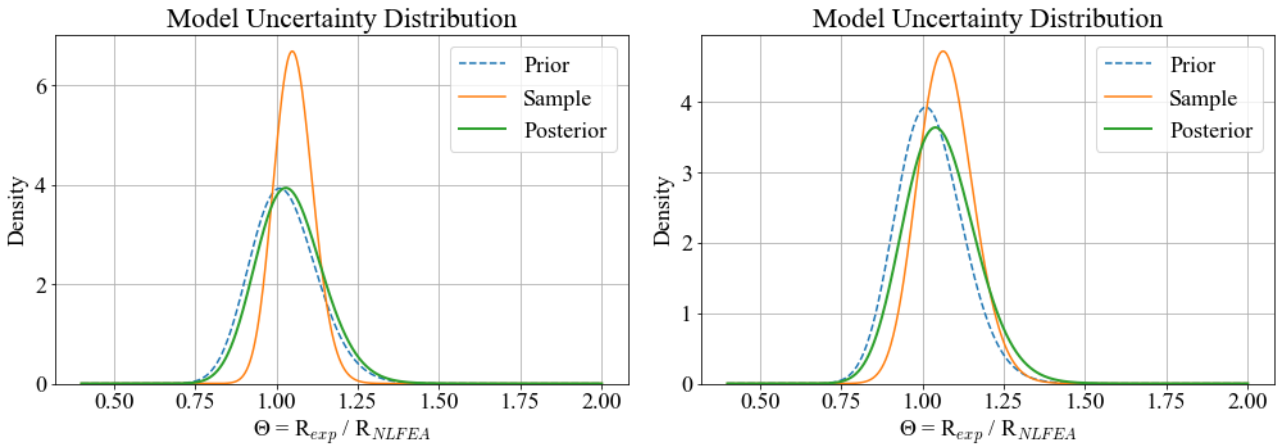

Figure 5-1: Probability density functions (PDF)for the prior, sample, and posterior distributions of the NLFEA model uncertainty Θ associated with two different modelling strategies for concrete in compression (left: model A based on the Saenz model for concrete in compression; right: model B based on the EC2 model).

Figure 5-1 shows that the posterior distributions represent a compromise between the informative sample and the broader prior. Both solution strategies (A, B) yield updated mean values μ_Θ slightly above unity (1.04–1.06), indicating a minor positive bias in the predicted ultimate load. The scatter is modest, with coefficients of variation of around 0.1 on the Θ-scale, which corresponds to typical levels of model uncertainty for nonlinear FE analyses reported in the literature [95]. It should be noted that differences in density peak height between prior, sample and posterior PDFs cannot be interpreted directly as differences in scatter, because the distributions are lognormal and the updating is carried out in ln(Θ). Shifts in the mean on the original Θ-scale influence the height of the density peak independently of the underlying statistical variability.

The similarity of the posterior MU distributions for Model A and Model B supports the conclusion that the dominant contributions to model uncertainty in these cases do not originate from the compressive concrete model but from other aspects of the NLFEA solution strategy. This might have been expected because both sets of benchmark beams are dominated by flexural or flexure-related failure modes, where other parameters including the reinforcement detailing, and the mechanical behaviour of steel govern the resistance to a greater extent than subtle differences in the compressive concrete constitutive law. Thus, the effect of the concrete model (enhanced Saenz vs EC2) on the global load capacity of the benchmark beams is modest. Consequently, the updated parameters μ_Θ, V_Θ, and γ_{Rd} for A and B are very close.

For an annual target reliability of $\beta_t = 3.3$ in line with JCSS, ISO2394 and fib MC recommendations, the analysis yields partial factors $\gamma_{Rd} \approx 1.04 - 1.05$. For the higher target aligned with Eurocode provisions, β_t = 4.7, both strategies produce $\gamma_{Rd} \approx 1.09$. The key observation of this case study is that these updated factors are significantly lower than the γ_{Rd} of, respectively 1.26 (basis for comparison to the γ_{Rd} based on $\beta_t = 3.3$) and 1.3 (basis for comparison to the γ_{Rd} based on the Eurocode for $\beta_t = 4.7$) that would be recommended when no benchmarking data are available, see Table 5-4. This demonstrates a strong incentive for engineers to undertake focused NLFEA benchmarking: a validated modelling strategy can justify substantially lower partial factors, leading to less conservative, more efficient, and evidence-based structural assessments.

5.5 Design actions and action effects

When structural assessment is performed using numerical methods, design values of the relevant actions should be incrementally applied in the correct sequence. Typically, this means that the design value of the permanent actions is applied first, followed by the design value—or, where relevant, the design combination value—of the leading and accompanying variable actions. This sequencing ensures that nonlinear effects, such as cracking, plasticity, time-dependent, or 2nd order effects, are appropriately captured within the numerical analysis. The superposition principle does not apply in case of non-linear structural behavior, see e.g., [68].

Design values and design combination values of the actions are to be determined by using the corresponding load PFs indicated in the relevant standards, regardless if the PFM or the GFM is concerned. Eurocode prEN 1990-2 [50] prescribes the use of fixed load PFs, unless conditions for an adjustment of PFs for actions are given in the National Annex. Such an adjustment can be justified for example in case additional observations on the loads of the structure in question can be gained and the probabilistic models are updated (see section 5.3), see e.g. [99].

It should be noted that the standardised load PFs in codes and standards account for uncertainties associated with the models to establish the corresponding *load effects*. For calculation of the design load effects with NLFE models, this is a conservative approach since it might be assumed that such uncertainties are covered by the γ_{Rd} accounting for model uncertainty, resulting from a benchmark study considering the relevant load configurations and corresponding load effects. It might hence be argued that the contribution of load effect model uncertainty should be excluded from the load PF. Future studies could address this apparent inconsistency in the safety format for structural verifications based on NLFEA.

5.6 Partial factor method

For the verification of structural reliability based on the PFM, two approaches can be distinguished, the indirect and direct assessment method, as further specified in sections 5.6.1 and 5.6.2 below.

5.6.1 Indirect assessment method

In the indirect assessment approach, referred to in prEN1990 [72], as well as in section 30.10.4 of [45], NLFEA can be used to determine action effects for subsequent capacity control of critical cross-sections. Under this approach, the design value of the action effects, F_d, are obtained from the numerical model by sequential application of design values and design combination values of actions (section 5.5). As for the establishment of actions, it is recommended to use updated representative values for material or geometrical parameters when defining the input to the numerical model with the aim of determining F_d. In case uncertainties associated with material properties are not reduced by means of testing, it is advised to check the sensitivity of F_d to the characteristics of the probabilistic distributions of the material properties. Depending on the situation, using mean or even upper characteristic values (e.g., 95% fractile) might lead to higher design actions F_d than when lower characteristic values (e.g., 5% fractile) are used.

The resulting F_d is then compared to the design value for structural resistance (R_d), which is based on codified resistance models representing cross-section capacities as provided in the relevant standard (e.g. Eurocode or National Annex):

$$\mathrm{R}_d = R_{code}(X_{d,code}) \tag{65}$$

Where:

$R_{code}()$ = Structural capacity based on codified resistance models
$X_{d,code}$ = Design values for material properties based on codified material PFs.

The resistance models $R_{code}()$ are applied in conjunction with the material PFs used for ordinary ultimate limit state verifications, which, in addition to material and geometrical uncertainties, account for resistance model uncertainties. Table 5-6 shows the well-known standard PFs recommended in prEN1992-1-1 [50] for design of new structures (γ_C = 1.5, γ_S = 1.15), likewise recommended for the assessment of existing structures in the absence of tests that would allow for a reduction of uncertainties associated with the mechanical or geometrical properties characterising structural resistance - see [50], Annex I. These standard PF have been derived based on Eq. (66), valid as long as the coefficient of variation V_M remains below 0.3 (in this case the error margin of Eq. (66) is around 5%), a target reliability index β_t=3.8 and a standardised sensitivity coefficient $\alpha_{R,D}$ = 0.8 for dominant resistance variables, both associated with a reference period of T_{ref} = 50y, and specific probabilistic modelling assumptions for the relevant basic variables (including resistance model uncertainties) summarised in Annex A of [50]. See [68] for further background on these assumptions.

$$\gamma_M = \frac{\exp(\alpha_{R,D}\beta_t V_M)}{\delta_M} \quad (66)$$

Where:
$\alpha_{R,D}$ = Sensitivity factor for dominant resistance variables
β_t = Target reliability index, see section 5.2
V_M= Coefficient of variation of local structural resistance (i.e. at cross-sectional level, e.g. concrete in compression)
δ_M= Bias factor of local structural resistance (i.e. at cross-sectional level, e.g. concrete in compression)

Similar PFs (γ_C= 1.47, γ_S = 1.14) are obtained when using the indicative annual target reliabilities based on economic optimisation principles recommended in the [73, 74, 45] for the assumption of normal safety costs usually adopted in connection with design of new structures (section 5.2), while keeping the same probabilistic modelling assumptions. Note that while the target reliability index ($\beta_{t,eco}$ = 4.2), has increased with respect to the 50-year Eurocode value, β_t = 3.8, the sensitivity coefficient α_R has been reduced from 0.8 to 0.7 to adjust to the circumstances of an annual reference period (T_{ref} = 1 year) following recommendations in [45].

Table 5-6 further shows that when large safety costs are assumed ($\beta_{t,eco}$ = 3.3), typically relevant for assessment of existing structures (section 5.2), the PFs experience a significant decrease (γ_C= 1.31, γ_S = 1.08) with respect to the normal situation. As already stated in section 5.2, it should be carefully checked if human safety (or eventually environmental) requirements might require higher target reliability levels than the $\beta_{t,eco}$ values assumed for the derivation of the PFs in Table 5-6.

The PFs given in Table 5-6 should be adjusted in case new information on e.g. relevant material or geometrical parameters is obtained from the existing structure (section 5.3). Updating the codified resistance model uncertainties is also possible, see e.g. [100], but comparatively cumbersome and associated with destructive testing, and therefore usually not undertaken in individual structural assessments. Further guidance on adjustment of PFs for existing structures based on site-specific information can be found in [101, 87, 102, 90, 103].

Table 5-6: Partial factors (PFs including resistance model uncertainties) for concrete and reinforcing steel for the assessment of existing concrete structures in conjunction with the indirect assessment method in absence of updated resistance variables.

Partial factor	Eurocode prEN 1990 [72]	Based on indicative values for $\beta_{t,eco}$ (CC2) given in Table 5-2)	
		Normal relative safety costs	Large relative safety costs
T_{ref} (years)	50	1	1
γ_C	1.5	1.47	1.31
γ_S	1.15	1.14	1.08

Finally, it should be mentioned that, while the indirect assessment method is a comparatively straightforward approach for verification of structural safety based on NLFEA, the analyst is advised to carefully check if the simplified standardized resistance models are indeed appropriate for a representation of the non-linear problem under consideration. Contrarily, the direct assessment method (section 5.6.2) or the global factor method (5.7) should be applied instead.

5.6.2 Direct assessment method

Both Annex F to [50] and [45] advocate for the direct assessment method. In this method, both the internal forces or stresses and the structural resistance are, more consistently than under the indirect approach, obtained from the same (numerical) model. Due to its nature to globally represent the structural capacity (not the safety factors), accounting for load redistributions in consequence of non-linear behavior, this method, as well as the global factor methods described under section 5.7, usually lead to a certain safety margin gain compared to local approaches based on component verifications using the partial factor format [104].

The direct assessment method requires an explicit treatment of resistance modelling uncertainty, as this uncertainty is considered on the global capacity level. The design value of the structural capacity is given as:

$$R_d = \frac{R_{NLFEA}(X_d^*)}{\gamma_{Rd}} \tag{67}$$

Where:
$R_{NLFEA}()$ = Structural capacity based on non-linear numerical model
X_d^* = Design values of material properties based on material PFs excluding model uncertainties.
γ_{Rd} = Partial factor accounting for uncertainties of the NLFEA model.

Since the model uncertainties are globally considered, they should not be included in the formulation of the PFs for resistance variables that are input to the numerical analysis. Table 5-7 provides recommendations for default PFs for concrete and reinforcing steel, which consider only material and geometrical uncertainties according to [50, 68]. In an equivalent manner to the derivation of the PFs shown in Table 5-6, these values have been derived based on Eq. (66), in this case excluding model uncertainties. Interestingly, the PFs for the reinforcing steel are higher than compared to the standard case when model uncertainties are included (Table 5-6), what can be attributed to a relatively large bias factor of the resistance model uncertainty for members in bending, as compared to the corresponding coefficient of variation.

It should again be highlighted that care should be taken when relying on the β_{eco} targets, assuring the fulfilment of minimum requirements for human safety (section 5.2). In addition, it is insisted here that both characteristic values and the provided default PFs should, whenever possible, be updated based on

information on material or geometrical properties obtained from the existing structure object of the assessment, see section 5.3.

Table 5-7: Partial factors (excluding resistance model uncertainties) for concrete and reinforcing steel for the assessment of existing concrete structures in conjunction with the direct assessment in absence of updated resistance variables.

PF	Eurocode prEN 1992-1-1, Annex A [50]	Based on indicative values for $\beta_{t,eco}$ (CC2) in Table 5-2	
		Normal relative safety costs	Large relative safety costs
T_{ref} (years)	50	1	1
γ_c	1.46	1.43	1.30
γ_s	1.20	1.19	1.14

To determine the ultimate structural capacity $R_{NLFEA}()$, design values of the actions in the considered combination must be increased incrementally until structural failure occurs (according to a previously defined failure criterion). As expressed by Eqs. (50) and (67), structural safety according to the direct assessment method is verified if $R_{NLFEA}(X_d^*)$ equals or exceeds $\gamma_{Rd} \cdot F_{Ed}$, with partial factor γ_{Rd} accounting for model uncertainty obtained from Eq. (64). While it is possible to stop the incremental loading once this criterion is fulfilled, doing so omits valuable information on the structure's reserve capacity.

5.7 Global factor method

5.7.1 General

Different global safety factor approaches have been developed in the past, with different conclusions regarding the effectiveness and level of user-friendliness of structural safety assessments as well as regarding the associated safety margins [104, 105, 97, 106, 107]. In this report, the global factor methods (GFM) put forward in [50] (section 5.7.2) and [45] (section 5.7.3) are referred and corresponding background information provided.

5.7.2 Eurocode

The GFM as included in Annex F of [50], also known as ECoV method, see e.g. [104], follows a similar approach as the direct PFM (section 5.6.2). Both approaches treat resistance model uncertainties globally, i.e. at the structural capacity level. The main difference lies in the consideration of material and geometrical uncertainties.

In the GFM, the design value of the structural capacity, R_d, is represented by the mean value of structural resistance based on the numerical simulation $R_{m,NLFEA}(x, a)$ divided by a global factor γ_R^* that accounts for the uncertainties affecting material and geometrical properties, and γ_{Rd} considering model uncertainties according to Eq. (68):

$$R_d = \frac{R_{m,NLFEA}(x, a)}{\gamma_R^* \cdot \gamma_{Rd}} \cong \frac{R_{NLFEA}(x_m, a_{nom})}{\gamma_R^* \cdot \gamma_{Rd}} \quad (68)$$

Where:

$R_{m,NLFEA}()$ = Mean value of structural capacity based on non-linear numerical model

$R_{NLFEA}()$ = Structural capacity based on non-linear numerical model

x = Material properties.

x_m = Mean values for material properties.
a = Geometrical properties.
a_{nom} = Nominal values for geometrical properties.
γ_{Rd} = Partial factor accounting for uncertainties of the NLFEA model, determined as described under section 5.6.2.
γ_R^* = Global factor accounting for aleatoric uncertainties in material and geometrical properties.

The mean value of structural capacity $R_{m,NLFEA}(x, a)$ can be obtained based on a probabilistic analysis, e.g. crude Monte Carlo or Latin hypercube sampling, and include aleatory uncertainties inherent to material and geometrical variables. Alternatively, and for sake of simplicity, [50] allows the approximation of $R_{m,NLFEA}(x, a)$ by $R_{NLFEA}(x_m, a_{nom})$, i.e. performing the numerical analysis based on mean values for material properties x_m and nominal values a_{nom} for geometrical properties. This simplification, which implies the assumption of a unitary bias factor for structural resistance (δ_R = 1.0), has been found to lead to relatively small errors in several investigations, e.g. [105]. Note that for the assessment of existing structures, updated values for material and geometrical properties should be preferably used as input to the numerical model $R_{NLFEA}()$, see section 5.3.

The global safety factor γ_R^* is determined according to Eq. (69):

$$\gamma_R^* = \exp(\alpha_{R,D}\beta_t V_R^*) \tag{69}$$

Where:
V_R^* = Coefficient of variation of structural capacity, accounting for material and geometrical uncertainties.
$\alpha_{R,D}$ = Sensitivity factor for dominant resistance variables.

The coefficient of variation V_R^* can be obtained by means of a probabilistic analysis of the structural capacity. However, the efforts for conducting such an analysis with the aim to subsequently use the results in a safety verification format with a comparatively lower level of detail regarding the uncertainty representation (safety factor format vs full probabilistic format) does not seem to be justified. Alternatively, [50] proposes to determine V_R^* from Eq. (70):

$$V_R^* = \sqrt{V_{R,M}^2 + V_{R,G}^2} \tag{70}$$

Where:
$V_{R,M}$ = Coefficient of variation of structural resistance accounting for uncertainties of material properties.
$V_{R,G}$ = Coefficient of variation of structural resistance related to geometrical uncertainties, evaluated in line with Annex A of [50].

It should be noted that geometrical uncertainties can be neglected in many cases ($V_{R,G}$ = 0). However, there might be situations where structural resistance and failure modes might be sensitive to such uncertainties, as for example is the case for slender columns [68].

The CoV accounting for uncertainties in the material properties $V_{R,M}$ can be inferred from Eq. (71), which assumes a lognormally distributed structural resistance and a corresponding characteristic value associated with a 5% fractile:

$$V_{R,M} = \frac{1}{1.65} \ln \left(\frac{R_{NLFEA}(x_m, a_{nom}}{R_{NLFEA}(x_k, a_{nom}} \right) \quad (71)$$

Where:
$R_{NLFEA}(x_m, a_{nom})$ = Structural capacity based on non-linear numerical model and mean values of material properties, see Equation (68).
$R_{NLFEA}(x_k, a_{nom})$ = Structural capacity based on non-linear numerical model and characteristics values of material properties.

If available, updated geometrical or material properties should be used when evaluating $V_{R,M}$ and $V_{R,G}$ (section 5.3). In absence of a proper estimation of $V_{R,M}$, [50] proposes to adopt a value of 0.15, assuming that the most conservative situation is the one where material uncertainty of concrete governs and propagates linearly through the resistance model (unless the National Annex proposes another value).

5.7.3 Fib Model Code

On the other hand, the fib MC 2020 advocates for a different formulation of R_d, where aleatory uncertainty (e.g. material and geometrical uncertainties), on one hand, and model uncertainties, on the other, are merged into one global safety factor γ_R, as defined by Eqs. (72) and (73):

$$R_d = \frac{R_{m,NLFEA}(X,a)}{\gamma_R} \cong \frac{R_{NLFEA}(x_m, a_{nom})}{\gamma_R} \quad (72)$$

$$\gamma_R = \frac{\exp(\alpha_{R,D} \beta_t V_R)}{\mu_\Theta} \quad (73)$$

Where:
V_R = Coefficient of variation of structural capacity, accounting for material and geometrical uncertainties as well as model uncertainty.
μ_Θ = Mean value of the model uncertainty θ (see section 5.4.3).
$\alpha_{R,D}$ = Sensitivity factor for dominant resistance variable covering both aleatory and epistemic uncertainties
γ_R = Global factor accounting for uncertainties in material and geometrical properties, as well as model uncertainties.

Assuming statistical independence between model uncertainty, material and geometrical variables, V_R can be estimated by means of the following expression:

$$V_R = \sqrt{V_{R,M}^2 + V_{R,G}^2 + V_\Theta^2} \quad (74)$$

Where:
$V_{R,M}$, $V_{R,G}$: as defined under the Eurocode approach.
V_Θ = Coefficient of variation of the model uncertainty θ (see section 5.4).

Recent research suggests that the approach based on a single global safety factor for structural resistance outperforms the simplified approach with separate treatment of aleatory and epistemic uncertainties. A set of NLFEAs of 56 different RC columns, walls and deep beams, representing a broad spectrum of structural failure modes, evaluated based on these two methods, showed a slightly higher accuracy for the single factor

approach in the estimation of the global safety factors when compared to the safety factors derived from a full probabilistic analysis of structural resistance [105]. Similarly, Gino et al. determined global safety factors in non-linear analysis of RC beams failing in shear for the two methods and compared the result to safety factors based on a probabilistic simulation of structural resistance [107]. The findings indicate that the approach based on the separate safety factors may lead to unconservative estimates in cases of ductile shear failures where stirrups have yielded, whereas the joint safety factor approach provided a closer match across all observed shear failure modes.

The sensitivity of the results of a NLFEA-based safety assessment with respect to the variability in the structural failure modes is an ongoing research field. The adoption of a single global safety factor eliminates the need to make assumptions about the dominance or non-dominance of either type of uncertainty (aleatory vs. model uncertainty), what constitutes especially an advantage for situations where the expected failure mode is *a priori* not evident and where it is uncertain that the usual assumption of non-dominant model uncertainties will hold [105].

Specific attention should be paid when the global failure mode is the result of two or more local mechanisms concurrently reaching failure at the approximately same load level since this will contribute significantly to a system failure probability. The local failure mechanisms might be correlated through correlations in common basic variables involved. In case of two correlated mechanisms, Eq. (72) applies. For two or more uncorrelated local failure mechanisms, the formulation of the global PF should account for system behavior under distinction of parallel or series systems. In this case, a more thorough assessment is needed. The reader is referred to [45] section 30.10.3.4 for more specific guidance.

It should be noted that within the global safety format based on a joint safety factor accounting for both aleatory and epistemic uncertainties, it is not possible to make use of default PFs γ_{Rd} in case no benchmark test are available for assessing the model uncertainty (MU). The Model Code advises the user to always do benchmarking when using the GFM.

5.8 Application example

5.8.1 Objective and scope

A case study is presented to demonstrate the structural assessment of a RC beam by integrating i) the insights obtained from the NLFE modelling described in section 2, ii) the proposed reduction factors to represent the effects of reinforcement corrosion on the geometric and material properties of steel (section 4), and iii) the different formats for interpreting results of NLFEA in terms of structural safety, introduced in the preceding subsections.

The case study adopts several simplifying assumptions. These simplifications are intentional: the objective is to illustrate the application of the proposed procedure and the associated methods for safety verification using NLFEA, rather than to reproduce the full complexity of a specific real-world structure. Nevertheless, the adopted assumptions remain sufficiently representative of practical assessment conditions to provide meaningful insight for practicing engineers.

The case study compares structural performance and safety outcomes under the assumptions of sound and corroded steel, illustrating the influence of degradation on both capacity prediction and safety margins. Safety verifications are demonstrated using the following methods introduced in earlier sections:

- A. Partial Factor Method (PFM) based on the direct assessment approach (section 5.6.2).
- B1. Global Factor Method (GFM) based on the two-factor approach (section 5.7.2).

- B2. Global Factor Method based (GFM) on the one-factor approach (section 5.7.3).

Section 5.8.2 sets out the assumptions on the structural system and loads, deterioration scenarios, as well as on the material and geometrical parameters. Subsequently, section 5.8.3 briefly outlines the NLFE solution strategy, followed by section 5.8.4, which presents the results of the numerical simulations. Based on these results, section 5.8.5 illustrates the structural safety verifications, including a comparative discussion of the resulting safety margins.

5.8.2 Assumptions

5.8.2.1 Structural system and loads

The case study assumes an 50y old, simply supported RC beam representative of a bridge girder. Structural safety of the girder in its current condition should be assessed by means of a NLFEA.

The beam spans over L= 2.6 m between supports and is loaded by two concentrated design loads $F_{Ed}/2$ at 800mm from the supports, see Figure 5-2. For sake of simplicity, self-weight and other loads to be accounted for in realistic assessment conditions are neglected here.

The beam's cross-section dimensions (T cross-section between supports, while rectangular cross-section beyond supports) and reinforcement arrangement correspond to case study CS7 in section 2.6.1, see also Figure 5-2 below. The longitudinal reinforcement consists of 2 rebars of ϕ = 20 mm in the tensile layer and 4ϕ4 rebars in the compression layer. Shear is resisted by ϕ = 6 mm stirrups disposed at a typical distance of 120 mm.

The structure is assumed to be classified into consequence class CC2. Expected economic failure consequences (e.g. due to need for bridge closure and replacement) are considered to prevail over potential risks to persons.

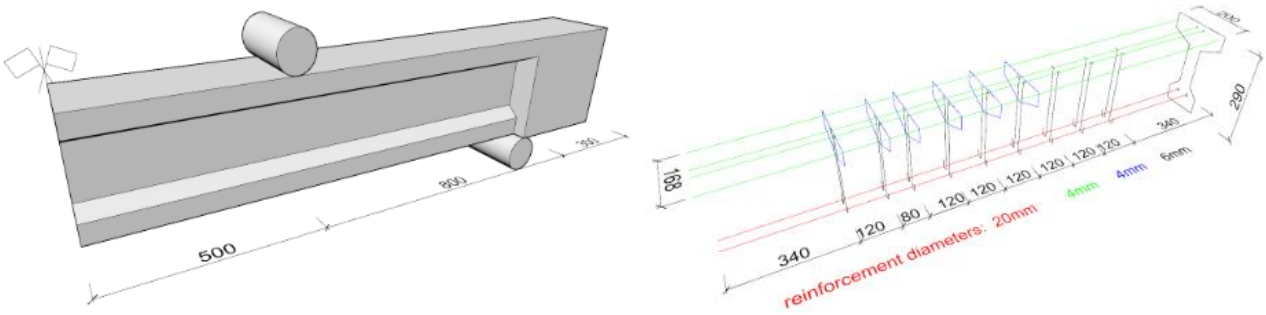

Figure 5-2: Representation of the case study beam geometry and reinforcement arrangement

5.8.2.2 Corrosion scenario

The beam is assumed to have experienced a 50-year exposure to cyclic wet and dry conditions favouring carbonation-induced corrosion while not exposed to chlorides. It is out of scope of this case study to describe how these exposure conditions translate into an estimation of a corrosion penetration depth P_x of the rebars and how to account for the associated uncertainties. It is also not considered herein how corrosion rate measurements can potentially lower such uncertainties. For deeper insight into these aspects, the reader is referred to e.g. [108, 109, 110, 45]. Herein, it is assumed that that the depassivation front has reached the rebar surface of the three beam reinforcement types (tensile, compression, and shear reinforcement) at the same time and induced an estimated average corrosion penetration depth P_x of 0.3 mm after the 50 year exposure of the beam. From P_x, an average corrosion rate ξ reflecting mass loss is then derived depending

on the rebar diameter based on Eq. (27), where a pitting factor of $\alpha = 2$ is adopted, representing carbonation-induced, uniform corrosion. The resulting ξ are summarised in Table 5-8.

Table 5-8: Average corrosion degree based on an assumed average penetration depth P_x = 0.3mm

Reinforcement type	Tensile (ø=20 mm)	Compression (ø=4 mm)	Shear (ø=6 mm)
Average corrosion degree ξ	0.059	0.278	0.19

5.8.2.3 Material and geometrical properties

For sake of this case study, it is assumed that information on the grades of both concrete and reinforcing steel is available from design project documentation. It is further assumed that the engineer in charge of the structural assessment decides, in a first approximation, to base the structural performance assessment on this prior information. As stated before, narrowing down the uncertainties associated with the material properties by testing and subsequent updating of the prior information is recommended whenever technically and economically feasible. In general terms, such an uncertainty reduction will reflect in lower characteristic values and safety factors and hence in a benefit when it comes to the assessment of structural safety. Especially in the context of cost and time-intensive NLFEA-based assessment, the efforts and corresponding costs required for conducting material testing may be considered relatively small. In this case study, however, the assessment will be based exclusively on prior data.

The material properties for sound reinforcing steel and concrete assumed in the assessment are summarised in Table 5-9 andTable 5-9: Material properties of reinforcing steel assumed in the calculations

Table 5-10 below. The indicated properties are in line with Eurocode 2 models for steel B500 (ductility class B) and concrete C35/40. To enable a comparison of the different safety formats described in the previous sections, mean values, characteristics values as well as design values are indicated. To demonstrate safety verifications based on the partial factor method (approach A), the indicated design values have been obtained with partial safety factors γ_s and γ_c that exclude the influence of model uncertainties (see Table 5-7), distinguishing two different scenarios, i.e. scenario X_{d1}: $\gamma_s = 1.2$ and $\gamma_c = 1.46$ based on target reliability β_t as formulated in [72] and scenario X_{d2}: $\gamma_s = 1.14$ and $\gamma_c = 1.3$ based on an annual $\beta_{t,eco} = 3.3$ as proposed in [45, 74]. Human safety considerations that may generally condition the choice of β_t (see section 5.2) are not considered of relevance for this case study.

It should be noted that in a realistic assessment situation, material properties should align with the definitions, models and statistical characterizations underlying the structural standards used when the structure was designed, rather than reflecting provisions and models in current codes. A realistic assessment should also account for time-dependent alterations of the material properties, such as the effect of sustained loading on concrete resistance, creep or shrinkage effects, and the potentially substantial increase of the concrete strength over time (with respect to the 28d strength). Herein, such effects have been ignored.

Geometrical properties of the concrete cross-section and the sound rebar cross-section sound bars are represented by their nominal values throughout the study.

Table 5-9: Material properties of reinforcing steel assumed in the calculations

Property	Variable	*Mean values (X_m)*		*Characteristic values (X_k)*		*Design values (X_{d1}) based on $\beta_{t,prEN1990}$*		*Design values (X_{d2}) based on $\beta_{t,ISO2394/fibMC2020/JCSS}$*	
		Sound	*Corr.*	*Sound*	*Corr.*	*Sound*	*Corr.*	*Sound*	*Corr.*
Yield strength	f_y (N/mm²)	538.4	473.8	500	440	416.7	367	438.6	386
Ultimate strength	f_u (N/mm²)	581.5	520.4	540	483.3	450	402.8	473.7	423.9
Yield strain	ε_y (-)	0.00269	0.00255	0.0025	0.00237	0.00208	0.00197	0.00219	0.00207
Ultimate strain	ε_u (-)	0.05	0.04285	0.05	0.04285	0.04167	0.03571	0.04386	0.03759
Modul. of elasticity	E_s (N/mm²)	200000	186000	200000	186000	200000	186000	200000	186000

Table 5-10: Material properties of concrete assumed in the calculations

Property	Variable	*Mean values (X_m)*	*Characteristic values (X_k)*	*Design values (X_{d1}) based on $\beta_{t,prEN1990}$*	*Design values (X_{d2}) based on $\beta_{t,ISO2394/fibMC2020/JCSS}$*
Compressive strength	f_c (N/mm²)	41.3	35	24	26.9
Strain at max. stress	ε_{c1} (-)	0.00242	0.00242	0.00242	0.00242
Ultimate strain	ε_{cu1} (-)	0.0035	0.0035	0.0035	0.0035
Modulus of elasticity	E_c (N/mm²)	32827	32827	22484	25251
Tensile strength	f_{ct} (N/mm²)	3.2	2.2	1.51	1.69

The impact of the carbonation-induced corrosion on the rebar properties is estimated based on the formulations for approximate reduction factors k_{red} given in section 4.3.4 and the average corrosion degrees ξ given in Table 5-8.

Table 5-11 summarises these factors for the three different rebar diameters corresponding to the three reinforcement types. The modified material properties based on k_{red} are shown in Table 5-9.

According to prEN1992-1-1 (Annex I), it may be assumed that the complete concrete section contributes to the resistance for penetration depts P_x < 0.2 mm to 0.4 mm. Consequently, corrosion-induced concrete spalling has not been accounted for in this case study, nor any other deterioration mechanisms of concrete.

Table 5-11: Reduction factors for reinforcing steel assumed in the calculations

Reinforcement type		Tensile (ø=20 mm)	Compression (ø=4 mm)	Shear (ø=6 mm)
Material property	**Variable**	**Reduction factors k_{red}**		
Rebar cross-section	A_s	0.941	0.723	0.81
Yield strength	f_y	0.929	0.667	0.772
Ultimate strength	f_u	0.938	0.709	0.801
Yield strain	ε_y	0.969	0.828	0.89
Ultimate strain	ε_u	0.916	0.604	0.729
Modulus of elasticity	E_s	0.959	0.806	0.867

5.8.3 NLFEA solution strategy

The NLFEA model used for simulating the beam performance is elaborated using Abaqus 2019 with the following modelling attributes - analysis type: displacement-control with step size maximum of 0.01; element types: truss 2-node linear T2D2 element for rebars and a continuum 8-node linear brick C3D8 element for concrete; mesh size: 25-100 mm rectangular mesh; material models: ideal elastic-plastic behaviour for reinforcing steel., modified Sanz model for concrete in compression and concrete damaged plasticity (CDP) for concrete in tension; boundary conditions: rebars embedded in concrete without bond-slip.

The loads *Q* are applied until numerical instability occurs in the post-peak range. The ultimate (maximum) load-carrying capacity R_{NLFEA} is registered. Note that in this simplified case with only one load, no partial factors have been applied to the loads. In a realistic situation, where combinations of both permanent and variable loads might be expected, one would typically first apply the design value of the former, followed by a step-wise increment of the latter until failure.

5.8.4 Results of the numerical simulation

Figure 5-3 shows the load-deflection curves of the beam as obtained in the numerical simulation of the beam under the assumed loading scenario and the different realisations for material properties given in Table 5-9 and Table 5-9: Material properties of reinforcing steel assumed in the calculations

Table 5-10. Table 5-12 provides the corresponding maximum load bearing capacity R_{NLFEA} of the beam. As expected, the results based on mean values entail the highest load-bearing capacity, followed by the characteristic value combination, and the design value combinations X_{d2} and X_{d1}. The loss of load bearing capacity R_{NLFEA} of the beam with deteriorated reinforcement with respect to the sound beam is of the order of, respectively 13%, 8% and 14% when interpreted in terms of mean, characteristic, and design values. Given that for all these situations (mean, characteristic and design values) the same reduction factors k_{red} have been used for defining the stress-strain relationships of the deteriorated steel, the comparatively lower percentage for the characteristic combination is unexpected.

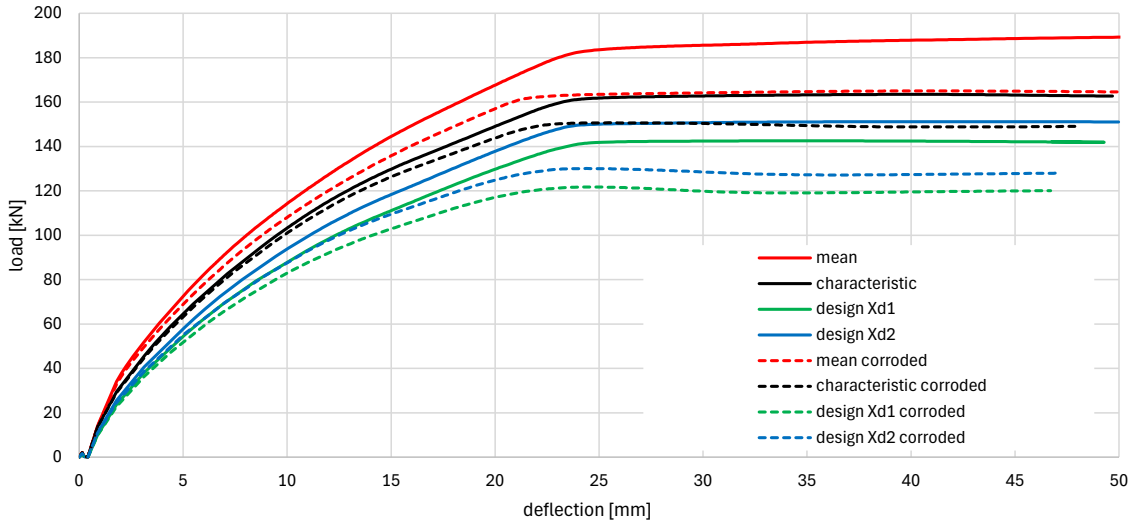

Figure 5-3: Results of the numerical simulations of the beam with sound and corroded reinforcement under use of mean, characteristic and design values (X_{d1} and X_{d2}).

Table 5-12: Maximum load resisted by the simulated beam

	$R_{NLFEA}(X)$ [N]			
Assumption for condition of reinforcing steel	Mean values (X_m)	Characteristic values (X_k)	Design values (X_{d1})	Design values (X_{d2})
Sound steel	189354	163487	142565	151177
Corroded steel: P_x = 0.3mm	165043	150674	121789	130065
Difference [%]	12.8%	7.8%	14.6%	14.0%

5.8.5 Structural safety assessment

5.8.5.1 Model uncertainty

The partial factor γ_{Rd} accounting for model uncertainty is adopted from the case study described in section 5.4.6 of this report, where four benchmark studies were performed using the same numerical solution strategy as used in the present case study – in particular solution strategy *i* using the enhanced Saenz Model for representing the performance of concrete in compression. As summarised in Table 5-5, the assessment of these benchmark studies concluded with γ_{Rd} = 1.09 based on the annual reliability requirement $\beta_{t=4.7}$ in the Eurocodes, and slightly lower γ_{Rd} = 1.05, when β_t =3.3 as advocated for in [74, 45]. Partial factor γ_{Rd} is used in connection with the safety verifications based on the direct PFM, as well as for the GFM as formulated in the Eurocodes [50].

For assessing structural safety based on the GFM as proposed in the fibMC 2020, the updated parameters of the model uncertainty Θ, μ_Θ =1.043 and V_Θ = 0.098 are adopted for computing the design value of the global structural resistance R_d, see Table 5-5.

As stated in section 5.4.5, it is recommendable to analyse the sensitivity of the NLFEA model to the variability of the material parameters, especially if the assessment relies on prior information only as assumed herein. For this purpose, Eurocode prEN1992 Annex F proposes to analyse the structural response based on different combinations of mean and design values for, respectively, concrete and steel: *a*: mean values for concrete and design values for steel; *b*: design values for concrete and mean values for steel; *c*: design values for both (i.e. concrete and steel). In case either combination *a* or *b* leads to a more unfavourable result than combination *c*, the model response should be judged as sensitive to variability in the material parameters with a corresponding increase of the γ_{Rd}.

Figure 5-4 shows the results of this sensitivity analysis. Regardless of the combination of mean and design values analysed, the structural response is governed by flexural, ductile behaviour. The design value combination X_{d1} (which is the critical among X_{d1} and X_{d2} due to the higher partial factors γ_C and γ_S), entails the lowest load bearing capacity, i.e. in this context the most unfavourable result. Hence, under the studied load scenario, the NLFE model response might be judged as insensitive to variations in the material properties. Note that this could change e.g. if more shear-critical load scenarios would be studied, such as e.g. significant point loads close to the beams supports.

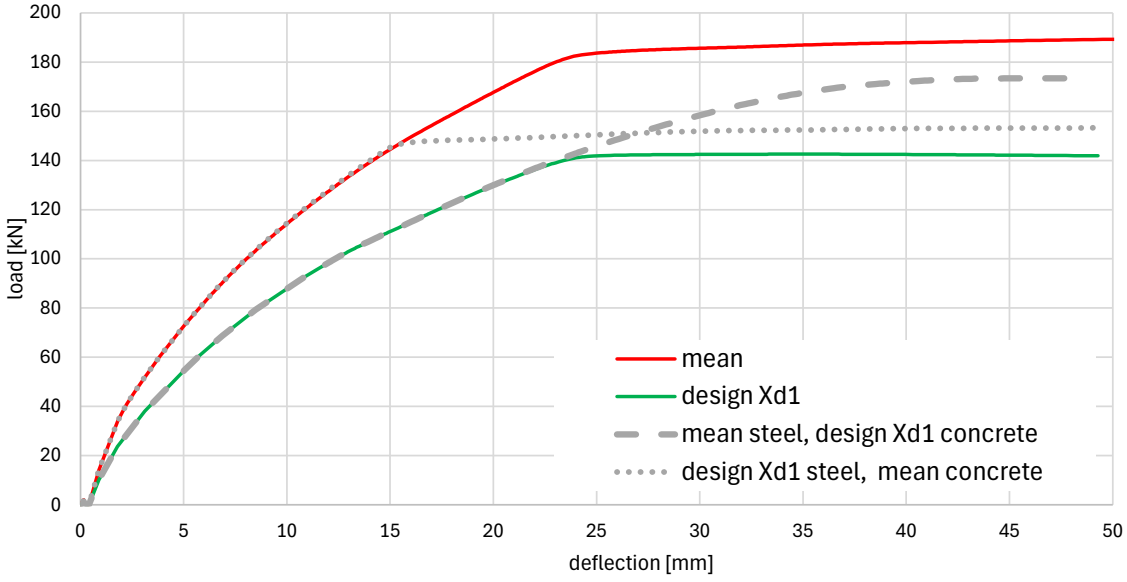

Figure 5-4: Results of the model sensitivity analysis under varying combinations of mean and design values for the material parameters.

5.8.5.2 Verifications

A: PFM (direct assessment approach)

Table 5-13 summarizes the design values R_d of structural resistance of the beam according to the PFM (section 5.6.2). For design value combination X_{d1}, based on the conservative Eurocode requirements for the target reliability level, the assessment concludes with a design resistance of around 131 kN for the assumption of sound reinforcing steel, and around 112 kN for the corroded steel. For combination X_{d2}, we obtain a design resistance R_d of the order of 10% higher, resulting in around 144 kN and 124 kN, respectively for sound and corroded steel.

Table 5-13: Summary of results for approach A

Design value combination			X_{d1}	X_{d2}
Partial safety factors		**Unit**	**Value**	
Concrete	γ_C	-	1.46	1.3
Steel	γ_S	-	1.20	1.14
Model uncertainty	γ_{Rd}	-	1.09	1.05
Design value of structural resistance				
Sound steel	$R_{d,sound}$	kN	130.8	144.0
Corroded steel	$R_{d,corr}$	kN	111.7	123.9
Difference	$\Delta R_{d,sound-corr}$	%	-14.6	-14.0

B1: GFM (two-factor approach)

Table 5-14 summarizes the results for approach B1, i.e. the GFM based on the two-factor approach treating aleatory and epistemic uncertainties with separate safety factors, as recommended in prEN1992-1-1 (section 5.7.2).

The coefficient of variation representing variability of the material parameters, $V_{R,M}$ has been obtained according to Eq. (71). The comparatively lower result for corroded steel is due to the closer approximation of mean and characteristic capacity $R_{NLFEA}(X)$ than for the sound beam, clearly visible in Figure 5-3. For the geometrical uncertainties, $V_{R,G} = 0.05$ has been adopted, representing variability in the static depth *d* of the critical beam cross-section, see [68, 50]. The coefficient of variation of structural resistance V_R* (excluding model uncertainty) is then estimated based on Eq. (70). Table 5-14 depicts the results for the sound and corroded beam, respectively, $V_{R,sound}$* and $V_{R,corr}$* - the latter somewhat lower due to the comparatively lower $V_{R,M}$. This appears to be a counter-intuitive result, since one might expect the corrosion attack to increase the uncertainties associated with structural resistance. This highlights the need for more sophisticated modelling approaches to represent both the physical impacts of corrosion on the properties of reinforcing steel as well as the associated uncertainties.

Taking the derived V_R* as input, the global safety factors γ_R* are then obtained based on β_t=4.7 and $\alpha_{R,D}$=0.7 - the results are shown in Table 5-14. Factoring in model uncertainty factor γ_{Rd}, the design values of structural resistance R_D are finally inferred from Eq. (68), resulting in around 124 kN and 119kN, respectively for sound and corroded steel.

Table 5-14: Summary of results for approach B1

Coefficients of variation		Unit	Value
Material, sound steel	$V_{R,M,sound}$	-	0.089
Material, corroded steel	$V_{R,M,corr}$	-	0.055
Geometry	$V_{R,G}$	-	0.050
Structural resistance, sound steel	$V_{R,sound}$*	-	0.102
Structural resistance, corroded steel	$V_{R,corr}$*	-	0.074
Safety factors			
Global safety factor, sound steel	$\gamma_{R,sound}$*	-	1.40
Global safety factor, corroded steel	$\gamma_{R,corr}$*	-	1.28
Model uncertainty	γ_{Rd}	-	1.09
Design value of structural resistance			
Sound steel	$R_{d,sound}$	kN	124.2
Corroded steel	$R_{d,corr}$	kN	118.5
Difference	$\Delta R_{d,sound-corr}$	%	-4.5

B2: GFM (one-factor approach)

Table 5-15 summarizes the results for approach B2, i.e. the GFM based on the one-factor approach treating aleatory and epistemic uncertainties with a common safety factor, as recommended in the fib MC2020 (section 5.7.3).

The coefficients of variation V_R shown in Table 5-15 account for model uncertainties, explaining their substantially higher values compared to the V_R* values in Table 5-14.

Global safety factors are then obtained – note that unlike the γ_R* given in Table 5-14, the obtained γ_R are based on β_t=3.3, given that the assessment is performed in the fib MC2020 environment. Finally, the design values of structural resistance R_d are derived from Eq. (72), leading to around 142 kN and 130 kN, respectively for sound and corroded steel.

Table 5-15: Summary of results for approach B2

Coefficients of variation		Unit	Value
Model uncertainty	μ_Θ	-	1.043
	V_Θ	-	0.098
Structural resistance, sound steel	$V_{R,sound}$	-	0.142
Structural resistance, corroded steel	$V_{R,corr}$	-	0.123
Safety factors			
Global safety factor, sound steel	$\gamma_{R,sound}$	-	1.33
Global safety factor, corroded steel	$\gamma_{R,corr}$	-	1.27
Design value of structural resistance			
Sound steel	$R_{d,sound}$	kN	142.4
Corroded steel	$R_{d,corr}$	kN	129.5
Difference	$\Delta R_{d,sound-corr}$	%	-9.0

5.8.5.3 Comparison

The results presented in the previous section can be compared from different perspectives. First, as expected, do the approaches based on lower target reliability β_t, which follow the recommendations in the fib MC2020 and the consensus in the scientific literature that the assessment of existing structures is typically associated with large relative costs for incrementing the safety level, lead to higher design capacities R_d than compared to the Eurocode assessments. Depending on whether the comparison is conducted within the PFM or within the GFM (), the different reliability requirements β_t (Approach A, X_{d1} vs. X_{d2}; Approach B1 vs. B2) translate into differences in R_d of the order of 10-15%.

When focusing on results based on the same β_t, consistent comparisons between the PFM and the GFM can be conducted. In the Eurocode environment (β_t=4.7), the PFM (A-X_{d1}) leads to a design resistance R_d about 5% higher than the GFM (B1) if the uncorroded situation is considered. Contrarily, for the corroded beam scenario, the results of the GFM exceed those of the PFM by about 6%. As mentioned before, this can be attributed to a comparatively low ratio of mean to characteristic capacity $R_{NLFEA,corr}(X_m)/R_{NLFEA,corr}(X_k)$, i.e. low in comparison to the same ratio obtained under the sound reinforcement assumption. A similar conclusion is obtained when conducting the comparison between PFM and GFM under the β_t=3.3 assumption. In this case, the results for the sound rebar assumption are almost identical, while for the deterioration assumption the R_d for approach B2 exceeds the result for approach A-X_{d2} in about 5%. It can be concluded that for the case study conducted, both approaches, the PFM and the GFM, deliver similar and consistent results.

The findings discussed above are strictly valid for the specific case study considered herein and should not be interpreted as generally applicable without further examination, as the relative performance of the PFM and GFM may be influenced by a range of factors. These include, e.g., the structural typology and geometry, the governing failure modes (especially in case of several, simultaneously concurring failure modes), or the applied loading scenarios and load combinations. Furthermore, differences in uncertainty levels associated with material properties, geometry, and model uncertainty may affect the design resistances. Consequently, while the present case study demonstrates internal consistency between the investigated approaches, care should be taken when extending these conclusions to other problems.

6 Necessary input on deterioration from field observations and service life models

6.1 ASR

As described in section 3.2 all concrete expansion-based models are based on the concept of free ASR expansion. i.e, the ASR induced expansion that would have occurred for the same concrete under the same environmental conditions but without stress. This parameter is, however, in almost all cases unknown in an arbitrary concrete structure which has not been monitored from the start of the service life. The magnitude and distribution of the free expansion may also vary in different parts of the structure. This may be a significant contributor to restraint moments and axial forces. Such cases typically occur if some parts of the structure have a higher moisture than others due to for example weather conditions or lack of membrane. Variations in concrete compositions, e.g. use of different types of aggregates in different parts of a structure or due to reconstruction and rehabilitation may also lead to variable expansion.

6.1.1 Estimation of the free expansion using mechanical testing

The R&D-project “Better Bridge Maintenance” carried out by the Norwegian Public Road Administration had through the PhD-work by Kongshaug and Stemland [19] [20] a large focus on estimating the expansion in an arbitrary structure through material testing.

In [19] [20] specimens with a reactive concrete similar to that used for Norwegian infrastructure in the 50s and 60s are expanded to different expansion levels and tested according to a particularly mechanical test method, the Stiffness damage test (SDT) to characterize the material degradation. This test consists of five load cycles in compression up to 40 % of the specimens' 28-day strength [111]. The difference between the loading and unloading secant modulus creates an energy dissipation (hysteresis), which can be directly related to microcrack activity. In [20] the main damage parameters from the tests are the Stiffness Damage Index (SDI), which is the ratio between the sum of the hysteresis or dissipated energy and the total applied energy to the system for the five cycles, and the average secant E-modulus of the last loading and unloading curve (cycle number 5) divided by a reference E-modulus for undamaged concrete (E_5/E_{ref}). The relationships between these damage parameters and the expansion of the samples in the test direction are shown in **Figure 6-1**, for the SDI and E_5/E_{ref} relationships, respectively. Here, both a linear and polynomial regression function are shown in addition to the regression function by [24], similarly to the results in Figure 3-2 for the same concrete. The samples shown in these figures was not exposed to any stress in the test direction. It is suggested that these relationships may be applied to estimate the free expansion of cores from a structure if they are tested similarly. The cores must then be drilled perpendicular to the main reinforcement. However, it is expected that these relationships might be different for other concretes, as shown in [112], and, therefore, not necessarily the same for the concrete in the considered structure. However, the concrete used in these laboratory experiments is assumed to represent Norwegian structures from the 1950s and 1960s.

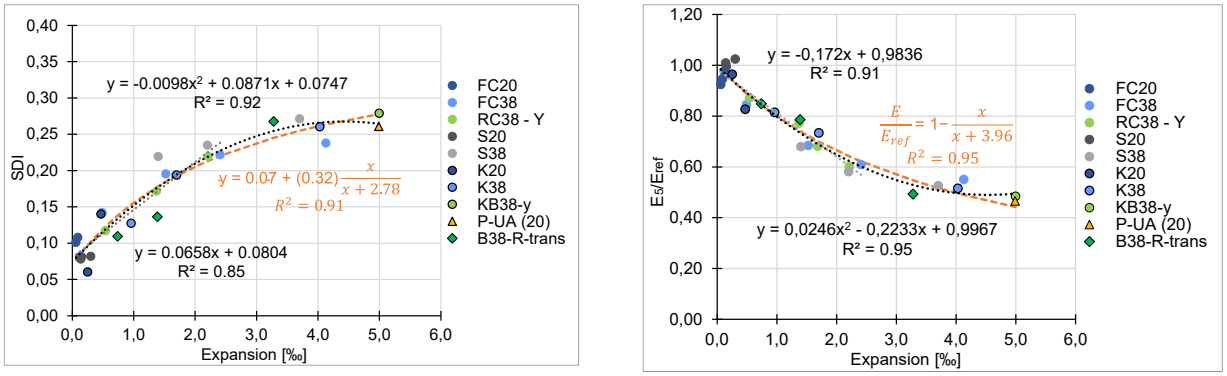

a) SDI vs expansion **b) E_5/E_{ref} vs expansion**

Figure 6-1: Damage parameters from the SDT for free samples plotted towards the expansion and shown with a curved and linear regression line [20]**. A regression line from** [24] **(β=3.96, R^2=0.95) is also shown with an orange line**

The regression function by [24] gives the following equations to calculate the free expansion:

$$\varepsilon_{free} = \frac{-2.78 \cdot SDI + 0.1946}{SDI - 0.39} \quad (75)$$

$$\varepsilon_{free} = \frac{3.96 \cdot (1 - E_5/E_{ref})}{E_5/E_{ref}} \quad (76)$$

As discussed in [20], if the *SDI*- and E_5/E_{ref}-values are outside the range of the laboratory curves (SDI > 0.28 or E_5/E_{ref} < 0.45), an estimate based on this method must be considered cautiously as such values may be due to special conditions such as coarse macro- and delamination cracks and frost damage. Estimates can be made from both *SDI* and E_5/E_{ref}, and if data are available to determine both, the final free expansion can be determined as the mean value of the two.

As the expansion is expected to vary, several cores (2-3) should be drilled both at each location and from several locations along the structure. Even if the estimated expansion from the *SDI* and E_5/E_{ref}-values is quite uncertain, it may be the best estimate that can be made if no additional information about the elongation of the structure in different directions is provided. Even then, an initial assumption must be made, which can be adjusted further to match the additional information.

Cores may also be cored from a “undamaged” part of the structure which can provide input, such as a reference E-modulus and to the material model in the analysis.

6.1.2 Input from field surveys

An alternative way of modelling is using the free expansion as a variable that is adjusted according to the structural response obtained from the analysis and whether model and field observations correspond. For example, by adjusting the free expansion so that the final elongation from the analysis fits with a measured elongation, or that observed cracks on the structure fit with those obtained from the analysis. It must here be divided between the surface cracks, which is a characteristic feature of ASR affected structures, which primarily occurs due to leaching of alkali-ions in the surface layer of the concrete, and the structural cracks that may occur due to additional loads on the structure which may be obtained from an analysis. When performing an assessment, the extent of cracking may, however, also be considered, as it may lead to more favourable conditions for other deterioration mechanisms such as reinforcement

corrosion and frost and in some severe cases also delamination of the cross-section, which may be critical for the structural capacity.

A sub-aim within the EXCON project is developing innovative methods for non-destructive field surveys, monitoring and laboratory analysis of cored samples. Some of the most relevant were used on three case dams as described in [113]. The focus was here on monitoring cracking caused by ASR. In addition to the "Cracking Index" (CI) method, crack detection by use of photogrammetry and advanced NDT measurements (ultrasound scanning) was also performed. One aim was to assess the accuracy of using those tools for the measurement of the extent of cracking. The result was therefore compared to the cores tested for the SDT method described above.

The CI-method is "well-established" method and is a good tool for following the extent of surface cracking over time. This initial survey shows that it gives corresponding ranking of the extent of damage on different locations as SDT analyses. However, the CI-values indicate higher strains in ‰ (mm/m) compared to the estimated expansion from SDT-testing, as the correlation between surface cracking and the extent of internal micro-cracks is not expected to be linear. The ultrasound scanning also proved promising for detecting subsurface cracks and acoustic discontinuities, for example due to delamination cracks, caused by ASR and visualizing their extent.

Laser scanning also proved to be a good tool for structural health monitoring of structures affected by ASR, as it by capturing detailed spatial data enables engineers to monitor deformation changes over time. Photogrammetry was employed as a complementary method to laser scanning to evaluate surface conditions and detect cracking. This proved to be an affordable alternative to laser scanning, especially for large-scale structural assessments by rapidly capturing high-detailed pictures.

6.2 Corroded reinforcing steel

To incorporate reinforcement corrosion into NLFEA of concrete infrastructures, the analysis requires the specification of corrosion degrees (ζ) and their distribution within the structure, e.g. as defined in Eq. (12) and (27).

Uncorroded reinforcement must be properly classified based on one or a combination of the methods mentioned in Section 4.3.5.1. Accordingly, the relevant reinforcement bar dimensions from the structure under assessment must be classified to enable reliable determination of the properties of the uncorroded and corroded material.

The methodology (see flowcharts in Figure 4-3 and Figure 4-5) also enables predictive assessments of future structural performance, provided that anticipated corrosion depths (P_X) and the corresponding corrosion degrees (ζ)—along with their distribution—are specified for a selected future time. In practice, this information can be represented using "heat maps" on structural drawings, illustrating the corrosion degrees (ζ) defined by Eq. (27) for both the current condition (t_1) and a future condition (t_2), based on parameters such as:

- nominal concrete cover (C_{nom})
- environmental exposure conditions
- reinforcement diameter (Ø)
- distribution factor (α)

It should be noted that determining corrosion depth (P_X) and its distribution is outside the scope of this report. These aspects are expected to be addressed by other work packages within the project that focus specifically on corrosion development and modelling.

7 Concluding remarks

7.1 Summary

A framework for applying NLFEA to assess the current and future condition of reinforced concrete infrastructures has been established. It proposes two approaches for composing material models applicable for that purpose. Both approaches open for either composing available material models or by programming them as user supplied subroutines in commercial general purpose finite element software. Furthermore, methods to account for material degradation due to ASR and reinforcement corrosion were formulated along with a safety format applicable for that purpose.

7.2 Material models applicable for NLFEA of deteriorated concrete structures

Two general approaches have been found to be applicable for NLFEA of deteriorated concrete infrastructures.

Following conclusion can be drawn for the first approach described in subchapter 2.2

- Both Kotsovos [5] and Total strain [4] predict correct failure modes, and both provide relatively good responses up to peak irrespective of i) the failure mode and ii) using a tension chord model or naked steel behaviour for the steel reinforcement.
- Kotsovos [5] provide the best response, in particular for the post-peak behaviour.
- The use of tension chord model provides best estimate of the stiffness, which is paramount in not overestimating the deformation capacity in accordance with [2]. This becomes important for static indeterminate systems to capture realistic ductility and thus behaviour of the structure.
- Both Kotsovos [5] and Total strain [4] are suitable for NLFEA of large concrete infrastructures, being computationally efficient.
- The simplicity of applying the concrete cylinder strength as the only input to Kotsovos [5] makes it recommendable as a practical and pragmatic approach for analysing large concrete infrastructures with NLFEA.

Following conclusion can be drawn for the second approach described in subchapter 2.3

- Concrete Damaged Plasticity can correctly predict both stiffness, capacity and failure mode for all studied cases where complex stress states occur for concrete strengths within 20-80MPa
- Early cracking and crashing damage can be estimated from CDP models and simulation
- Damaged plasticity formulation requires extensive material input, including two stress-strain curves and two strain-damage curves for compressive and tensile properties, as well as yield surface parameters (dilation angle, eccentricity, bi-axial stress ratio) and viscosity. All data are considered necessary for universal application of the model
- Damaged plasticity model is most practical for analyzing structural details and components with focus on complex failure modes mechanism and corrosion and degradation effects
- Convergence and computational time are main issues in large infrastructure application but careful material input selection can dramatically improve performance.

7.3 Modelling deterioration of concrete affected by ASR

Alkali–silica reaction (ASR) in concrete is a chemical process that induces expansion and material degradation, leading to structural consequences. The primary effects include reduced tensile strength and modulus of elasticity, while compressive strength is less affected. Expansion is stress-dependent—compressive stress reduces expansion in the load direction, resulting in anisotropic behavior.
For structural analysis, ASR effects are incorporated at the concrete scale using smeared material models. Expansion is typically modeled as an imposed strain, decomposed into thermal, shrinkage, and ASR

expansion. A key input to the ASR expansion model is the free ASR expansion (stress-free condition), which depends on environmental factors such as temperature and humidity. Stress dependency is captured through reduction functions, which adjust expansion under compression.

Material degradation due to ASR significantly reduces stiffness and tensile strength even at small expansion levels, which may in turn influence the shear capacity. Plates/shells without shear reinforcement should be evaluated with particular care, as their shear capacity relies solely on the concrete's contribution.

Structural modeling must account for reinforcement to capture the pre-stressing effect. Cracking and creep should be included for accurate stiffness representation. Safety assessment requires considering both stress changes and material deterioration. NLFEA may be employed to determine cross-section load effects (F_d) of ASR expansion for capacity checks of critical sections, which should then be compared against the corresponding resistance (R_d) while accounting for material deterioration caused by ASR.

7.4 Modelling deterioration of reinforcing steel affected by corrosion

The following conclusion can be drawn from chapter 4

- Both cross-sectional loss and additional material degradation due to governing corrosion mechanisms can be accounted for by adjusting the stress-strain curves of corroded rebars
- The corrosion degree ζ is the necessary input required to adjust the stress-strain curves accordingly
- The ability of the structure to redistribute internal forces due to corrosion can be accounted for by providing stress-strain curves at distinct times

7.5 Safety format

Chapter 5 of this report aimed to facilitate informed method selection and consistent implementation of NLFEA-based safety assessment of existing structures in engineering practice by systematically presenting available safety formats and discussing the background of current and emerging code provisions.

The section focused on semi-probabilistic verification methods, which represent the current state of practice. The Partial Factor Method and the Global Factor Method were introduced and discussed in terms of their conceptual basis, practical applicability, and consistency when applied in conjunction with NLFEA. Particular attention was given to issues that are specific to existing structures, such as the choice of specific target reliability levels accounting for assessment-specific circumstances and the role of information updating. Moreover, emphasis was placed on model uncertainty, which plays a central role in NLFEA-based safety assessment. The chapter illustrated how model uncertainties can be explicitly addressed and how their quantification and reduction may benefit from updating procedures based on benchmark studies, thereby improving the transparency and reliability of the assessment.

A case study was presented to illustrate the practical application of the different safety formats and methods, as well as of the simplified treatment of reinforcement corrosion within a safety assessment, based on the approach presented in section 4.3. The results demonstrate that, for the considered example, the investigated safety formats lead to consistent safety assessments and comparable design resistances, while also highlighting how differences in reliability requirements and uncertainty representation may affect the outcome. The case study was not intended to represent a specific real-world structure, but rather to demonstrate the application of the procedures and to support understanding of the conceptual differences between the methods.

7.6 Necessary input on deterioration from field observations and service life models

The necessary input required to assess the current and future condition of concrete infrastructures subjected to deterioration caused by ASR and reinforcement corrosion are

- The free ASR strains and the distribution of them within a structure
- The corrosion degrees and the distribution of them within a structure

These could be indicated, e.g. by providing “heat maps” of a structure. These should be provided for the current condition of the structure as a minimum. The future behaviour of the structure could also be predicted with NLFEA if the development of the necessary inputs is also provided, e.g. at a certain time in the future.

8 References

[1] Excon, “State-of-the-art report - NLFEA of deteriorated concrete structures. Report No: 2024:01542.,” SINTEF, 2023.

[2] J. Mata-Falcón, D. Tran, W. Kaufmann and J. Navrátil, “Computer-aided stress field analysis of discontinuity concrete regions,” in *Computational Modelling of Concrete Structures*, 2018.

[3] V. Cervenka, A. Rimkus, V. Gribniak and J. Cervenka, “Simulation of the crack width in reinforced concrete beams based on concrete fracture,” *Theoretical and Applied Fracture Mechanics,* vol. 121, 2022.

[4] M. Hendriks, A. de Boer and B. Belletti, Guidelines for Nonlinear Finite Element Analysis of Concrete Structures, Rijkswaterstaat Ministry of Infrastructure and the Environment, 2016.

[5] M. Engen, M. Hendriks, J. Øverli and E. Ålstedt, “Non-linear finite element analyses applicable for the design of large reinforced concrete structures,” *European Journal of Environmental and Civil Engineering,* vol. 23, no. 11, pp. 1381-1403, 2019.

[6] P. Marti, M. Alvarez, W. Kaufmann and V. Sigrist, “Tension Chord Model for Structural Concrete,” *Structural Engineering International,* 1998.

[7] O. Terjesen, T. Kanstad and R. Tan, “Simplified modified tension chord model: An alternative crack width calculation model to Eurocode 2 and fib model codes,” *Structural Concrete,* 2024.

[8] CEN, Eurocode 2: Design of concrete structures - Part 1-1: General rules and rules for buildings, European Committee for Standardization, 2004.

[9] T. L. Tomasz JANKOWIAK, “IDENTIFICATION OF PARAMETERS OF CONCRETE DAMAGE PLASTICITY CONSTITUTIVE MODEL,” *Foundations of Civil and Environmental Engineering,* vol. 6, 2005.

[10] F. J. a. S. W. Vecchio, “Experimental and Analytical Reexamination of Classic,” *Journal of Structural Engineering,* 2004.

[11] M. D. Kotsovos, “A fundamental explanation of the behaviour of reinforced concrete beams in flexure based on the properties of concrete under multiaxial stress,” *RILEM Publications SARL,* 1982.

[12] K. P. M. Seraj M.S., “THREE-DIMENSIONAL FINITE-ELEMENT MODELLING OF NORMAL- AND HIGH-STRENGTH REINFORCED CONCRETE MEMBERS, WITH SPECIAL REFERENCE TO T-BEAMS,” *Computers and Structures,* pp. 699-716, 1992.

[13] M. H. El-Feky, A. Elsisi, G. Mohamed, A. S. Eisa, M. Zelenakova and D. Katunsky, “Performance of RC frames strengthening by external post-tensioning tendons under vertical and lateral loads,” *Case studies in Construciton Materials,* vol. 20, 2024.

[14] G. Brådland and K. Kloster, “Consistent material modelling for nonlinear finite element analysis of corroded concrete infrastructures,” Norwegian University of Science and Technology, Master's thesis in Civil and Environmental Engineering, Trondheim, 2024.

[15] R. N. Swamy and M. M. Al-Asali, “Engineering properties of concrete affected by alkali-silica reaction,” *Materials Journal,* 1988.

[16] G. Giaccio, R. Zerbino, J. M. Ponce and O. R. Batic, “Mechanical behaviour of concretes damaged by alkali-silica reaction,” *Cement and Concrete Research,* 2008.

[17] N. Smaoui, B. Bissonnette, M. A. Bérubé, B. Fournier and B. Durand, “Mechanical properties of ASR-affected concrete containing fine or coarse reactive aggregates,” *Journal of ASTM International,* 2005.

[18] R. Esposito, C. Anac, M. Hendriks and O. Copuroglu, “Influence of the Alkali-Silica Reaction on the Mechanical Degradation of Concrete,” *Jounral of Materials in Civil Engineering,* 2016.

[19] S. S. Kongshaug, O. W. Oseland, T. Kanstad, M. Hendriks, E. Rodum and G. Markeset, “Experimental investigation of ASR-affected concrete - The influence of uniaxial loading on the evolution of mechanical properties, expansion an damage indices,” *Construction and Building Materials,* 2020.

[20] K. M. Stemland, Experimental and Structural Basis for Analysis and Assessment of Concrete Structures exposed to Alkali-Silixa Reactions, Trondheim: PhD-thesis NTNU, 2024.

[21] R. Esposito and M. Hendriks, “Literature review of modelling approaches for ASR in concrete: a new perspective,” *European Journal of Environmental and Civil Engineering,* 2019.

[22] R. Courtier, “The assessment of ASR-affected structures,” *Cement and Concrete composites,* 1990.

[23] I. May, H. X. Wen and R. Cope, “The modelling of the effects of AAR expansion on reinforced concrete members,” in *The Ninth International Conference on Alkali-Aggregate Reaction in Concrete*, 1992.

[24] H. Wen, “Prediction of structural effects in concrete affected by alkali-aggregate reaction,” *PhD Thesis,* 1993.

[25] P. Léger, P. Côté and R. Tinawi, “Finite element analysis of concrete swelling due to alkali-aggregate reactions in dams,” *Computers & structures,* 1996.

[26] V. Saouma and L. Perotti, “Constitutive model for alkali-aggregate reactions,” *ACI materials journal,* 2006.

[27] S. Multon, J. Seignol and F. Toutlemonde, “Chemomechanical assessment of beams damaged by alkali-silica reaction,” *Journal of materials in civil engineering,* 2006.

[28] S. S. Kongshaug, R. M. Larssen, M. A. Hendriks, T. Kanstad and G. Markeset, “Load effects in reinforced concrete beam bridges affected by alkali–silica reaction—Constitutive modelling including expansion, cracking, creep and crushing,” *Engineering structures,* 2021.

[29] S. Kongshaug, M. Hendriks, T. Kanstad and G. Markeset, “Toward identifying the ASR-induced stresses from displacement measurements and crack observations—Demonstration on a beam bridge in Norway,” *Engineering Structures,* 2022.

[30] C. Larive, “Apports combinés de l'expérimentation et de la modélisation à la compréhension de l'alcali-réaction et de ses effets mécaniques,” Ecole nationale des ponts et chaussees, 1997.

[31] S. Multon and F. Toutlemonde, “Effect of applied stresses on alkali-silica reaction-induced expansion,” *Cement and Concrete Research,* 2006.

[32] B. Gautam, D. Penesar, S. Sheikh and F. Vecchio, “Effect of Multiaxial Stresses on Alkali-Silica Reaction Damage of Concrete,” *ACI Materials Journal,* 2017.

[33] M. Berra, G. Faggiani, T. Mangialardi and A. E. Paolini, “Influence of stress restraint on the expansive behaviour of concrete affected by alkali-silica reaction,” *Cement and Concrete Research,* 2010.

[34] H. Kagimoto, Y. Yasuda and M. Kawamura, “ASR expansion, expansive pressure and cracking in concrete prisms under various degrees of restraint,” *Cement and Concrete Research,* 2014.

[35] J. Liaudat, I. Carol, C. López and V. Saouma, “ASR expansions in concrete under triaxial confinement,” *Cement and Concrete Composites,* 2018.

[36] A. Jones and L. Clark, “The effects of restraint on ASR expansion of reinforced concrete,” *Magazine of Concrete Research,* 1996.

[37] C. Gravel, G. Ballivy, K. Khayat, M. Quirion and M. Lachemi, “Expansion of AAR concrete under triaxial stresses: Simulation with instrumented concrete block,” in *11th International Conference on Alkali-Aggregate Reaction*, Quebec, Canada, 2000.

[38] T. Ahmed, M.A, E. Burley and S. Rigden, “The effect of alkali—silica reaction on the fatigue behaviour of plain concrete tested in compression, indirect tension and flexure,” *Magazine of Concrete Research,* 1999.

[39] C. Dunant and K. Scrivener, “Effects of uniaxial stress on alkali-silica reaction induced expansion of concrete,” *Cement and Concrete Research,* 2012.

[40] R. Charlwood, S. Solymar and D. Curtis, “A review of alkali aggregate reactions in hydroelectric plants and dams,” in *The international conference of alkali-aggregate reactions in hydroelectric plants and dams*, 1992.

[41] M. Herrador, F. Martínez-Abella and J. Rabuñal Dopico, “Experimental evaluation of expansive behavior of an old-aged ASR-affected dam concrete: methodology and application,” *Materials and Structures,* 2008.

[42] M. S. Pourbehi and G. P. van Zijl, “Seismic analysis of the kleinplaas dam affected by alkali-silica reaction using a chemo-thermo-mechanical finite element numerical model considering fluid structure interaction,” *Journal of Advanced Concrete Technology,* 2019.

[43] H. E. J. Z. Y. a. Y. T. Xi Ji, “Time-dependent Effect of Expansion due to Alkali-silica Reaction on,” *Journal of Advanced Concrete Technology,* 2021.

[44] S. G. H. H. B. J. Jesper Kierkegaard Hansen, “Exploring Alkali-Silica Reaction Effects on Concrete Bond Strength: Literature Review and Novel Experimental Approach,” in *15th fib International PhD Symposium in Civil Engineering*, 2024.

[45] fib, “fib Model Code for concrete structures 2020,” fédération internationale du béton (fib), Lausanne, 2023.

[46] Institution of Structural Engineers, “Structural effects of alkali-silica reaction. Technical guidance on the appraisal of existing structures.,” 1992.

[47] H. Johansen, “Bæreevneklassifisering av bruer med alkalireaksjoner, Svv Rapport Nr. 855,” 2022.

[48] K. Stemland, H. Johansen and T. Kanstad, “Load Effects of ASR-induced Expansion in Reinforced Concrete and Their Consequences for Structural Assessment,” *NCR Journal,* vol. 68, pp. 39-63, 2023.

[49] EN 1992-1-1:2004, “EN 1992-1-1:2004 Eurocode 2: Design of concrete structures – Part 1-1: General rules and rules for buildings”.

[50] CEN, “prEN1992-1-1:2023. Eurocode 2 - Design of concrete structures - Part 1-1: General rules and rules for buildings, bridges and civil engineering structures,” CEN, Brussels, 2023a.

[51] S. Haefliger, Load-deformation behaviour of reinforced concrete structures affected by local corrosion, vol. PhD Thesis, Zürich: ETH Zürich, 2022.

[52] J. Cairns, G. Plizzari, Y. Du, D. Law and C. Franzoni, “Mechanical properties of corrosion-damaged reinforcement,” *ACI Materials Journal,* vol. 102, no. 4, 2005.

[53] Y. Du, L. Clark and A. Chan, “Residual capacity of corroded reinforcing bars,” *Magazine of Concrete Research,* vol. 57, no. 3, pp. 135-147, 2005.

[54] J. Osmolska, T. Kanstad, H. M. A.N. and M. G, “Numerical investigation into the effects of corrosion on the shear performance of pretensioned bridge girders with cast-in-place slabs,” *Structures,* pp. 1447-1468, 2022.

[55] fib Bulletin 111, “Modelling structural performance of existing concrete structures. State-of-the-art report,” fédération internationale du béton (fib), 2024.

[56] Faraz Tariq, Pradeep Bhargava, “Stress-strain curves and mechanical properties of corrosion damaged super ductile reinforcing steel,” *Structures,* pp. 33: 1532-1543, 2021.

[57] Fernández, I., Bairán, J.M., and Marí, A.R., “Corrosion effects on the mechanical properties of reinforcing steel bars. Fatigue and σ–ε behavior,” *Construction and Building Materials,* pp. 101: 772-783, 2015.

[58] H. Stemland, “Service life of concrete structures (Betongkonstruksjoners livsløp). DP2- B3 Structural Analysis of Concrete Structures Affected by Corrosion,” SINTEF, Tronheim, 2001.

[59] Zhu, W., Francois, R., Poon, C.S., and Dai, J.-G., “Influences of corrosion degree and corrosion morphology on the ductility of steel reinforcement,” *Construction and Building Materials,* pp. 148: 297-306, 2017.

[60] NS 3473:1989, “Concrete structures — Design rules”.

[61] fib CEB Bulletin 188, “Fatigue of Concrete Structures. State-of-the-art report,” fédération internationale du béton (fib), 1988.

[62] Faraz Tariq and Pradeep Bhargava, “Post-Corrosion Bond-Slip Models for Super Ductile Steel with Concrete,” *Construction and Building Materials,* pp. Vol. 285, Article No. 122836, 2021.

[63] fib Bulletin 65, “Model Code 2010 – Volume 1,” fédération internationale du béton (fib), 2012.

[64] DNVGL-ST-C502:2018, “DNVGL-ST-C502:2018 (Amended 2021). Offshore Concrete Structures,” DNV GL AS.

[65] EN ISO 15630-1:2019, “EN ISO 15630-1:2019 Steel for the reinforcement and prestressing of concrete – Test methods – Part 1: Reinforcing bars, wire rod and wire”.

[66] EN ISO 15630-2:2019, “EN ISO 15630-2:2019 Steel for the reinforcement and prestressing of concrete – Test methods – Part 2: Welded fabric and lattice girders”.

[67] fib Bulletin 66, “Model Code 2010 – Volume 2,” fédération internationale du béton (fib), 2012.

[68] Vrouwenvelder et al., “Reliability background of the Eurocodes,” CEN, Brussels, 2024.

[69] P. Tanner, R. Hingorani and C. Lara, “New or Existing. Does it matter?,” in *Acta Polytechnica CTU Proceedings 36(0)*, Prague, 2022.

[70] R. Melchers and A. Beck, Structural Reliability Analysis and Prediction, John Wiley & Sons Ltd., 2018.

[71] D. Diamantidis, P. Tanner, M. Holicky, H. Madsen and M. Sykora, “On reliability assessment of existing structures,” *Structural Safety,* p. 113; 102452, 2025.

[72] CEN, “Draft EN 1990:2023, prA1: Eurocode - Basis of structural and geotechnical design - Part 1: New Structures,” CEN, Brussels, 2023.

[73] JCSS, “Probabilisitc model code,” Committee on Structural Safety, 2001.

[74] ISO , “ISO 2394:2015 General principles on reliability for structures,” International Organization for Standardization (ISO), Geneva, 2014.

[75] T. Vrouwenvelder, “Developments towards full probabilistic design codes,” *Structural Safety,* pp. 24:2–4, 417-432, 2002.

[76] M. Holicky, D. Diamantidis and M. Sykora, “Reliability levels related to different reference periods and consequence classes,” *Beton und Stahlbetonbau,* 2018.

[77] N. Meinen and R. Steenbergen, “Reliability levels obtained by Eurocode partial factor design - A discussion on current and future reliability levels,” *Heron,* pp. 63:243-302, 2018.

[78] J. Nathwani, N. Lind and M. Pandey, “Affordable Safety By Choice: The Life Quality Method,” Inst. for Risk Research, University of Waterloo. , Waterloo, 1997.

[79] R. Rackwitz, “Optimization — the basis of code-making and reliability verification,” *Structural Safety,* pp. 22:1, 27-60, 2000.

[80] K. Fischer, C. Viljoen, J. Köhler and M. Faber, “Optimal and acceptable reliabilities for structural design,” *Structural Safety,* pp. 76: 149-161, 2019.

[81] B. Bhattacharya, “An appraisal of the LQI as an approach to setting target reliabilities in ISO 2394:2015,” *Structural Safety,* p. 109: 102482, 2024.

[82] M. H. Faber, J. D. Sørensen and A. (. O. & Vrouwenvelder, “On the regulation of life safety risk.,” in *12th International Conference on Applications of Statistics and Probability in Civil Engineering (ICASP 12)*, Vancouver, 2015.

[83] P. Tanner and R. Hingorani, “Acceptable risks to persons associated with building structures,” *Structural Concrete,* pp. 16:3, 314-322, 2015.

[84] F. Liljefors and J. Köhler, “Framework for rational decision-making in bridge,” *Structure and Infrastructure Engineering,* 2024.

[85] T. Vrouwenvelder and N. Scholten, “Assessment criteria for existing structures,” *Structural Enginnering International,* pp. 20:62-65, 2010.

[86] R. Steenbergen, M. Sykora, M. D. D. Holicky and T. Vrouwenvelder, “Economic and human safety reliability levels for existign structures,” *Structural Concrete,* pp. 16:323-332, 2015.

[87] fib, “Partial factor methods for existing concrete structures,” fédération internationale du béton (fib), Lausanne, 2016.

[88] R. Caspeele, W. Botte and E. Vereecken, “Bayesian performance assessment of existing concrete structures combining different types of information from inspections and monitoring,” *Structure and Infrastructure Engineering,* pp. 21,7-8: 1134-1150 , 2025.

[89] R. De Vries, E. Landsoght, R. Steenbergen, M. Hendriks and M. Naaktgeboren, “Structural reliability updating on the basis of proof load testing and monitoring data,” *Engineering Structures,* pp. 330, 119863, 2025.

[90] C. Lara, P. Tanner, C. Zanuy and R. Hingorani, “Reliability Verification of Existing RC Structures Using Partial Factors Approaches and Site-Specific Data,” *Applied Sciences,* pp. 11(4), 1653, 2021.

[91] E. Vereecken, W. Botte, G. Lombaert and R. Caspeele, “Influence of modeling choices and prior information on the Bayesian assessment of a reinforced concrete bridge,” *Structural Concrete,* p. 25:1713–1734, 2024.

[92] CEN, “prEN 1990:2022, Basis of structural and geotechnical design - Part 2 Assessment of existing structures,” CEN, Brussels, 2023b.

[93] RILEM TC, “Reliability Updating and Decision Analysis. In: Probabilistic Assessment of Existing Structures - JCSS Report,” RILEM Publications SARL, 2001.

[94] M. Engen, M. Hendriks, J. Köhler, J. Øverli and E. Åldstedt, “A quantification of the modelling uncertainty of non-linear finite element analysis of large concrete structures,” *Structural Safety,* p. 64:1–8, 2017.

[95] M. Engen, M. Hendriks, G. Monti and D. Allaix, “Treatment of modelling uncertainty of NLFEA in fib Model Code 202,” *Structural Concrete,* pp. 22:3202-3212, 2021.

[96] P. Castaldo, D. Gino, G. Bertagnoli and G. Mancini, “Partial safety factor for resistance model uncertainties in 2D non-linear finite element analysis of reinforced concrete structures,” *Engineering Structures,* pp. 176:746-762, 2018.

[97] P. Castaldo, D. Gino and G. Mancini, “Safety formats for non-linear finite element analysis of reinforced concrete structures. Discussion, comparison and proposals,” *Engineering Structures,* pp. 193:136-153, 2019.

[98] V. S. R. S. P. R. V. M. V. S. R. Y Shashank Babu, “A Review of mathematical models for prediction of Stress-strain and moment –curvature behaviour in concrete,” *2020, E3S Web of Conferences,* p. 01111, 2020.

[99] F. Shaker and C. Caprani, “Enhancing structural performance prediction through Bayesian updating with considering load and speed uncertainty,” in *Bridge Maintenance, Safety, Management, Digitalization and Sustainability*, Taylor and Francis group, CRC Press, 2024.

[100] P. L. C. Tanner and D. Sanz, “Understanding existing barriers to consistent decision making,” in *2025 fib International Symposium. Concrete structures: extended lifetime, limit impacts.*, Antibes, 2025.

[101] Orcesi A. et al., “Investigating Partial Factors for the Assessment of Existing Reinforced Concrete Bridges,” *Structural Engineering International,* pp. 34:1, 55-70, 2023.

[102] R. Caspeele, M. Sykora and D. S. R. Allaix, “The Design Value Method and Adjusted Partial Factor Approach for Existign Structures,” *Structural Engineering International,* pp. 23:4, 386-393 , 2013.

[103] D. Gino, P. Castaldo, G. Bertagnoli, L. Giordano and G. Mancini, “Partial factor methods for existing structures according to fib Bulletin 80: Assessment of an existing prestressed concrete bridge,” *Structural Concrete,* p. 21:15–31, 2019.

[104] M. Ferrara, D. Gino, E. Miceli, L. Giordano, M. Malavisi and G. Bertagnoli, “Safety assessment of existing prestressed reinforced concrete bridge decks through different approaches,” *Structural Concrete. 2024,* p. 1–21, 2024.

[105] E. Miceli, D. Gino and P. Castaldo, “Approaches to estimate global safety factors for reliability assessment of RC structures using non-linear numerical analyses,” *Engineering structures,* p. 311:118193, 2024.

[106] D. Allaix, V. Ilario Carbone and G. Mancini, “Global safety format for non-linear analysis of reinforced concrete structures,” *Structural Concrete,* pp. 14-1: 29-42, 2013.

[107] D. Gino, E. Miceli and P. Castaldo, “Comparison of approaches for determining global safety factors in NLNA of RC members failing in shear,” in *Proceedings of the 2025 fib International Symposium: Concrete structures: extended lifetime, limit impacts*, Antibes, 2025.

[108] C. Andrade, “Propagation of reinforcement corrosion: principles, testing and modelling,” *Materials and Structures,* p. 52:2, 2019.

[109] C. Andrade and M. Cruz Alonso, “RILEM TC 154-EMC. 'Electrochemical Techniques for Measuring Metallic Corrosion. Test methods for on-site corrosion rate measurement of steel reinforcement in concrete by means of the polarization resistance method,” *Materials and Structures,* pp. 37:623-643, 2004.

[110] K. Hornbostel, T. Danner and M. Geiker, “Non-destructive Test Methods for Corrosion Detection in Reinforced Concrete Structures,” *Nordic Concrete Research,* pp. NCR 62 – ISSUE 1 – Article 3, pp. 41-61, 2020.

[111] L. F. M. Sanchez, B. Fournier, M. Jolin and J. Bastien, “Evaluation of the Stiffness Damage Test (SDT) as a tool for assessing damage in concrete due to ASR: Test loading and output responses for concretes incorporating fine or coarse reactive aggregates,” *Cement and Concrete Research,* 2014.

[112] L. F. M. Sanchez, B. Fournier, M. Jolin, D. Mitchell and J. Bastien, “Overall assessment of Alkali-Aggregate Reaction (AAR) in concretes presenting different strenghts and incorporating a wide range of reactive aggregate types and natures,” *Cement and Concrete Research ,* 2017.

[113] W. B. K. R. C. K. R. H. E. K. K. M. S. H. R. I. D. I.-E. T. K. Ø. B. Jan Lindgård, “Alkali-silica reactions (ASR) in concrete dams - field survey, ND-testing and laboratory analyses,” in *Concrete Solutions 2025*, Lisbon, 2025.

EXCON

https://www.sintef.no/prosjekter/2023/excon-gronn-forvaltning-av-konstruksjoner-for-infrastruktur/

The project is funded by the Green Platform scheme, which is a collaboration between the Research Council of Norway, Innovation Norway, Siva and Enova, and the following partners: